
Editorial Office of *Earth's Cryosphere (Kriosfera Zemli)*
Institute of Geography, Russian Academy of Sciences
37 Vavilov str., office 22, Moscow, 117312, Russia
Editorial staff: *N.V. Arutyunyan*, *N.G. Belova*, *O.M. Lisitsyna, G.E. Oblogov*
Phone: (499) 124-54-22, e-mail: kriozem@gmail.com

Journal promoted by
Russian Academy of Sciences, Siberian Branch, Novosibirsk
Earth's Cryosphere Institute, Tyumen Scientific Centre SB RAS, Tyumen
Melnikov Permafrost Institute, SB RAS, Yakutsk

Editorial Manager *M.A. Trashkeeva*
Designed by *N.F. Suranova*
Typeset by *N.M. Raizvikh*

English text by *M.A. Korkka, V.V. Kuzovkin, G.E. Oblogov*

RUSSIAN ACADEMY OF SCIENCES
SIBERIAN BRANCH
EARTH'S CRYOSPHERE INSTITUTE, TYUMEN SCIENTIFIC CENTRE

EARTH'S CRYOSPHERE
SCIENTIFIC JOURNAL

Founded in January 1997	6 issues per year	Vol. XXV, No. 1	January–February 2021

CONTENTS

EARTH'S CRYOSPHERE
SCIENTIFIC JOURNAL

Kriosfera Zemli, 2021, vol. XXV, No. 1, pp. 3–30

FUNDAMENTAL ISSUES OF EARTH'S CRYOSPHERE

LATE QUATERNARY SAND COVERS OF CENTRAL YAKUTIA (EASTERN SIBERIA): STRUCTURE, FACIES COMPOSITION AND PALEOENVIRONMENT SIGNIFICANCE

A.A. Galanin

Melnikov Permafrost Institute, Siberian Branch of the Russian Academy of Sciences, Merzlotnaya str. 36, Yakutsk, 677010, Russia; agalanin@gmail.com

An additional comprehensive study of the Peschanaya Gora (Sand Hill) outcrop and other sections of aeolian coversands in Central Yakutia has revealed that, together with loess-ice (Yedoma) covers, they were two related granulometric and mineralogical derivatives which had formed as a result of aeolian processing of Quaternary alluvium during the second half of the Late Neopleistocene. Episodes of desertification took place 22.0–14.0, 12.8–11.8, and 0.6–0.1 ka BP. A decrease in aeolian activity and consolidation of dune massifs by a soil-vegetative cover took place in the intervals of 14.0–13.0 and 10.0–0.6 ka BP. The largest episode of desertification took place during the last global thermic minimum (MIS-2) and led to a sharp decline in the mammoth biome, the disappearance of the wooly mammoth and rhinoceros in Central Yakutia.

Key words: *aeolian formation, D'olkuminskaya Series, cryogenic-aeolian, niveo-aeolian lamination, desertification, Late Pleistocene, Holocene, Bølling, Allerød, Younger Dryas, Eastern Siberia.*

INTRODUCTION

The studied region is located in the southern part of the Central Yakutian Lowland, within the Mesozoic Vilyuy Lowland of the Siberian platform. The sedimentary cover of the platform, which is exposed in the base of the Lena River's and its tributaries' high terraces, consists of Lower Paleozoic carbonate and Mesozoic-Cenozoic terrigenous deposits. Quaternary formations are represented by alluvial, lake, aeolian, and polygenic (cryogenic-aeolian) facies groups. The most abundant among them are Late Neopleistocene loess-ice deposits (Yedoma Series) with large polygonal ice wedges (PIW), as well as loess and sand covers and dune massifs (D'olkuminskaya Series) with a small ground ice content (Fig. 1, 2).

The climate of the region is sharply continental, with an average annual temperature of approximately –7 °C, annual precipitation varying from 140 to 250 mm, and a precipitation-evaporation ratio of 0.8–1.0. Permafrost 200–600 m thick with a temperature of –3 to –7 °C is distributed throughout the region. The thickness of the active layer varies from 0.5 to 2.5 m [*Ershov, 1989*].

Various types of larch forests (*Larix gmelinii*) dominate the region's vegetation cover, with a mixture of pine (*Pinus sylvestris*), spruce (*Picea obovata*), and birch trees (*Betula platyphylla*, *B. pendula*). Shrub birches (*Betula exilis*, *B. nana*), alder elfin (*Alnus fruticosa*), the genus *Rosa* (*Rosaceae* sp.) dominate the canopy layer; subshrub heath (Ericaceae fam.), spike moss (*Selaginella rupestis)*, creeping cedars (*Lycopodium annotinum*, *L. pungens*, *L. clavatum,* etc.), mosses (Bryophyta), fructicose lichens (*Cladina* sp., *Cetraria* sp., etc.) dominate the ground layer. Grasses, sedges, and Asteraceae (Poaceae fam., Cyperaceae and Asteraceae) dominate the herbaceous layer [*Kuznetsova et al., 2010*].

Forestless landscapes are distributed fragmentarily on floodplains, low terraces, alas basins, and on steep slopes with a southern aspect. They are represented by meadow, steppe, and semi-desert herbaceous groupings consisting of feather grass (*Stipa capillata*), fescue (*Festuca lenensis*), Kobresia *(Kobresia* filifolia), sedges (*Carex duriuscula*, *C. pediformis*), wheatgrass (*Elytrigia jacutorum*), sagebrush (*Artemisia frigida*, *A. tanacetifolia*, *A. karavajevii*), buttercup (*Anemone sylvestris*), etc. Halophytic species are common (*Goniolimon speciosum*, *Salicornia europaea*, etc.).

Semi-desert groups are more common within modern dune massifs (Tukulans). The extremely sparse vegetation cover is formed by single curtains of xerophytic semi-subshrubs (*Thymus sergievskajae*, *Krascheninnikovia lenensis*, *Ephedra monosperma*) and perennial grasses, many of which are endemic (*Koeleria skrjabinii*, *K. karavajevii*, *Artemisia karavajevii*, *Phlojodicarpus sibiricus*, *Rumex graminifolius*, etc.).

The Peschanaya Gora outcrop (62°88.21′ N, 129°80.68′ E), also called Shishkinskiy Yar and D'olkuma-Khayata (as cited in [*Kamaletdinov, Minuk,*

1991]), is located on the right bank of the Lena River, 100 km north of Yakutsk (Fig. 1), and is one of the key sections of cover dune deposits of Central Yakutia. The cross- and wavy-stratification sands (up to 20 m thick) which emerge in the 18–25 m cliff of the (Kerdyom) terrace were named the D'olkuminskaya Series and dated to the last MIS-2 (marine isotope stage) cryochrone of the Late Neopleistocene [*Kolpakov, 1983; Aleekseev et al., 1984, 1990; Kamaletdinov, Minuk, 1991*]. The relatively young age of the D'Olkuminskaya Series is evidenced by its top, which is clearly expressed in the modern relief as vegetated U-shaped and longitudinal dunes with a southeast axis orientation (Fig. 2, *a*, *b*). Individual dunes reach a length of 2 km, a width of 300–400 m, and a height of 10–15 m.

Aeolian cover sands similar in composition, structure and age are known in many cold regions of Northern Eurasia: Transbaikalia and Baikalia [*Ivanov, 1966; Ufimtsev et al., 1997; Vyrkin, 2010*], Western Siberia [*Volkov, 1971; Fedorovich, 1983; Velichko, Timireva, 2005; Sizov, 2015; Zykina et al., 2017; Konstantinov et al., 2019; Sizov et al., 2020*], Northern Europe [*Schwan, 1986, 1988; Kasse, 2002; Astakhov, Svensen, 2011*], and also in Alaska and Canada [*Black, 1951; Pewe, 1975; Carter, 1981; Koster, Dijkmans, 1988; Lea, 1996; Wolfe et al., 2011*].

In 1984 the Peschanaya Gora outcrop was added to the list of unique objects in the scientific excursion of the 27th International Geological Congress that took place in Yakutsk [*Alekseev et al., 1984*]. Later, D'olkuminskaya Series deposits were documented in different volumes in the structure of both the low and the highest terraces of the Lena River (Fig. 1) [*Kamaletdinov, Minuk, 1991; Waters et al., 1999; Bolshiyanov et al., 2016; Spektor et al., 2016, 2017; Pravkin et*

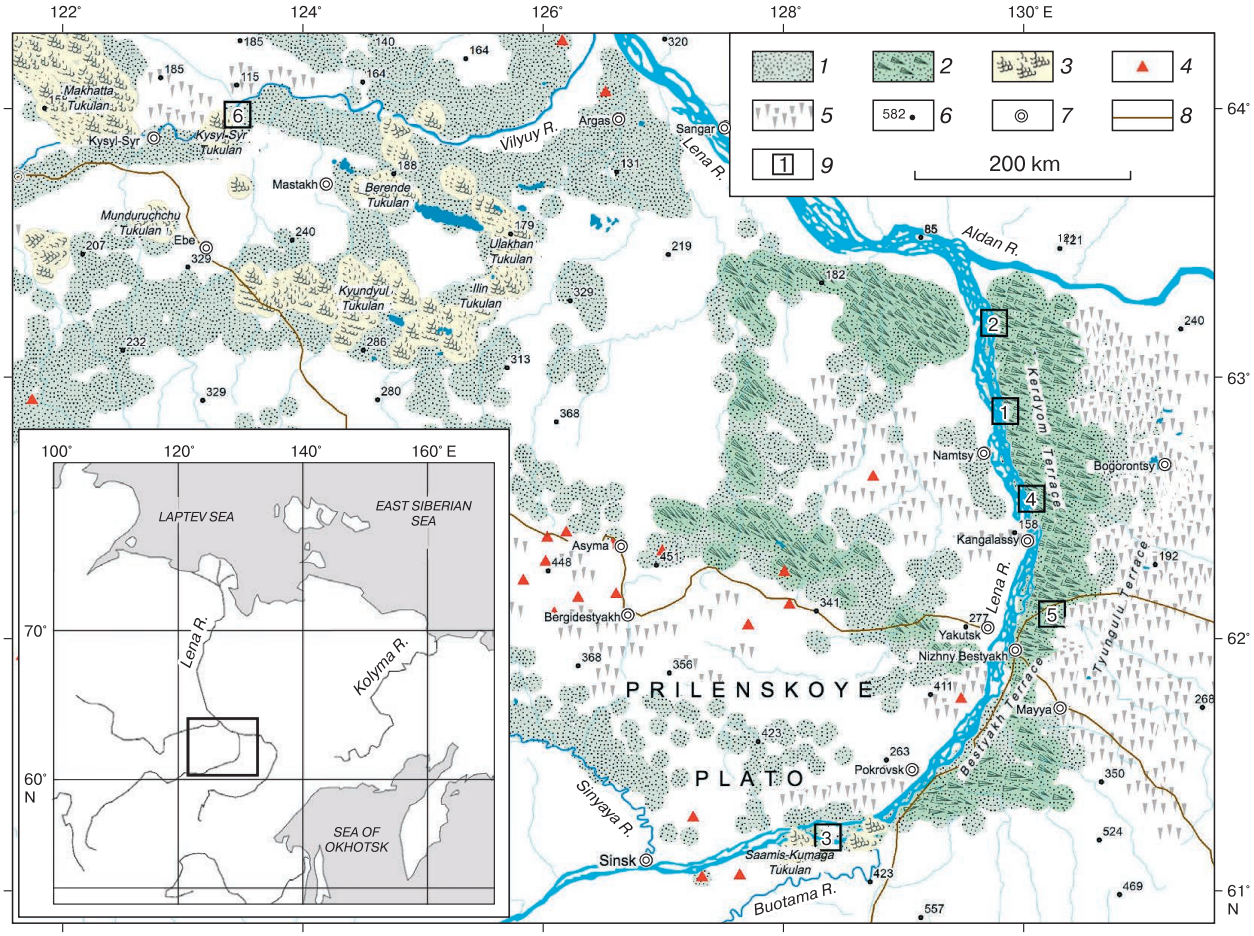

Fig. 1. Distribution of D'olkuminskaya Series cover aeolian deposits and modern unfixed dune massifs (Tukulans) in Central Yakutia.

1 – fixed sand covers of the last glacial maximum (MIS-2); *2* – fixed U-shaped and longitudinal dunes of the Younger Dryas; *3* – unfixed parabolic dunes (Tukulans) of the Little Ice Age; *4* – findings of large accumulations of ventifacts; *5* – accumulative plains and plateaus with Yedoma Series Late Neopleistocene ice-loess covers (MIS-3–MIS-2); *6* – height markers; *7* – populated areas; *8* – roads; *9* – D'olkuminskaya Series key sections discussed in the present article: 1 – Peschanaya Gora; 2 – Kharyyalakh; 3 – Ust'-Buotama; 4 – Suullar Myraan; 5 – Megin; 6 – Kysyl-Syr.

Fig. 2. Some forms of the aeolian and cryogenic-aeolian relief of Central Yakutia, composed of sand and loess-ice cover deposits of the second half of the Late Neopleistocene.

a, *b* – fixed U-shaped dunes on the surface of the 18–25-meter Kerdyom (*a*) and 45–75-meter Bestyakh (*b*) terraces of the Lena River in the territory surrounding Yakutsk; *c* – modern embryonic parabolic dune on the surface of the 30-meter terrace of the Vilyuy River; *d* – large modern dune massif (Tukulan), which intersects various elements of the Vilyuy River valley; *e* – modern dune massif (Ilin Tukulan) which partially blocks the Lungkha River valley (right tributary of the Vilyuy); *f* – 30-meter-tall cover dune on the brink of the Bestyakh terrace of the Lena River; *g* – thermodenudational relief within the distribution of ice-loess deposits of the Yedoma Series of the 75–150-meter (Tyungulu) terrace of the Lena River; *h* – Muus Appa deflational ventifact plateau within the Lena-Vilyuy drainage divide. Fig. 2, *a*, *b*, *g*, *h* – satellite images from the portal Yandex.Maps. Fig. 2, *c*, *d*, *e*, *f* – A.A. Galanin's photo from July–August 2019.

al., 2018], in the basin of the lower course of the Vilyuy River [*Galanin et al., 2016, 2018; Galanin, Pavlova, 2019*], and also identified in the terminal Middle and Late Neopleistocene moraines of the Verkhoyansk glaciers [*Siegert et al., 2007*]. The maximum thickness of the series (more than 70 m) is seen in the Ust'-Buotama outcrop of the Bestyakh terrace of the Lena River, 120 km south of Yakutsk.

To this day a fairly large amount of radiocarbon and optical luminescence (OSL) dates falling within the range of 30 to 10 ka has been obtained from D'olukminskaya Series deposits, which indicates the series' formation over the course of MIS-2 in the last cryochrone [*Galanin, Pavlova, 2019*].

Numerous lithological and structural features indicate an aeolian origin of the D'olkuminskaya Series [*Kolpakov, 1983; Pewe, Journaux, 1983; Kamaletdinov, Minuk, 1991; Waters et al., 1999; Siegert et al., 2007; Galanin et al., 2018*]. Aeolian genesis is also evidenced by a mantle-like bedding, the distribution

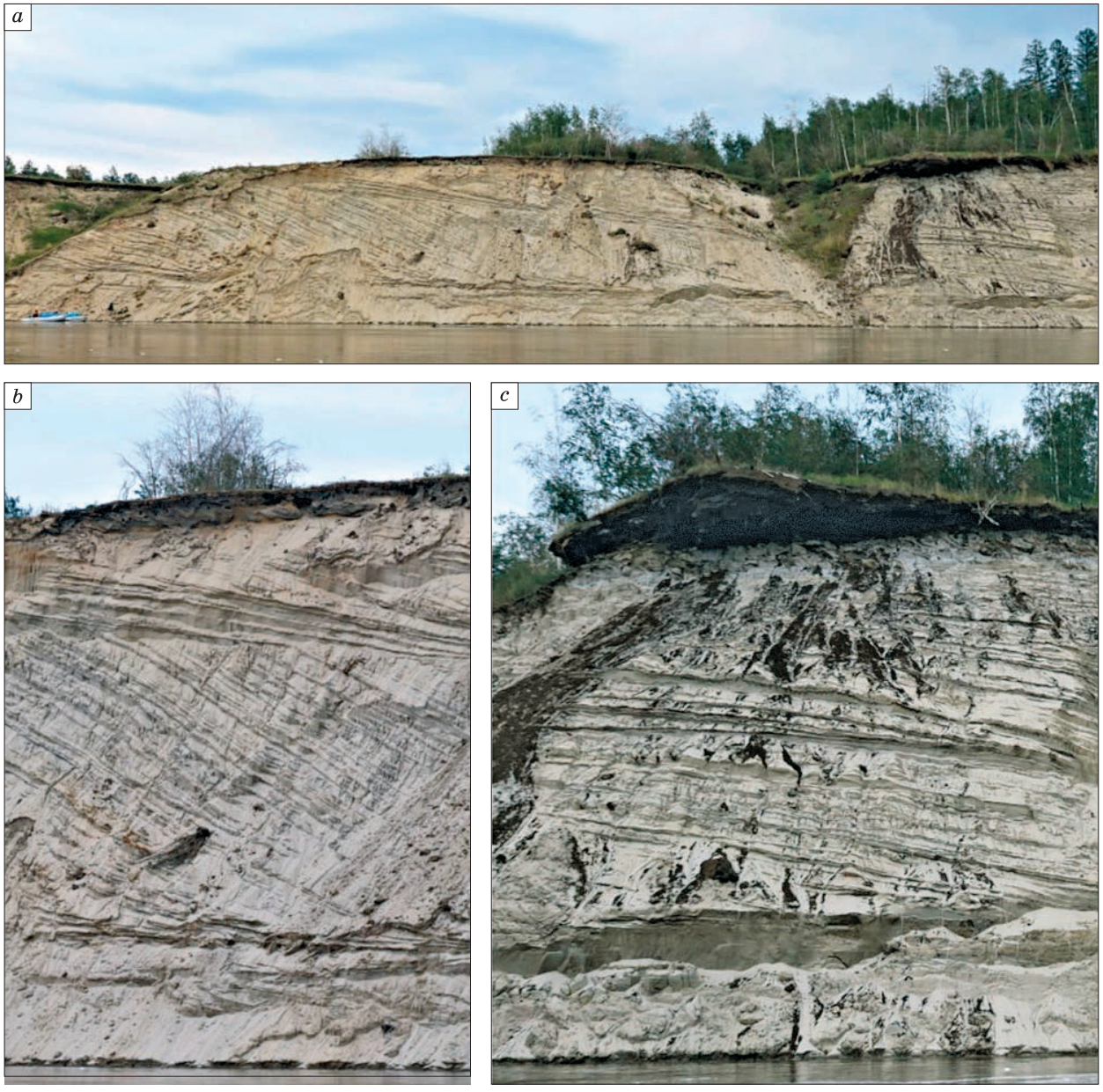

Fig. 3. Key outcrop Peschanaya Gora in the escarpment of the 18–25-meter (Kerdyom) terrace of the Lena River.

High overflow of the Lena River in August 2018 exposed expressive inclined, diagonal and cross-bedded D'olkuminskaya Series stratification types. *a* – overall appearance of the studied area; *b* – cross-bedded macrostructure of dune sands; *c* – Holocene peat bog in the roof of the D'olkuminskaya Series. A.A. Galanin's photo from August, 2019.

of sand covers across different hypsometric levels (Fig. 1), including watersheds, and the xerothermic composition of fossilized flora and fauna, in which cold steppe and desert taxa dominate [*Kolpakov, 1983; Kamaletdinov, Minuk, 1991; Filippov, Vasiliev, 2006; Galanin, Pavlova, 2019*].

Holocene and modern unvegetated dune massifs called Tukulans are widespread in the region in association with Late Neopleistocene D'olkuminskaya Series sand covers (Fig. 2, *c–f*). Their total area exceeds 3,000 km^2 [*Galanin et al., 2016; Galanin, Pavlova, 2019*]. The bigger ones – the Makhatta, Ulakhan, Kysyl-Syr, and other Tukulans – are located in the basin of the lower course of the Vilyuy River. The Saamis-Kumaga and Lenskaya Dune Tukulans, which model the surface of the 75–100-m (Bestyakh) terrace of the Lena River in the vicinity of the Ust'-Buotama outcrop and are comprised of unvegetated parabolic dunes up to 30 m in height (Fig. 2, *f*), are known in the territory surrounding Yakutsk.

For a long time the D'olkuminskaya Series was presented on geological maps as river and lake deposits [*Map..., 1959; Map..., 1983*]. It was assumed that cover sands were a particular type of "periglacial alluvium" and the dunes that lie atop the surface of the terraces had formed as a result of its wind reworking [*Soloviev, 1959; Alekseev, 1961*]. The lengthy denial of aeolian genesis of the D'olkuminskaya Series is also due to a lack of confidence in the existence of mixed-age river terraces in the Lena River Basin in this case, and the principle of distinguishing them by relative height is broken altogether.

Despite the appearance of Late Neopleistocene dune covers on the new geological map [*Map..., 2014*], the structure of the key outcrop Peschanaya Gora, the distribution areas, and the genesis of the D'olkuminskaya Series are currently under discussion. Some researchers are attempting to explain the series' "gigantic inclined and wavy stratification which has no modern analogues" (Fig. 3) using the activity of catastrophic floods and spillways moving transversely across the valley of the Lena River [*Spektor et al., 2016, 2017*]. Another group of authors [*Bolshiyanov et al., 2013, 2016; Pomortsev et al., 2017*] ties the origin of sand covers to a rise in the level of the Lena River by 100–150 m during MIS-3 as a result of "a change in the base of erosion and backwater from the sea" [*Pravkin et al., 2018, p. 225*].

Various types of stratification and lamination, the taxonomy and origin of which are poorly studied, are common in D'olkuminskaya Series deposits. The diagonal and gigantic oblique types of stratification (Fig. 3), referred to by some researchers as alluvial oblique stratification, are of particular importance. It was supposed for a long time that its formation is related to the unusual regimes of Late Neopleistocene watercourses and particular facies of "periglacial alluvium," modern analogues of which do not exist [*Soloviev, 1959; Alekseev, 1961; Ershov, 1989; Bolshiyanov et al., 2016; Spektor et al., 2016, 2017; Pravkin et al., 2018*]. Discussions arise not only from the unusual types of stratification and lamination, but also from the ubiquitous southeast strike of the strata. It completely diverges from the direction of the flow of modern rivers, but matches the southeast orientation of the dune relief on the surface of river terraces and corresponds to the main direction of atmospheric transport in the region (Fig. 1, 2, *a*, *b*).

In 2017–2020 the authors of the present article conducted an additional study of the structure and granulometric and mineralogical composition of Peschanaya Gora deposits and obtained new radiocarbon dates. Special attention was paid to the study of the structure of the deposits (stratification and lamination).

The goal of the present article is to provide a more complete description of the Peschanaya Gora outcrop and to discuss, taking into account both new data and data published earlier, the main features of the structure and origin of D'olkuminskaya Series deposits and the Late Quaternary relief of Central Yakutia and Eastern Siberia.

RESEARCH MATERIALS AND METHODS

The factual material of the present article is based on the study of natural outcrops using standard methods of Quaternary geology, geomorphology, structural and facies analyses.

The granulometric analysis (42 samples) was completed in accordance with GOST 12536-2014 [*2015*] methods of sieving and areometry in the Melnikov Permafrost Institute (MPI), SB RAS granulometric laboratory. V.V. Okhotin's [*1933*] granulometric classification denominations were used to describe deposits. Statistical processing of the results was completed in the Gradistat program [*Blott, Pye, 2001*] using the modified geometric method [*Folk, 1980; Blott, Pye, 2001*]. Mean (x) and median (Md) grain sizes were calculated in micrometres (μm); other values – grain sorting coefficient (σ), skewness (asymmetry) (α), and excess kurtosis (τ) – were calculated in dimensionless units of logarithmic scale [*Blott, Pye, 2001*]. The results of the analysis are shown in Table 1.

The quantitative immersion mineralogical analysis (28 samples) was completed in the MPI SB RAS laboratory using binocular and polarizing mineralogical microscopes, as well as immersion liquids. Mineral grain count was completed simultaneously for two fractions: 100–50 μm and 50–10 μm. 300–350 grains were taken from each sample and fraction from a random batch, based on which the percentage content of each mineral was calculated. The results of the mineralogical analysis are shown in Table 2.

Table 1. **Granulometric composition of the deposits of the 18–15-meter terrace of the Lena River in the Peschanaya Gora outcrop (Central Yakutia)**

Deposit unit number	Interval (m)	Number of samples	x, μm	σ	α	τ	Md, μm
Ia	0–2.45	8	316.8 ± 64.9	2.03 ± 0.16	0.04 ± 0.10	1.10 ± 0.18	317.8 ± 63.5
Ib	2.45–2.50	2	56.2 ± 1.1	4.43 ± 0.80	–0.25 ± 0.15	0.85 ± 0.03	71.7 ± 11.5
IIb	5.0–7.0	2	253.9 ± 10.9	1.84 ± 0.16	–0.06 ± 0.02	0.82 ± 0.06	260.9 ± 7.1
IIIa	10.0–17.0	2	298.4 ± 79.5	1.70 ± 0.04	0.02 ± 0.01	1.12 ± 0.36	290.3 ± 73.1
IIIb	17.0–17.4	2	649.0 ± 331.8	1.71 ± 0.23	–0.39 ± 0.10	1.23 ± 0.06	741.2 ± 411.7
IIIc	17.4–20.0	8	240.2 ± 17.0	1.69 ± 0.06	–0.16 ± 0.07	0.81 ± 0.07	253.7 ± 24.0
IVa	20.0–20.4	1	44.5	4.29	0.13	0.95	38.0
IVb	20.4–22.4	4	316.9 ± 30.7	1.67 ± 0.16	–0.21 ± 0.07	1.18 ± 0.15	334.4 ± 18.6

Note: x – mean grain size; σ – grain sorting coefficient; α – skewness; τ – excess kurtosis; Md – median.

Table 2. **Mineralogical composition of alluvial and aeolian sands in the 18–25-meter (Kerdyom) terrace of the Lena River in the Peschanaya Gora outcrop (Central Yakutia)**

Parameter			Unit number			
			I	II	IIIa	IIIc
Sampling interval*, m			0–2.45	2.50–9.95	10.0–17.0	17.0–22.5
Number of samples in fractions: 100–50 μm; 50–10 μm			6; 4	11; 5	5; 4	6; 2
Minerals		Fraction, μm	Grain content in sample**, %			
Primary	Quartz	100–50	17.4–55.1; 39.9	25.1–50.8; 44.2	42.3–50.4; 47.4	43.9–56.2; 50.7
		50–10	8.5–27.2; 18.8	22.0–43.3; 34.3	33.8–56.0; 46.0	36.0–46.8; 41.4
	Feldspars	100–50	9.0–40.4; 28.1	17.7–44.9; 36.8	28.1–39.6; 35.1	33.4–43.7; 38.8
		50–10	6.7–16.2; 11.1	19.0–37.9; 29.0	17.0–44.1; 34.0	41.8–44.2; 43.0
	Carbonates	100–50	1.4–68.4; 20.3	0.7–54.2; 9.7	0.9–11.7; 4.0	0.0–4.8; 0.9
		50–10	16.6–80.0; 46.6	16.6–54.9; 27.6	2.1–24.3; 8.3	0.0–10.5; 5.3
	Amphiboles	100–50	1.5–13.2; 7.4	1.6–9.8; 5.3	2.5–7.3; 5.1	3.1–8.4; 5.6
Secondary and accessory	Epidote	100–50	0.0–3.5; 0.8	0.0–3.8; 1.4	0.0–1.7; 0.6	0.0–3.4; 1.3
	Magnetite	100–50	0.0–1.9; 1.0	0.0–2.7; 1.1	0.0–4.8; 3.1	0.6–2.7; 1.7
	Biotite	100–50	0.0–1.1; 0.6	0.0–1.1; 0.2	0.0–0.6; 0.1	0.0–0.7; 0.2
		50–10	1.2–8.2; 4.2	1.6–5.7; 3.8	1.3–4.6; 2.4	3.2–4.1; 3.6
	Zircon	100–50	0.0–1.5; 0.6	0.0–1.4; 0.4	0.0–2.8; 0.8	0.0–0.7; 0.2
	Pyroxenes	100–50	0.0–1.2; 0.2	0.0–0.6; 0.2	0.0–0.6; 0.3	0.0–0.9; 0.2
	Chlorite	100–50	0.0–0.8; 0.3	single	0.0–0.6; 0.2	single
		50–10	0.0–3.0; 1.3	0.6–6.5; 2.6	0.0–1.8; 0.8	1.2–4.9; 3.1
	Garnet	100–50	0.0–1.3; 0.5	0.0–1.4; 0.3	none	0.0–0.5; 0.2
	Apatite	100–50	single	none	none	none
	Rutile	100–50	single	none	none	none
	Iron hydroxides	100–50	0.0–0.6; 0.1	0.0–0.5; 0.1	0.0–0.3; 0.1	0.0–0.3; 0.1
	Charcoal	100–50	0.5–1.5; 0.9	0.0–0.6; 0.5	0.0–11.7; 3.0	0.0–0.3; 0.1
		50–10	0.6–18.4; 6.7	1.0–4.5; 2.8	1.6–18.4; 7.7	0.0–3.5; 1.8

* Sampling interval bottom-up.

** Minimum and maximum values; mean.

Radiocarbon dating was completed in the MPI SB RAS radiocarbon laboratory (Yakutsk) using liquid scintillation counting on the Quantulus 1220 spectrometer-radiometer. Radiocarbon date calibration was completed using the OxCal 4.3 program for a 95 % level of significance [*Bronk, 2009*]. A portion of the cited dates, which had been obtained by predecessors before the mid-1990s, was published earlier without calibration. Consequently, for ease of interpretation all such dates were also calibrated and rewritten using calendar age. Radiocarbon dates are shown in Table 3.

Table 3. **Radiocarbon dates of the deposits in the 18-25-meter (Kerdyom) terrace of the Lena River in the Peschanaya Gora outcrop (Central Yakutia)**

Unit number	Dating laboratory number	Height from baseflow edge of Lena River, m	Deposit type, dated material	^{14}C age, y.a.	Calendar age*, y.a.	Cited reference
IVc	MPI-120	24.0	Paleosol, peat	6400 ± 300	7860–6650	Author's details
	MPI-119	23.5	Same	9500 ± 350	12 030–9890	Same
	MPI-118	23.0	Paleosol, shrub branches	6560 ± 350	8060–6720	Same
	GIN-2462	22.6	Paleosol, peat	7920 ± 60	8990–8600	[*Alekseev et al., 1984, 1990*]
	MPI-121	22.5	Same	8280 ± 250	9890–8580	Author's details
IIIb	GIN-2461	17.0	Same	11 850 ± 150	14 070–13 400	[*Kamaletdinov, Minuk, 1991*]
IIIa	MPI-760	11.0	Same	14 000 ± 500	18 330–15 680	[*Alekseev et al., 1984, 1990*]
	MPI-901	10.0	Paleosol, peat	14 450 ± 320	18 390–16 700	[*Kamaletdinov, Minuk, 1991*]
IIa	MPI-759	5.0	Alluvial vegetation detritus	17 200 ± 500	22 100–19 600	[*Alekseev et al., 1984, 1990*]

* Interval with $p > 94.9$ % level of significance.

Stratification and lamination analysis of sediments was completed with consideration of the modern understanding of aeolian deposition mechanisms in cold regions, which were examined in detail in the works of R.E. Hunter and his followers [*Hunter, 1977; Schwan, 1986, 1988; Kasse, 2002; Brookfield, 2011; Zieliński et al., 2015; Derbyshire, Owen, 2017; Kasse, Aalbersberg, 2019*].

A large variety of geometric and genetic types of stratification and lamination of cold region dune deposits has been described to this day. Some of them are seen in both aeolian and alluvial deposits. However, there are specific types of lamination that are typical only for aeolian sands. Among them are *translatent climbing ripple lamination*, *grain-fall lamination* and *sandflow lamination*, which are typical for the steep leeward dune slope facies [*Hunter, 1977; Brookfield, 2011*]. Some aeolian and alluvio-aeolian deposit facies demonstrate a wide distribution of *adhesion lamination*, the formation of which is related to aeolian deposition onto a humid sedimentation surface. *Planebed*, *crinkly parallel* types, including *adhesion ripple lamination* and others, are common among adhesive structures [*Hunter, 1977; Brookfield, 2011; Caputo, 2020*].

Modern aeolian deposits of cold regions frequently have interbedded snow and ice layers which are buried under layers of sand and dust. Such deposits are described in modern Antarctic dunes, in Alaska within the Kobuk dune massif, and are called *niveo-aeolian* [*Cailleux, 1974; Calkin, Rutford, 1974; Koster, Dijkmans, 1988; Brookfield, 2011*]. Numerous signs of syngenetic freezing and subsequent melting were identified in European, Canadian, and Alaskan cover aeolian deposits which had formed at the end of the Late Neopleistocene in the interval of 14.0–12.5 ka [*Koster, Dijkmans, 1988; Kasse, 2002; Brookfield, 2011; Zieliński et al., 2015; Derbyshire, Owen, 2017; Kasse, Aalbersberg, 2019*]. Structures related to the melting of buried snow and ice are called *denivation structures* and play a very significant role in facies analysis of aeolian deposits of cold regions [*Dijkmans et al., 1986; Koster, Dijkmans, 1988; Brookfield, 2011*].

Structure and facies composition of the key outcrop Peschanaya Gora

The Peschanaya Gora outcrop is located on the right bank of the Lena River, 60 km upstream of the Aldan River mouth and 14 km northeast of the small town of Grafskiy Bereg. Here, in the river cliff of the 18–25 m (Kerdyom) terrace (approximately 7 km long), the D'olkuminskaya Series structure is exposed (Fig. 3). The surface of the terrace is covered with parallel rows of U-shaped dunes (Fig. 2, *a*) with a southeast axis orientation (110–130° azimuth). The length of individual dunes varies from 500 m to 3 km, their width varies from 50 to 200 m, the maximum height of the dune brinks above the interdune basins is 5–10 m. A pine forest covers the dune brinks, and groups of birches, creeping shrub-sedge thickets, meadows, swamps, and small peat bogs and lakes are common in the interdune depressions. In the north part of the outcrop (62°88.21′ N, 129°80.68′ E), from the Lena River baseflow level up, the following stratigraphic units were highlighted in the R-537 section (Fig. 4).

Unit Ia (0.0–2.45 m) is composed of horizontally interlayering series of gravelly coarse sands, fine sands, and loamy sands with a mix of pebbles of local (limestone, dolomite) and distant transportation (gneisses, granitoids, quartzites, vulcanites, etc.). The color of the sediments varies from light-yellow to reddish-brown, occasionally intensely ochre. There are bright ochre-colored sand-loam crusts and lenses

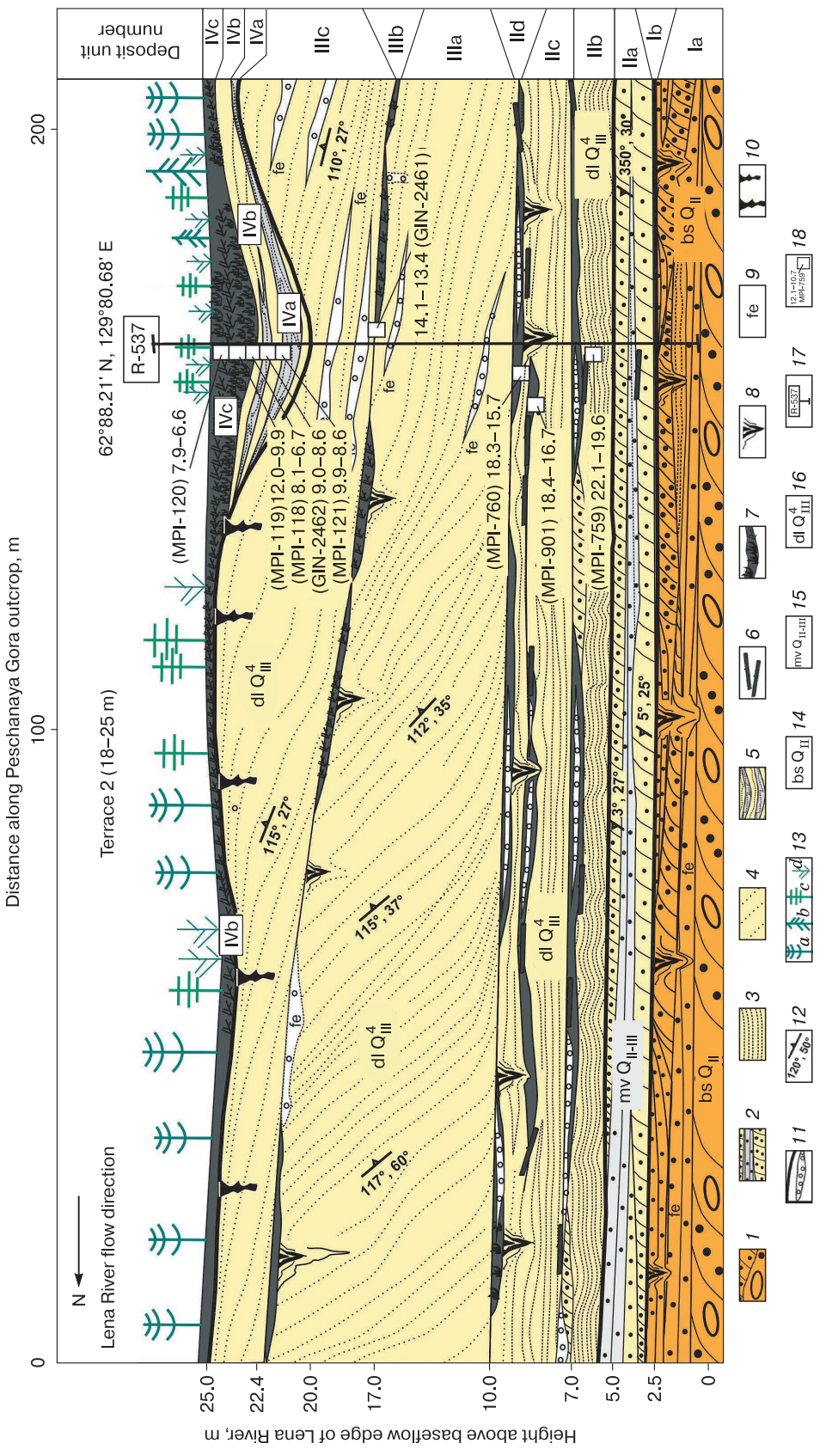

Fig. 4. Section of 18–25-meter Lena River terrace in the Peschanaya Gora outcrop (Central Yakutia).

1 – planar stratification of ochre sands with gravel and pebble with planar and oblique lamination; *2* – planar stratification of sands and dusty loamy sand with parallel, lens-like, and oblique lamination; *3* – planar interlayering of ochre sands and loamy sands with translatent climbing ripple stratification, adhesion and niveo-aeolian types of lamination, denivation structures, deflational interlayers of fine gravel; *4* – cross-bedded stratification of light sands with steep inclined grain-fall lamination of the dune slip face, translatent climbing ripple lamination, parallel lamination; *5* – interlayering of light sands of grey gleyed loamy sands with intensely deformed lamination and ambiguous lamination; *6* – driftwood; *7* – peat bogs and paleosol fragments; *8* – sandy wedges and veins; *9* – intense iron hydroxide colouration; *10* – humus nodules and veins; *11* – structural nonconformities and deflation; *12* – strike azimuth and dip angle of layers; *13* – vegetation (*a* – pine, *b* – larch, *c* – birch, *d* – willow); *14–16* – series designations in accordance with [*Kamaletdinov, Minuk, 1991*]: *14* – Bestyakh; *15* – Mavrin; *16* – D'oluminskaya; *17* – key clearing in which granulometric and mineralogical sampling was completed; *18* – radiocarbon dates in calibrated k.a. and their laboratory numbers.

everywhere which are densely cemented by epigenetic iron hydroxides and carbonates. The bottom of the unit is not outcropped and is located below the Lena River level. The top of the unit is weakly wavy and outcrops only during periods of severe baseflow.

The granulometric composition of the unit changes abruptly from layer to layer, indicating frequent changes in the energy of the flow, which is typical for aqueous conditions of particle transport and deposition. The mean grain size varies from 55 μm (dusty sand interlayers) to 460 μm (coarse sand layers with a mix of fine gravel). Overall, the average composition of the unit (8 samples) is indicative of moderate sorting and a symmetric normal distribution of particles: the mean grain size (x, μm) is 316.8 ± 64.9, the sorting coefficient (σ) is 2.03 ± 0.16, skewness (α) is 0.04 ± 0.10, excess kurtosis (τ) is 1.10 ± 0.18.

The mineralogical composition of the sand fraction (100–50 μm) of unit Ia (the average of nine samples) is represented by quartz (39.9 %), feldspar (28.1 %), carbonates (20.3 %), amphiboles (7.4 %), and magnetite (1 %).

The unit has planebed stratification composed of interchanging steady, thin (5–10 cm) sandy series with horizontal and oblique lamination typical for aquatic dunes and riffle facies [*Botvinkina, 1962; Kutyrev, 1968*]. The thickness of the elementary laminae in the oblique series is 1–3 mm, the north strike has a 25–30° dip, and its orientation matches the modern flow of the Lena River. The bottom portions of the elementary laminae are substantially enriched by large and heavy fractions. Series with horizontal lamination are composed of thin (1–5 mm) interchanging layers of light medium-grain sand and grey dusty loamy sand with a mix of fine alluvial organic detritus. Individual layers show small signs of water ripples.

Unit Ib (2.45–2.50 m) is a paleosol composed of ochre-coloured loamy sand with thin lenses (3–4 cm) of humified organic detritus and a mix of small charcoal pieces. The mean grain size (x, μm) is 56.2 ± 1.1, the sorting coefficient (σ) is 4.43 ± 0.8, skewness (α) is –0.25 ± 0.15, kurtosis is (τ) 0.85 ± 0.03. This indicates very poor sorting and a very platykurtic distribution with tails of fine fractions.

The stratification of unit Ib is gently wavy, the lamination is thin parallel. The top of the unit is sporadically disturbed by secondary vertical sandy veins and small wedges 10–15 cm thick, which extend up to 0.5–1.0 m deep into underlying deposits. The distance between neighboring wedges is 4–6 m. The lateral edges of the wedges are abrupt, deformations are absent in enveloping deposits.

Thus, the features of the structure of units Ia and Ib allow to relate them to a full alluvial cycle, the bottom part of which has channel facies (unit Ia), while the top is marked by floodplain facies (unit Ib) with paleosols and secondary sandy wedges of subaerial genesis.

Unit IIa (2.5–5.0 m) is composed of interchanging oblique light sands (5–10 cm) and grey loamy sands (3–10 cm) with thin parallel lamination. The oblique lamination is composed of interchanging elementary laminae from 1 to 10 mm thick, with a strike in the direction of the modern flow of the Lena River (north) and a 25–30° dip. The elementary laminae clearly differ from one another in color and granulometric and mineralogical composition. Dark laminae are enriched by heavy minerals, light laminae show a higher content of mica and quartz. The unit top shows evidence of ripple marks, alluvial organic detritus lenses, small charcoal pieces, thin interlayers of fine gravel (1–3 mm).

Unit IIb (5.0–7.0 m) is composed of well-sorted light sands with thin (0.5–2.0 mm) systematic horizontal and wavy colmatage interlayers of dark loamy sands which repeat every 2–5 cm. The step between adjacent interlayers is maintained at a long horizontal distance (3–5 m or more), the bends of each interlayer repeat the previous one. The top portion of the unit shows interlayers (1–3 cm) of large-grain, loose, gravelly quartz sand with a mix of humified organic detritus and small charcoal pieces (Fig. 5, *b*).

The granulometric composition (two samples) of unit IIb deposits indicates moderate sorting and a flat symmetric distribution: the mean grain size (x, μm) is 253.9 ± 10.9, the sorting coefficient (σ) is 1.84 ± 0.16, skewness (α) is –0.06 ± 0.02, kurtosis (τ) is 0.82 ± 0.06. Coarsening of the granulometric composition is seen inside the layers, upward from the bottom to the top (inverse grading).

Parallel wavy adhesion lamination is typical for unit IIb (Fig. 5, *e*). The distance between the interlayers is not continuous and changes from several millimeters to 3–4 cm. Each of the interlayers is ferruginated to a different extent. In some parts the thickness of the interlayers increases to 2–4 mm. Such structure types are called adhesive climbing ripple lamination, which forms from aeolian deposition of sand grains onto a humid sedimentation surface [*Huissteden et al., 2000; Brookfield, 2011; Caputo, 2020*]. Some colmatage interlayers are made more complex by vertical micro-wedge-like apophyses up to 1–2 cm in size, the origin of which most researchers relate to the melting of niveo-aoelian deposits and infiltration by surface waters [*Huissteden et al., 2000*].

Unit IIc (7.0–9.85 m) differs from the underlying unit in only one sedimentational structure type. Here, colmatage interlayers become rather thin, straight, and difficult to tell apart. The distance between neighboring interlayers becomes more steady, and the structure itself more uniform (Fig. 5, *b*). Unlike the underlying unit IIb, the colmatage interlayers are composed not of silty material, but of fine magnetite grains. This type of structure forms under the condition of sand particle deposition onto a dry surface and is called translatent climbing ripple lami-

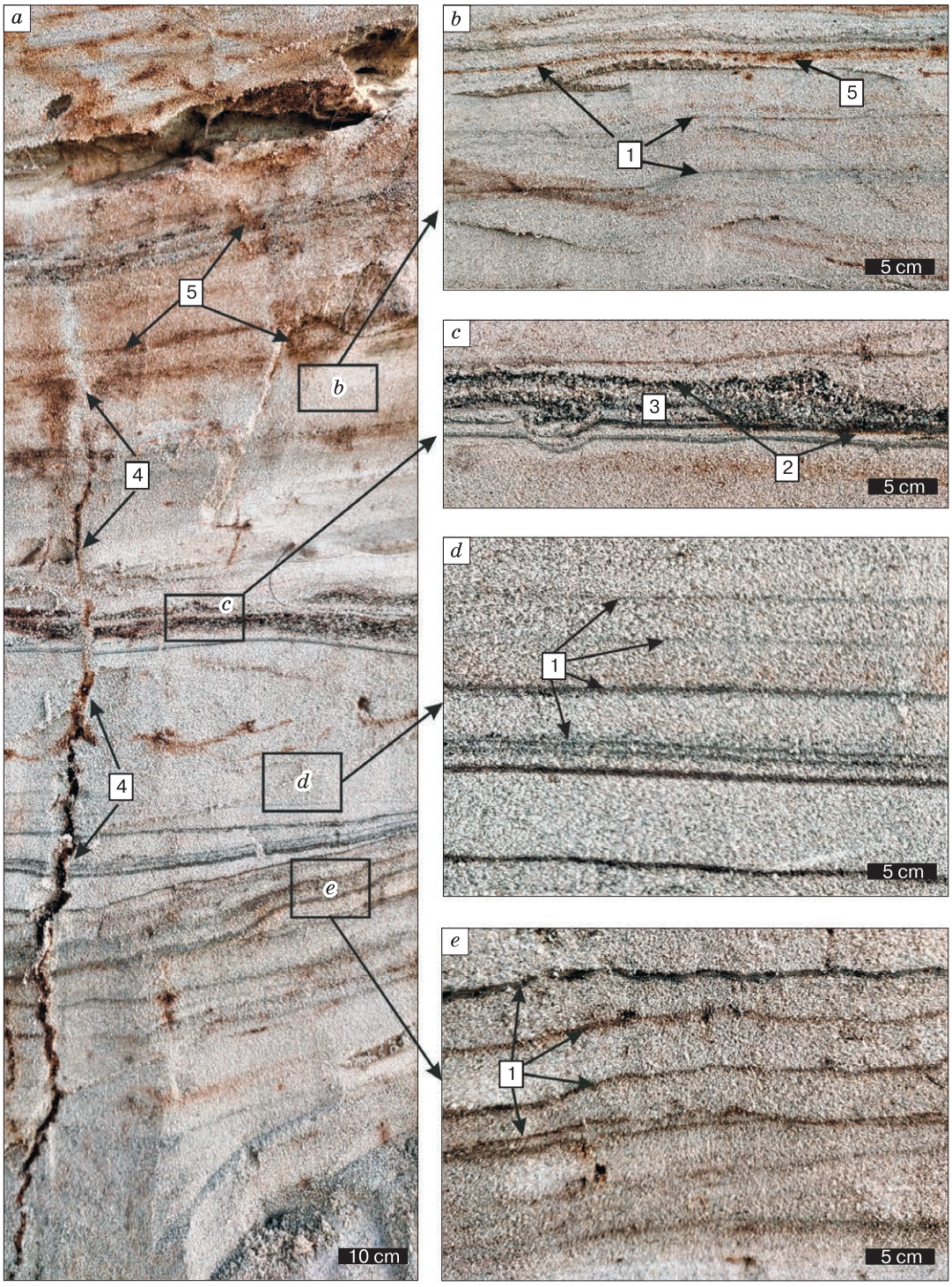

Fig. 5. Some types of adhesion lamination of the D'olkuminskaya Series in the Peschnaya Gora outcrop.

Units IIb, IIc (6.0–8.0 m): *a* – overall appearance; *b* – wavy adhesion climbing ripple lamination; *c* – deflation horizon with paleosol; *d* – parallel planebed adhesion lamination; *e* – wavy-crinkly stratification and adhesion lamination. 1 – elementary sedimentation surfaces; 2 – humified sand (paleosol); 3 – large sand with fine gravel; 4 – epigenetic fracture of vertical groundwater infiltration; 5 – post-sedimentational ochre striation. A.A. Galanin's photo from September, 2020.

nation [*Hunter, 1977; Huissteden et al., 2000; Boggs, 2009; Brookfield, 2011*].

Unit IId (9.85–10.0 m) is a paleosol which is composed of thin interlayering of large-grain sand and dark humified loamy sand with fine vegetative detritus, alluvial organic matter lenses, and is divided in places by secondary vertical sandy veins and wedges up to 1.5 m deep and up to 0.5 m wide, filled with quartz sand from overlying layers.

The mineralogical composition of the sand fraction (100–50 μm) of units IIb and IIc (the average of eight samples) is represented by quartz (44.2 %), feldspars (36.8 %), carbonates (9.7 %), amphiboles (5.3 %), epidote (1.4 %), and magnetite (1.1 %).

In general, intense diagenetic striation formed by lines, crinkly films and ochre stains (Fig. 5) is typical for units IIb and IIc. Sometimes the striation inherits the sedimentational stratification, but intersects it in most cases. The complex geometry of the striation is clearly related to the uneven upward movement of the bottom of the active layer during syngenetic freezing of the deposits. Numerous intensely ferruginated vertical fractures up to 2–3 cm thick and up to 1.5–2.0 m long (Fig. 5, *a*) are also seen in unit II.

Unit IIIa (10.0–17.0 m) is composed of well-sorted light sands with infrequent interlayers of large-grain quartz sand and thin lenses of fine gravel (2–4 mm). The mean granulometric composition of the unit (two samples) is indicative of moderate sorting and a leptokurtic symmetric distribution: the mean grain size (x, μm) is 298.4 ± 79.5, the sorting coefficient (σ) is 1.70 ± 0.04, skewness (α) is 0.02 ± 0.01, excess kurtosis (τ) is 1.12 ± 0.36. The bottom and top of the unit are abrupt, cut off by the deflation surfaces (Fig. 3, Fig. 6, *a*). The mineralogical composition of the sand fraction (100–50 μm) of unit IIIa (the average of four samples) is represented by quartz (47.4 %), feldspars (35.1 %), carbonates (4.0 %), amphiboles (5.1 %), magnetite (3.1 %), and small charcoal pieces (3.0 %).

The unit is composed of inclined (diagonal) series up to 2–3 m thick with clearly defined grain-fall cross-stratification of the dune slip-facies [*Hunter, 1977*]. The stratification has a southeast strike (112–115° azimuth) with a 35–45° dip, which matches the orientation of the dunes on the surface of the adjoining terrace and is opposite to the modern flow of the Lena River.

The texture is represented by grain-fall lamination [*Hunter, 1977; Brookfield, 2011*]. It is caused by granulometric and mineralogical heterogeneity, as well as the varying density of grain packing in elementary laminae, the thickness of which is 2–4 mm. Some laminae are enriched by humus, fine vegetative detritus, and present as poorly developed paleosols, which are indicative of a short-lived dune slip face fixing by a vegetative cover (Fig. 6, *a–c*). The epigenetic stratification and staining formed by colmatage interlayers and iron hydroxide stains are also indicative of this.

Unit IIIb (17.0–17.4 m) is a deflational surface underlain by dark sand and loamy sand with paleosol fragments. The surface discordantly cuts off the inclined series of the underlying unit (IIIa), has a southeast strike at 10–15°, and is disturbed by vertical sand veins up to 10–15 cm thick and up to 0.5–1.0 m deep. The paleosol is formed by discontinuous thin (0.5–1.0 cm) interlayers and lenses of fine vegetative detritus, small charcoal pieces, thin interlayers of bleached large-grain quartz sand with a mix of fine (2–3 mm) gravel, and abnormally high concentrations of magnetite and zircon in the fine fraction.

The granulometric composition (two samples) indicates moderate sorting. The mean grain size (x) varies from 980 to 317 μm, the sorting coefficient (σ) is 1.71 ± 0.23, skewness (α) is –0.39 ± 0.10, excess kurtosis (τ) is 1.23 ± 0.06. Clearly defined negative skewness, a leptokurtic distribution, and enrichment by the coarse fraction indicate a significant deflation lag.

Unit IIIc (17.4–20.0 m) is composed of well-sorted medium-grain sands with interlayers of large-grain bleached sand and rare inclusions of thin soil-peat interlayers up to 2–4 cm thick. The granulometric composition of the unit (eight samples) indicates moderate sorting, a flat asymmetric distribution with "tails" of fine fractions: the mean grain size (x, μm) is 240.2 ± 17.0, the sorting coefficient (σ) is 1.69 ± 0.06, skewness (α) is –0.16 ± 0.07, kurtosis (τ) is 0.81 ± 0.07. This indicates blowing out of then dusty fraction and enrichment by coarse particles.

The mineralogical composition (the average of six samples) of the sand fraction (100–50 μm) is represented by quartz (50.7 %), feldspars (38.8 %), amphiboles (5.6 %), magnetite (1.7 %), and carbonates (0.9 %).

The structure of unit IIIc is formed by several cross-bedded series divided by deflational surfaces and representing mostly steep leeward dune slope slipfaces and gentle windward slope faces consisting of climbing ripples. Translatent climbing ripple stratification with a southeast strike (110° azimuth) with a 15–25° dip dominates in most series. This strike matches the dune orientation at the surface adjoining the terrace outcrop and is opposite to the modern flow of the Lena River.

Some gently inclined series up to 30–40 cm thick demonstrate thin parallel lamination (Fig. 6, *e*), others show translatent climbing ripple lamination (Fig. 6, *e–g*). A signature feature of the deposits is the presence of bright epigenetic ochre striation.

The top of unit IIIc outcrops onto the modern surface as vegetated U-shaped and longitudinal dunes of southeast orientation. These dunes cover the entire surface of the Kerdyom terrace on the right bank of

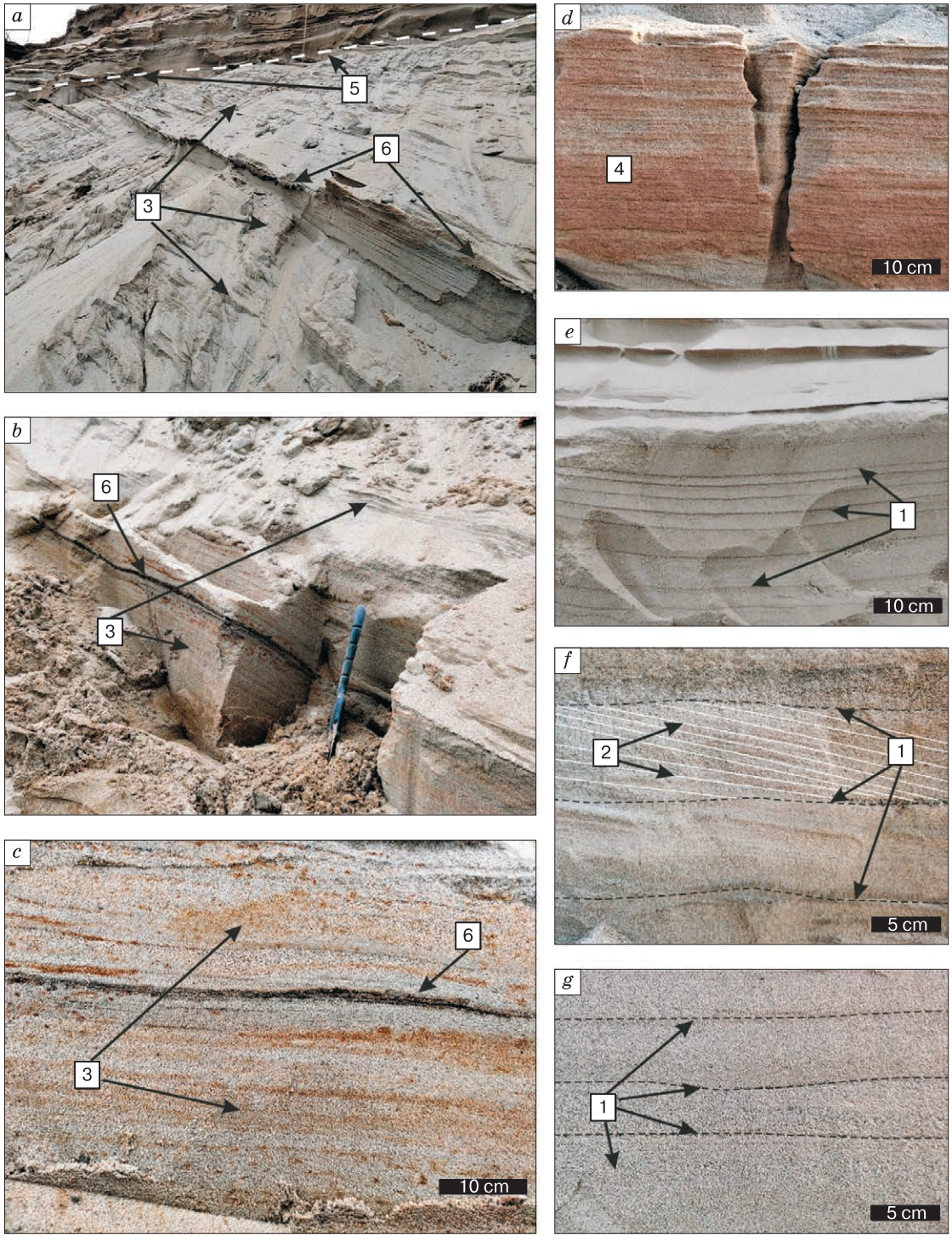

Fig. 6. Some types of D'olkuminskaya Series stratification and lamination in the Peschanaya Gora outcrop.

Units IIIa, IIIb (10.0–20.0 m): *a*, *b* – cross-bedded stratification of the dune slip face facies (unit IIIa); *c* – grain-fall dune slip face lamination facies (unit IIIa); *d* – planar parallel lamination (unit IIIb); *e*–*g* – translatent climbing ripple stratification (unit IIIb). 1 – translatent interlayers composed of magnetite grains; 2 – climbing ripple lamination; 3 – grain-fall dune slip face lamination; 4 – parallel planar lamination; 5 – structural nonconformity (deflation); 6 – paleosol marking a short-term period of dune slip face fixing by vegetation. A.A. Galanin's photo from September, 2020.

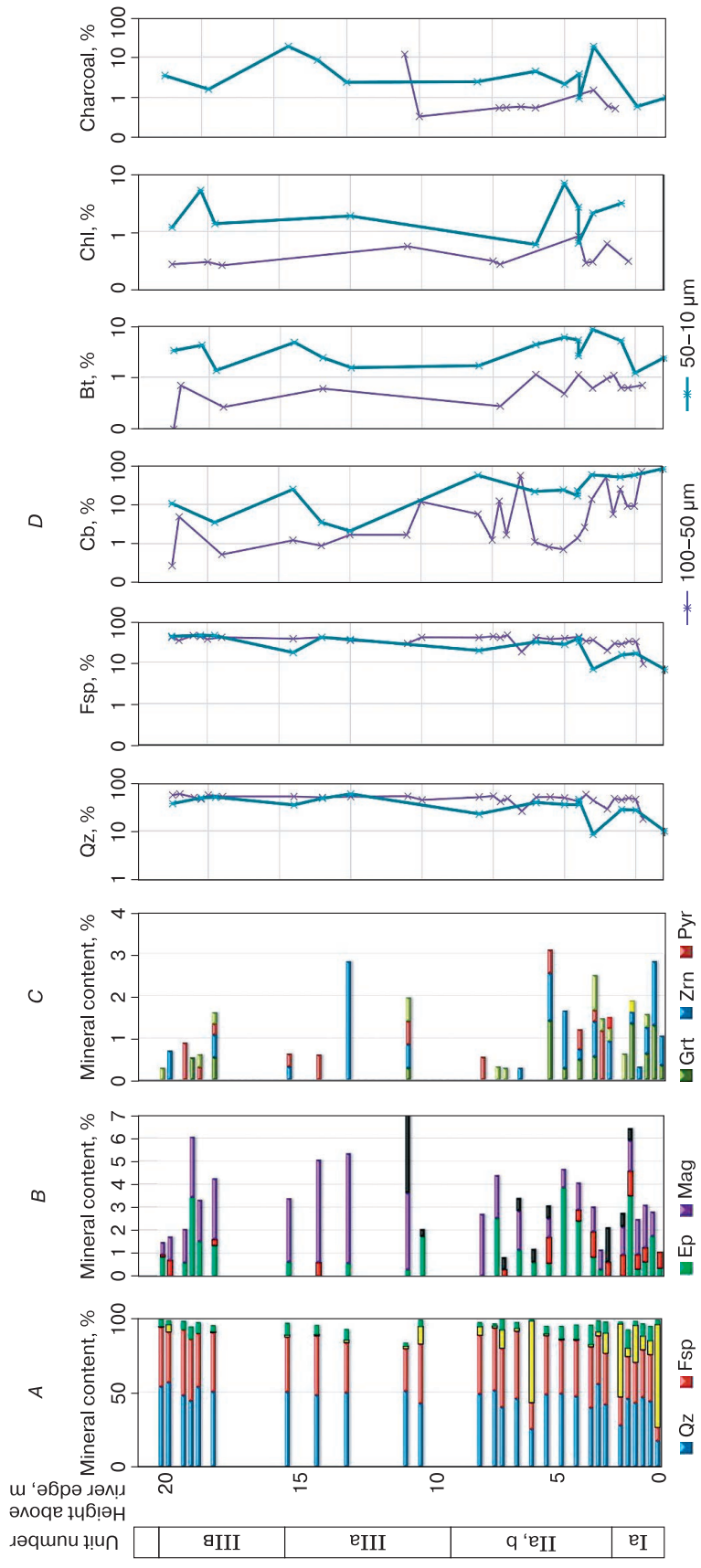

Fig. 7. Mineralogical composition of Peschanaya Gora key section deposits by the R-537 clearing (middle course of the Lena River, Eastern Siberia).

A–C – mineral content of 100–50 µm fraction (*A* – primary, *B* – secondary, *C* – accessory); *D* – mineral content of 100–50 µm and 50–10 µm fractions. Qz – quartz, Fsp – feldspar, Cb – carbonate, Amp – amphibole, Ep – epidote, Bt – biotite, Mag – magnetite, Grt – garnet, Zrn – zircon, Pyr – pyroxene, Chl – chlorite, Rt – rutile, Ap – apatite; charcoal.

the Lena River, from the Suola River mouth to the Aldan River mouth. The dune brinks are divided by gently sloping interdune depressions, which are currently occupied by lakes and swamps. One such paleobasin is exposed by natural erosion in the southern part of the Peschanaya Gora outcrop at the R-537 section (Fig. 4).

Unit IVa (20.0–20.4 m) is composed of interchanging layers (5–10 cm) of well-sorted light sand and interlayers (4–5 cm) of dense bluish-grey gleyed light loam without visible organic matter. The granulometric composition (one sample) of the loam indicates very poor sorting and positive skewness with a modal value bias toward fine fractions: the mean grain size (x, μm) is 44.5, the sorting coefficient (σ) is 4.29, skewness (α) is 0.13, excess kurtosis (τ) is 0.95. The stratification of the deposits is gently wavy, sometimes deformed into microfolds with signs of boudinage.

Apparently, the reason for poor sorting of the deposits is the interchanging lake and aeolian sedimentation regimes under conditions of a small seasonal body of water surrounded by unvegetated dunes.

Unit IVb (20.4–22.4 m) is composed of interchanging light well-sorted sands with thin interlayers of dark grey fine sands and dusty loamy sands. There are no visible organic remains. The granulometric composition (five samples) is as follows: the mean grain size (x, μm) is 316.9 ± 30.7, the sorting coefficient (σ) is 1.67 ± 0.16, skewness (α) is –0.21 ± 0.07, excess kurtosis (τ) is 1.18 ± 0.15. This indicates moderate sorting and enrichment by large fractions. The stratification is subhorizontal, intensely deformed here and there in the form of traction microfolds, microdiapirs, vertical fractures with a 10–15 cm displacement. Lamination is unclear.

Unlike the underlying unit (IVa), there is coarsening of the granulometric composition from the bottom to the top of the unit (inverse grading). Intense layered coloring of deposits by iron hydroxide is also typical. The top of the unit is abrupt, clear, composed of well-sorted bleached sand.

Unit IVc (22.4–25.0 m) is a dense, dark brown peat bog with numerous large fragments of moss and subshrub vegetation, wood fragments. It delaminates well into horizontal plates, has interlayers of bleached coarse sand in the bottom portion. Sedge peat with a mix of quartz sand and numerous small (1–4 mm) mollusk shells dominates the bottom portion. The top portion is a moss-subshrub peat with a mix of wood fragments. Apparently, the peat bog formed by way of a small lake overgrowing.

Mineralogical composition of aeolian sand covers

The mineralogical composition and features of mineral distribution in the section are important facies attributes of aeolian deposits in the cryolithozone [*Pewe, Journaux, 1983; Dijkmans et al., 1986, 1988*].

The main minerals in both studied fractions (100–50 and 50–10 μm) of the deposits of the Peschanaya Gora outcrop 25-meter Kerdyom terrace are quartz, feldspars, calcium carbonates, amphiboles, and magnetite (Table 2, Fig. 7).

In the 100–50 μm fraction the total composition of the main minerals exceeds 95 %. The mean quartz content increases up the section approximately by 10 % from 39.9 % in unit Ia to 50.7 % in unit IIIc. The mean feldspar content also increases from 28.1 % to 38.8 %. Carbonate mineral distribution is quite uneven. Their maximum content (20.3 %) is concentrated in the secondary thin iron-carbonate crusts (calcretes) of unit Ia, and in some individual samples of this unit the carbonate mineral content reaches 68 %. The minimum contents (0.9 %) are found in unit IIIb. Amphibole content decreases insignificantly up the section from 7.4 % in unit Ia to 5.4 % in unit IIIc.

Magnetite, biotite, and epidote are always present among secondary and accessory mineral groups in the 100–50 μm fraction. Most samples also have zircon, garnet, chlorite, grains of hard coal. Some samples show individual grains of pyroxenes, apatite, rutile, ochre-colored iron hydroxides. A characteristic feature is a significant (threefold) increase in heavy fraction and magnetite content up the section. Thus, the gravel-pebble-sand deposits of unit Ia have a mean magnetite content of approximately 1 %, and it reaches 3.1 and 1.7 % in units IIIa and IIIc, respectively, while in some samples from the top of unit IIIa the magnetite concentration reaches 4.8 %. At the same time, some of the higher concentrations of zircon (2.8 %) and micro particles of charcoals (11.7 %) are seen here.

From the bottom to the top of section the variation of primary and secondary minerals is even more contrasting in the 50–10 μm fraction, but, overall, repeats their distribution in the 100–50 μm fraction. Thus, the mean quartz content increases from 18.8 % in unit Ia to 41.4 % in unit IIIc. Feldspar content increases from 11.1 % in unit Ia to 43.0 % in unit IIIc. Carbonate content decreases from 46.6 % in unit Ia to 5.3 % in unit IIIc. Variations of accessory minerals in this fraction are significantly smaller, but are 2–3 times higher overall in comparison to the 100–50 μm fraction. The concentration of readily solvable carbonates in some samples of unit Ia reaches 70–80 %. The carbonates are represented both by whole grains and by fine crystalline aggregates coating the grains of other minerals as a crust. The minerals dissolve completely in a 5 % HCl solution.

The lithological source of aeolian sand cover formation

Based on primary mineral proportions, all studied samples of D'olkuminskaya Series sand covers from the Peschanaya Gora outcrop are oligomictic

arkose-quartz sands. The same series' sands, studied by the author earlier [*Galanin et al., 2018*] in the basin of the lower course of the Vilyuy River, differ significantly in their mineralogical composition. The series is composed of monomictic quartz sands with an 80–95 % quartz content and small amounts of feldspars (<9 %) on the Kysyl-Syr portion of the outcrop. Furthermore, significant concentrations of magnetites, zircons, and secondary carbonates have not been identified here. At the same time, accessory mineral content is significantly higher, and their composition is more diverse (garnet, epidote, hornblende, pyroxene, ilmenite, leucoxene, agate, chalcedony, etc.). Such significant differences can be explained by different origins of feeding sources of Quaternary alluvium in the basins of the Vilyuy and Lena rivers.

Indeed, the identified differences in the mineralogical composition of the D'olkuminskaya Series in the Peschanaya Gora (middle course of the Lena River) and Kysyl-Syr (lower course of the Vilyuy River) outcrops agree with the mineralogical zoning map of the Vilyuy syneclise of A.G. Kossovskaya [*1962*]. The Peschanaya Gora outcrop is linked to the Yakut-Sinskiy garnet-zircon sub-province, the formation of which is related to the denudation of the crystalline base rocks within the Aldan and Stanovoy highlands. A direct feeding source of Quaternary deposits (including alluvium) here is the Jurassic greywacke-quartz sandstones with a quartz content of 50–66 %. Their characteristic feature is the presence of zircon and high concentrations of magnetite, which explains the constant presence of these minerals in the deposits of Peschanaya Gora.

The Kysyl-Syr outcrop is linked to the Vilyuy-Tyungsk epidote-ilmenite-amphibole mineralogical province, the feeding areas of which are the Archean-Proterozoic crystalline rocks of the Patomsk Highland [*Kossovskaya, 1962*]. A direct source of Quaternary alluvium and D'olkuminskaya Series sands in the basin of the lower course of the Vilyuy River is the Late Cretaceous quartz-oligomictic sandstones which compose long areas of river cliffs. They are weakly cemented and break easily, forming vast quartz-kaolinite weathering rinds on gently sloping drainage divides. Cretaceous sandstones are enriched by quartz (65–80 %) and are extremely lacking in heavy minerals. This explains the high quartz content (80–95 %) and rather low magnetite content in the D'olkuminskaya Series deposits of the Kysyl-Syr outcrop. Among secondary minerals epidote, amphiboles, kaolinite, opal are always present in this mineralogical province [*Kossovskaya, 1962*].

Sand and loess-ice (Yedoma) covers – two lithological derivatives of Quaternary alluvium

T.L. Pewe and A. Journaux's work [*Pewe, Journaux, 1983*] is dedicated to the study of the mineralogical composition of cover loess-ice and sand deposits of the high terraces of the Lena River. The authors studied the mineralogical composition of 28 samples collected within the Lena-Amga interfluve. It was established that the primary components of both sand and loess-ice covers in Central Yakutia are quartz, mica, and feldspars, which, together, total 80–90 %. There are calcium carbonates, the content of which reaches 7.6 % in all the samples, with the exception of modern alluvium. Amphiboles and epidote dominate in the heavy fraction, small amounts of pyroxenes, titanite, garnet, zircon are present, rutile, tourmaline, kaynite, monazite, anatase, and others are occasionally seen. Overall, researchers conclude that the loess-ice (Yedoma) and sand covers (D'olkuminskaya Series) of the Lena-Amga interfluve belong to aeolian deposits and are two granulometric derivatives – the products of wind reworking of the Lena River's Quaternary alluvium [*Pewe, Journaux, 1983*].

A clear signature of aeolian genesis of the cover sands is the high concentration of magnetite and other heavy minerals, as well as secondary, readily solvable carbonates. The latter can be found in the form of carbonate-ferruginous films (carbonate mycelium) and are called calcretes [*Dijkmans et al., 1986, 1988*]. Constant presence of calcretes and iron hydroxides is typical for the Late Quaternary aeolian sands of the Kobuk dune massif in the Alaskan northwest and is an important genetic attribute which indicates hyperarid deposition conditions [*Dijkmans et al., 1986, 1988*].

The aforementioned mineralogical attributes are typical for units IIb, IIc, IIIa, IIIc of the Peschanaya Gora outcrop (Table 2). In comparison to the underlying alluvium (unit Ia) they show a threefold increase in magnetite content. The deflational lag (unit IIIb), which divides the lower (unit IIIa) and upper (unit IIIc) parts of the D'olkuminskaya Series sands, is most enriched by zircon (2.8 %), magnetite (4.8 %), and small pieces of charcoal (11.7 %) at the 17.0–17.4 m interval from the water edge of the Lena River. A high concentration of the heavy fraction at the unit borders may be related to a significant deflation lag and accumulation of wind eluvium.

A constant presence of trivalent iron hydroxides (limonite, ochre) which create an epigenetic striation of a bright ochre color, which indicates good aeration and alkaline sedimentation conditions, is typical for D'olkuminskaya Series deposits. The light and, in some spots, ochre color of the deposits, the lack of reduction minerals (vivianite) are additional criteria for subaerial origin of the deposits.

Stratification and lamination of aeolian sand cover

The structure of aeolian sand cover forms under the influence of numerous factors: wind speed, presence and volume of source loamy sandy material, strike and extent of humidification of the surface at

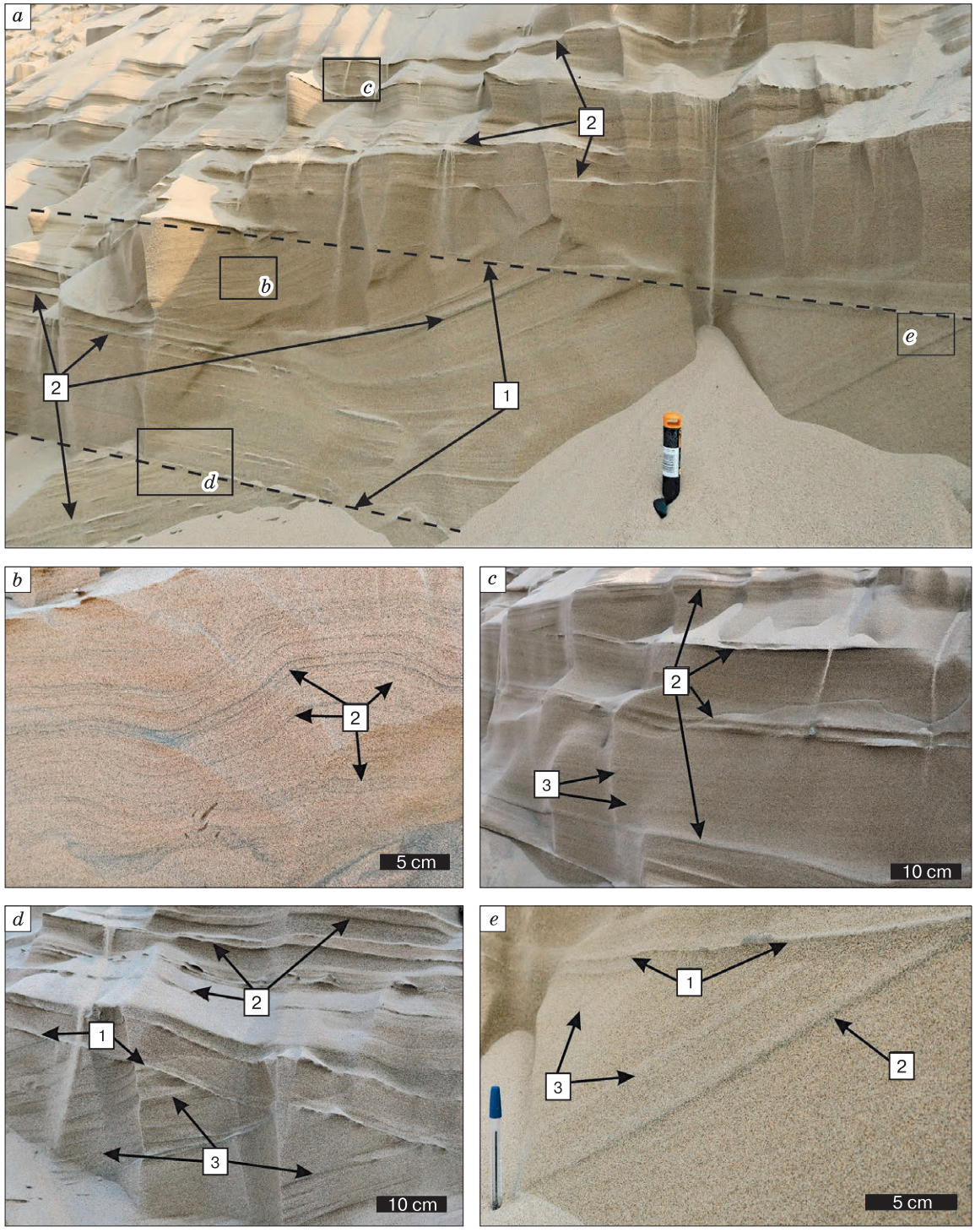

Fig. 8. Cross-bedded structure and translatent climbing ripple lamination in D'olkuminskaya Series dune deposits (Ust'-Buotama outcrop of the 75–100-meter terrace (Bestyakh) of the Lena River, lower portion).

a – overall appearance of the unit with a clear cross-bedded structure and translatent climbing ripple lamination; *b*–*e* – enlarged fragments of individual series with different geometric characteristics (dip angles) of stratification and lamination. 1 – abrupt deflation borders between sandy series; 2 – translatent interlayers (pseudo-stratification) composed of magnetite grains; 3 – elementary translatent climbing ripple lamination laminae. A.A. Galanin's photo from August, 2020.

the moment of sedimentation, temperature of the deposits, presence of snow cover, vegetation type. According to R.E. Hunter [*1977*] and his followers, the structure of aeolian sand cover differs drastically from other genetic types of deposits, including alluvium. The structure of aeolian sand cover is characterized by several key types of stratification and lamination.

Planebed stratification and *planebed lamination* [*Hunter, 1977; Brookfield, 2011*] form simultaneously in areas of more intense wind load. Such conditions are not favorable for aeolian ripple formation, and accumulation is very slow. The deposits have a coarsened composition and are characterized by dense packing of sand grains (minimal porosity). These stratification and lamination types are more typical for aeolian sand covers of small thickness, gently sloping windward dune slopes, and deflation basins. In the D'olkuminskaya Series deposits planed parallel lamination series are usually found on the borders of large cross-bedded units, as well as near the top.

Cross-bedded stratification [*Hunter, 1977; Brookfield, 2011*] is represented by large units from 1 to 6–10 m thick, separated from one another by structural nonconformities – deflation surfaces (Fig. 6, *a* and Fig. 8, *a*), also called *deflation lags* by Western authors [*Waters et al., 1999; Brookfield, 2011; Derbyshire, Owen, 2017*]. Each elementary unit is different in the nature and incline orientation of the bottom and top, the thickness of the elementary laminae, the amplitude and nature of the inclination. Essentially, each unit is a particular fragment of the fossil dune. Each unit forms owing to continuous movement of dunes across the dune field, as a result of which each consecutive dune creeps over and/or partially cuts off the previous ones. The individual segments of the deflational surfaces are often enriched by wind eluvium – large and heavy fractions sometimes containing fine gravel, ventifacts, vegetation detritus, small charcoal pieces, bones of small animals, remains of thin soil-divot horizons. Deflational surfaces are usually flat, sometimes gently sloping, nonconformingly cut off the inner stratification of elementary units in their top and bottom.

Cross-bedded mesostratification (Fig. 6, *b*) has a principally different originating mechanism. In aeolian deposits it is typical for the slip face facies and is called *grain-fall cross-stratification* or *dune-slipfacies cross-bedding* [*Hunter, 1977; Kasse, Aalbersberg, 2019*]. The formation of this facies occurs as a result of systematic falling (rolling down) of sand grains from the dune brink and their deposition on the leeward dune-slope or slip face. Fixing of falling grains on the steep leeward slope occurs by way of rather weak cohesion with the bedding surface, which leads to the formation of a thin and loose, barely noticeable *grain-fall lamination* [*Hunter, 1977; Brookfield, 2011*]. In the longitudinal section of a parabolic dune the elementary laminae dip at 35–45° in the direction of its movement.

Sandflow lamination is also common within the dune slip face facies [*Hunter, 1977; Brookfield, 2011*]. It forms as a result of periodic gravitational slumping of small portions of sand down from the slip face brink, as a result of which fan-shaped cones form at the foot of the lee-slope. Aeolian dune deposits with cross-bedded stratification, including the Peschanaya Gora outcrop, are often incorrectly interpreted by some researchers as oblique alluvial stratification [*Bolshiyanov et al., 2016; Pravkin et al., 2018*]. Aside from numerous other differences, aeolian dune cross-bedded stratification has a larger size, comparable with the size of elementary parabolic dunes, the height of which varies from 4 to 8 m in Central Yakutia.

Wavy bedding is widely presented in D'olkuminskaya Series deposits, and forms by way of burial of aeolian ripple marks that migrate across the surface on the border of aeolian units. The length of the ripples usually varies from 20–30 cm to 1–2 m, the height from 2–3 cm to 5–15 cm. An indicator of aeolian genesis of the ripple marks is their distribution not only on gently sloping, but also on steep areas of the dunes, while water-formed ripples are linked only to horizontal areas and are limited to the height of the water surface. Furthermore, the relationship between the length of the ripple and its height in water-formed ripple marks (equal to 15) is always higher than in aeolian ripple marks (9) [*Brookfield, 2011*]. The texture of dune deposits with wavy bedding more often manifests as *ripple foreset cross-lamination* and *ripple-form lamination* [*Hunter, 1977*].

Translatent climbing ripple stratification is a specific genetic structural group which is typical only for aeolian deposit dune facies [*Hunter, 1977; Brookfield, 2011*]. This structure, also known as pseudo-stratification, forms in the process of rather intense aeolian accumulation on gently inclined, predominantly windward dune slopes and horizontal surfaces covered with aeolian ripple marks (Fig. 9).

Aeolian ripple migration across a bedding surface occurs by way of a wind current flow dragging thin parallel laminae on slip face microslopes. This leads to the formation of *climbing ripple lamination*, the elementary laminae of which are parallel to each other and whose strike coincides with the direction of aeolian transfer. The thickness of the laminae usually does not exceed 0.5–3.0 mm, the dip varies from 2–3° to 10–15°. This type of lamination is usually almost unidentifiable on humid outcrop walls and manifests after they dry naturally (Fig. 8, *c–e*).

With a sufficient influx of sandy material and moderate wind loads, the bedding surface continuously moves upward as the ripples move, which leads to the formation of thin translatent interlayers or pseudo-stratification [*Hunter, 1977*]. Its key differ-

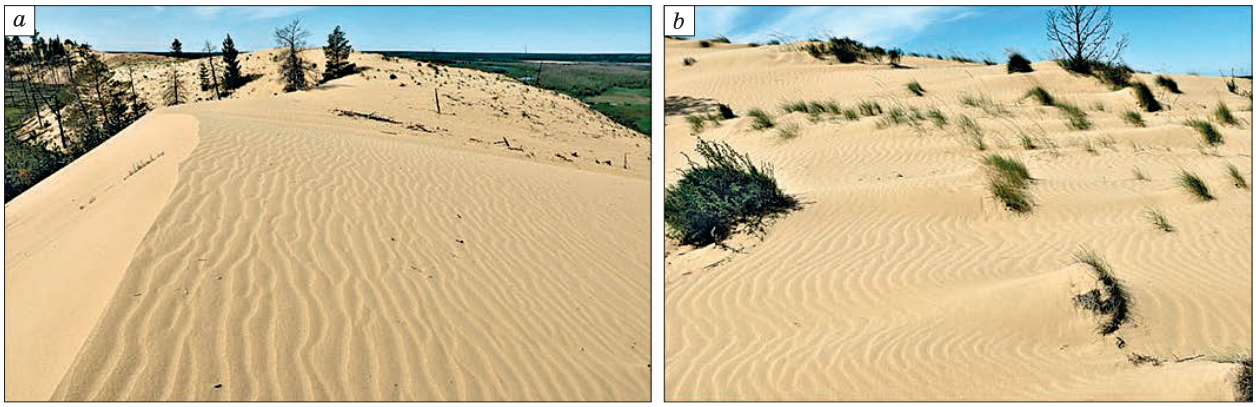

Fig. 9. Climbing aeolian ripple on some elements of the modern dune relief in the basin of the lower course of the Vilyuy River (Central Yakutia).

a – inclined windward slope near the brink of the parabolic dune; *b* – on the subhorizontal surface, partially fixed by cereal tussocks. A.A. Galanin's photo from July, 2019.

ence from regular stratification is that translatent interlayers are not sedimentation surfaces, but are pointed toward it at an angle.

The formation of all translatent interlayers in the elementary sand series takes place simultaneously and is linked to the accumulation of heavy minerals in the crests of aeolian ripples. Because of this, the translatent interlayers are usually composed of magnetite and stand out sharply against the light quartz sand in which they are contained (Fig. 8, *e*).

Translatent interlayers are clearly visible in sections, while the lamination of the ripples themselves, which are composed of mineralogically and granulometrically homogenous elementary laminae, is hard to identify. It is necessary to keep in mind that the azimuths and dips of translatent interlayers and lamination are opposite one another. The former is oriented against the wind, and the latter in the direction of the wind.

The identification of translatent climbing ripple lamination and the assessment of its geometry play a defining role in the analysis of facies composition and deposit genesis, the reconstruction of the direction of aeolian transport of material. Contrasting and noticeable translatent interlayers (pseudo-stratification), represented widely in some D'olkuminskaya Series sand units, have been interpreted by many predecessors as regular alluvial stratification [*Map..., 1959; Map..., 1983; Ershov, 1989; Bolshiyanov et al., 2016; Spektor et al., 2016, 2017; Pomortsev et al., 2017; Pravkin et al., 2018*], which has led to an incorrect understanding of the overall structure of the deposits and their facies affiliation alike. The taxonomy and formation mechanisms of translatent climbing ripple stratification and lamination are reviewed in detail in many works [*Hunter, 1977; Brookfield, 2011; Fenton et al., 2013*].

Adhesion stratification and lamination form as a result of adhesion of aeolian particles to humid surfaces [*Kasse, 2002; Zieliński et al., 2015; Kasse, Aalbersberg, 2019*]. Their characteristic feature is contrasting and clearly visible, systematic, thin, crinkly interlayers of dark dust which deposit on dune surfaces while they are humid and there is no deflation. Wide distribution of adhesion structures in sand deposits indicates significant fluctuations in humidification during deposition. The nature of humidification of the sedimentation surface is affected by the frequency and amount of atmospheric precipitation, exposure, depth of permafrost aquitard position, river flood level, etc.

For convenience of facies analysis of aeolian deposits C. Kasse and G. Aalbersberg [*Kasse, 2002; Kasse, Aalbersberg, 2019*] suggested dividing all types of sedimentational aeolian structures into two genetic groups. The first includes structures which form during aeolian sedimentation of particles onto a dry sedimentation surface (dry aeolian lamination). Such structures include grain-fall lamination of dune slip face slopes, some types of translatent climbing ripple lamination, etc. [*Kasse, Aalbersberg, 2019*]. The second group of structures is related to the sedimentation of aeolian particles onto humid and wet surfaces (wet aeolian lamination). It includes different types of adhesion lamination, including *planebed*, *crinkly*, *ripple*, etc. [*Kasse, Aalbersberg, 2019*].

Seasonal humidification dynamics lead to pulsation of aeolian processes and the formation of numerous microfacies environments which manifest in a wide variety of sedimentational structures. Thus, the drying of windward dune slopes always occurs before that of slip face slopes. Consequently, when the former already begin to be actively impacted by wind deflation, the latter remain in a humid state for some

time. In such cases polygenetic types of structures form, for example, *adhesion grain-fall lamination*, etc. [*Kasse, Aalbersberg, 2019*].

Adhesion structures are identified in large amounts in Late Quaternary aeolian and alluvial-aeolian deposits of Eastern Europe (European Sand Belt), the formation of which is linked to an extremely unstable specific regime of periglacial zone rivers and syngenetic aeolian processing of alluvial deposits [*Kasse, 2002; Zieliński et al., 2015; Kasse, Aalbersberg, 2019*]. It has been noted that during cryochrones, under conditions of weak surface runoff and excess fine disperse particle sedimentation, the absence of wood vegetation in valleys, watercourse beds were extremely volatile and constantly shallowed and branched out. Bed and floodplain alluvium facies underwent intense aeolian processing during continuous low-water periods.

Recently, widespread Late Pleistocene and Holocene alluvial-aeolian deposits containing buried Belling-Allered soil horizons (14.0–12.2 ka) have been noted in Western Siberia [*Zykina et al., 2017; Konstantinov et al., 2019*]. It is notable that these soil horizons, which are regional stratigraphic markers, are overlapped by dune deposits of the Younger Dryas.

Seasonal and perennial cyclical stratification of dune deposits is related to significant differences in the rate and mechanism of aeolian sedimentation in warm and cold times of the year, seasonal and quasi-periodic climatic processes. Among these are seasonal freezing-thawing of dune surfaces, snow cover, snowfields, flooding of interdune depressions as a result of fluctuations in the level of supra-permafrost waters, short-term fixing of dune surfaces by vegetation.

In some sections of dune deposits the cyclicality of aeolian sedimentation manifests in the interchange of sand series with various sets of specific types of stratification and lamination. Among them, cryogenic-aeolian and niveo-aeolian stratification typical for dune deposits in cold regions should be noted.

Cryogenic-aeolian seasonal stratification was first described within one of the largest dune massifs of Kobuk (northwestern Alaska) by E.A. Koster and J.W. Dijkmans [*Koster, Dijkmans, 1988*]. As a result of year-round observations of the nature of aeolian deposition it was established that at the beginning of the winter period there is dune surface adfreezing, snow cover formation, and an almost complete termination of deflation and accumulation. During the winter period intense redistribution of the snow cover and its partial sublimation lead to the exposure of significant areas of the dunes. Adhering and adfreezing atmospheric dust deposits onto the dune surface as a thin dusty interlayer.

During the summer period the dune surfaces thaws, aeolian activity intensifies, and the accumulation of a new sand layer occurs. This process repeats year after year and leads to the formation of specific annual cyclicality, which is reasonable to name *cryogenic-aeolian stratification* [*Koster, Dijkmans, 1988*]. Morphologically similar types of cyclical stratification have been noted in the sand dunes of Soviet Central Asia in the works of A.F. Ivchenko (as cited in [*Botvinkina, 1962*]).

The works of N.A. Kulik [*1928*] point to the specific conditions of aeolian deposition in cold regions (Pechorskaya Lowland). The author notes that, unlike deserts in cold and temperate latitudes, here there is a specific mechanism of cryogenic fixing of dune massifs by way of their syngenetic freezing and climbing movement of the active layer bottom syngenetically with aeolian accumulation.

Thin (0.5–1.0 mm) systematic colmatage films of dark dust are found quite often in D'olkuminskaya Series sections (Fig. 10, *a*, *d*) and match descriptions of the cryogenic-aeolian stratification of the Kobuk massif [*Koster, Dijkmans, 1988*]. They also match translatent pseudo-stratification, but, unlike it, are composed not of a heavy (magnetite), but of a thin and light (dusty) fraction and often include a mix of fine vegetation remains, plant seeds, and microcoals. The mineralogical analysis shows that the dust which forms these films is rich in hydrocarbonates and iron hydroxides. Near the dune surface the films gradually oxidize and obtain a bright ochre color.

The films are even, abrupt, but are much less steady and, unlike translatent stratification, often branch out. The distance between neighboring films defines the annual stratification interval of dune sands, which changes from a few millimeters to 10–15 cm and more. The aggregate of the films dividing the broad, light layers is resemblant of the annual growth rings of trees.

Overall, by its formation mechanism the cryogenic-aeolian stratification is related to adhesion stratification. The difference is that the former forms during the cold time of the year, when the dune surface is frozen, and deposition of dusty particles occurs by way of their freezing to the sedimentation surface. The latter forms during the warm time, when the dune surface is melted, deposition occurs by way of adhesion of particles to the humid surface.

Niveo-aeolian seasonal stratification is an important diagnostic indicator of aeolian deposits in cold regions. Its formation relates to the burial of winter snow cover in dune sand fragments and its subsequent recrystallization into thin horizontal schlieren of sedimentary-metamorphic (atmospheric) ice [*Dijkmans et al., 1986, 1988; Koster, Dijkmans, 1988; Brookfield, 2011; Dinwiddie et al., 2012*].

Modern niveo-aeolian formations composed of thin interlayering of sand, loamy sand, and firn (total ice content 40–50 %) were found in the dunes of the dry valley of Victoria in Antarctica [*Cailleux, 1974;*

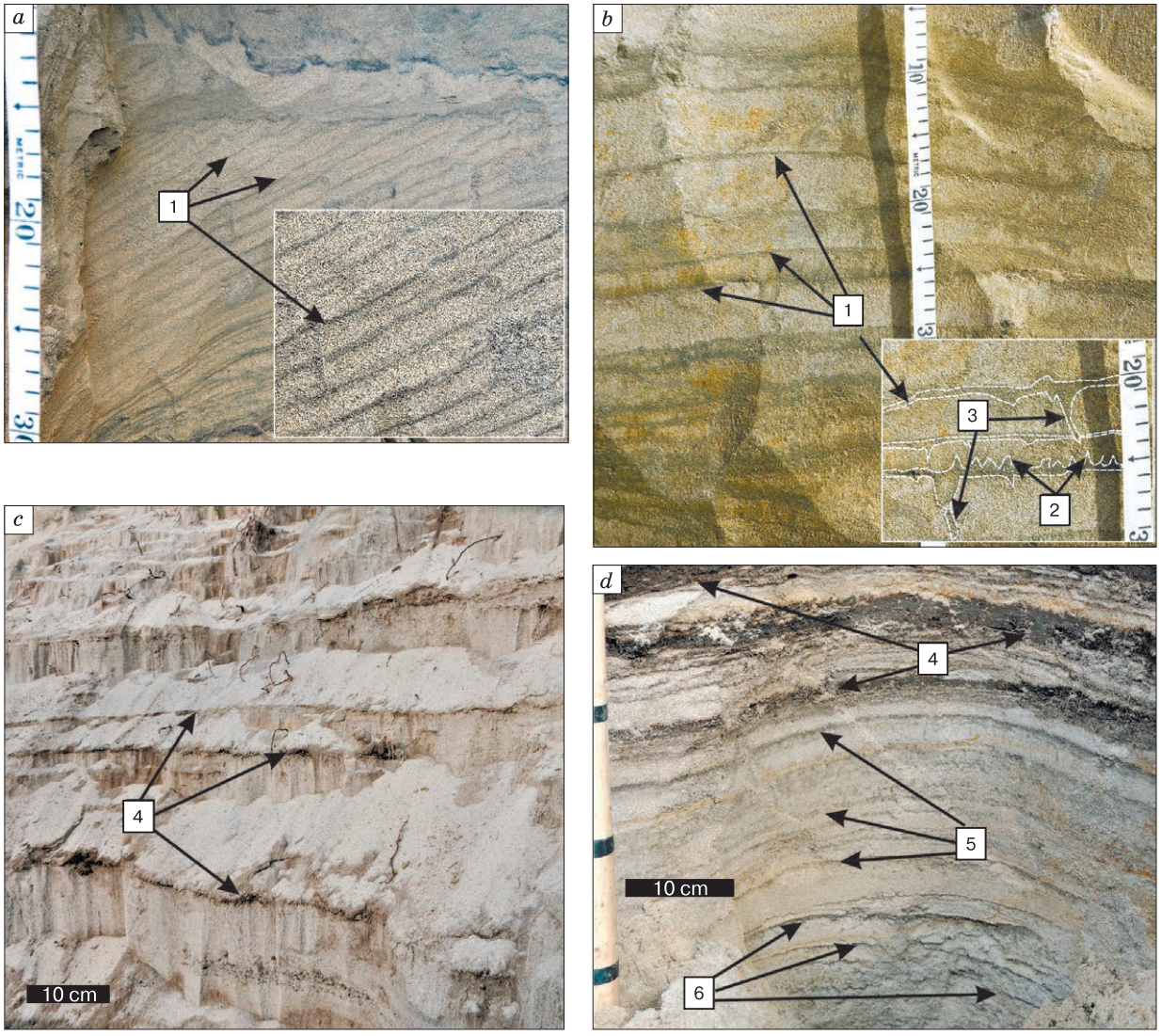

Fig. 10. Some types of cyclical stratification of D'olkuminskaya Series cover sands in key outcrops in Central Yakutia.

a – inclined cryogenic-aeolian; *b* – gently sloping niveo-aeolian; *c* – biogenic; *d* – primary cryogenic-aeolian and biogenic. 1 – inverse denivational silty interlayers; 2 – vertical inverse small wedges and apophyses; 3 – funnels of vertical drainage of meltwaters; 4 – peat-humus interlayers (paleosols); 5 – denivational colmatage interlayers; 6 – syngenetic schlieren and interlayers of fossil depositionally metamorphic ice. A.A. Galanin's photo from 2015–2019.

Calkin, Rutford, 1974; Ayling, McGowan, 2006]. The thickness of individual firn interlayers varies from 1 mm to 4–6 cm, some reach a thickness of 10 cm and more. Systematic burial of the snow cover in sand dune deposits occurs here under conditions of low summer temperatures (near 0 °C and lower) as a result of syngenetic freezing of deposits and continuous upward movement of the bottom of the active layer. Snow cover layers buried in the dune sands subsequently become denser and transform into ground ice shlieren lying either horizontally or at an angle, but parallel to the deposition surfaces.

Primary niveo-aeolian structures are seldom seen in sections in more moderate climates because the seasonal snow cover, including buried snow patches, has enough time to completely melt during the warm time of the year. As a result of permafrost degradation primary niveo-aeolian deposits melt, which leads to the formation of specific denivation structures.

Denivation structures form as a result of the melting of the seasonal snow cover. Atmospheric dust, sand, and fine organic detritus which accumulate in them deposit onto the dune surface as a thin (0.5–

4.0 mm) crinkly inversive dark-coloured warp called the denivational interlayer [*Dijkmans et al., 1988; Dinwiddie et al., 2012*].

Denivation structures also include specific types of stratification related to the melting of ancient niveo-aeolian deposits which contain interlayers and schlieren of fossil firn-ice of sedimentary genesis. The denivation structures manifest as crinkly silt interlayers with distinctive vertical micro-wedge-like apophyses and protuberances, vertical filtration funnels of meltwater, etc. Melting of niveo-aeolian deposits with a high ice content is frequently accompanied by complex microfolding, microsubsidences, fractures, and other types of deformations [*Dijkmans et al., 1988*].

J.W. Dijkmans and colleagues [*Dijkmans et al., 1988*] observed melting snow and summer rain waters which flow into enclosed interdune depressions and form microdeluvial, microproluvial facies, as well as inner microdeltas composed of thin denivational warp layers on the Kobuk dune massif. Because of high hygroscopy and poor permeability the denivation interlayers make meltwater and rainwater drainage difficult, which leads to permafrost aggradation, an increase in the permafrost aquitard, and an even higher seasonal flooding of interdune depressions. Denivation stratification is vastly represented in D'olkuminskaya Series deposits in many outcrops of Central Yakutia (Fig. 10, *b*, *d*).

Ultimately, the freezing of interdune basins floors and the increase in atmospheric precipitation on the border of the Neopleistocene and Holocene led to the formation of numerous shallow ephemeral water pools in which there was an accumulation of aeolian-lake deposits first, then swamp deposits. Such formations are widespread in the top of the D'olkuminskaya Series and are identified in the top part of the Peschanaya Gora outcrop (unit IV). They formed during the first half of the Holocene during the beginning stages of fixing of Younger Dryas dunes of the Kerdyom and Bestyakh terraces of the Lena River.

Many researchers [*Kasse, 2002; Zieliński et al., 2015; Kasse, Aalbersberg, 2019*] captured the wide distribution of niveo-aeolian and denivation structures in the aeolian deposits of the last cryochrone (MIS-2) within the periglacial European Sand Belt. Analogous structures are identified in aeolian sand covers within North American cryolithozones [*Koster, Dijkmans, 1988; Ayling, McGowan, 2006; Dinwiddie et al., 2012*].

Biogenic-aeolian cyclical stratification is found in some D'olkuminskaya Series outcrops. It is composed of systematically interchanging thin, parallel, divot-loamy sand interlayers 3–5 mm thick and layers of bleached quartz sand from 2–3 to 10–15 cm thick. The stratification origin is related to short episodes of fixing of sand dune surfaces by grass vegetation. On individual parts of the D'olkuminskaya Series territory, especially near its top, units with dozens of divot laminae (Fig. 10, *c*, *d*) which include buried grass tussocks, can be observed.

Biogenic-aeolian humus veins and nodules are widespread near the top of the D'olkuminskaya Series and reach 1.5–2.0 m in width and 0.5–1.5 m in thickness (Fig. 11). These veins form at the stage of fading aeolian activity, when a curtain herbaceous cover consisting of dense sedge-cereal tussocks forms on the dune surface. Continuous accumulation of new sand layers leads to a rise in the dune surfaces and depresses lateral tussock growth, as a result of which they continuously grow upward (Fig. 11, *b*). The grassy organic material of the tussocks decomposes quite quickly, which leads to the formation of isolated intensely humified spots, nodules, and diversely shaped veins. In more humid areas, because of high hygroscopy, the humus veins begin to freeze intensely with the formation of massive ice-ground veins (Fig. 11, *d*).

Cryogenic structures and textures in the D'olkuminskaya Series dune deposits is significantly diverse, but does not reach a large scale compared to the ice-loess covers of the Yedoma Series. The content of cementing porous ice varies from 5 to 30 % [*Galanin et al., 2018*]. "Sublimational" cryostructures represented by hoar-ice on grain contacts, thin ice films, and schlieren are more frequent in frozen sands which are extremely undersaturated with water. Massive cryotextures, the formation of which is related to the freezing of vertical and horizontal ground water infiltration zones, are often seen near the bottom of the series.

M.S. Ivanov [*1984*] points out that within the Peschanaya Gora outcrop he has discovered interlayers, schlieren, and fossil ice deposits from several millimeters to 3–4 meters thick. The majority of ground ice is concentrated in inclined bedding facies. Ice interlayer orientation repeats the stratification of enclosing dune deposits, based on which a sedimentary-metamorphic (atmosphere) origin of this ice by way of recrystallization of buried snow patches can be assumed.

V.B. Spektor and colleagues [*2011*] also point out the presence of fossil ice strata of firn origin in the Yedoma Series deposits of the Lena-Amga interfluve. According to the authors, the main indicators of their formation are strata type deposits, thin horizontal and wavy stratification, a light isotope composition ($\delta^{18}O = -30.8 \pm 0.9$ ‰; $D = -227.9 \pm 6.9$ ‰), and the presence of a significant amount of cryophytic herbaceous vegetation pollen.

Secondary sand veins and small wedges and pseudomorphs after PIW are usually linked to buried soil horizons in the bottom and top of the D'olkuminskaya Series, as well as buried Belling-Allered soils. These formations have an epigenetic origin related to episodes of soil-vegetative cover fixing of dunes, in-

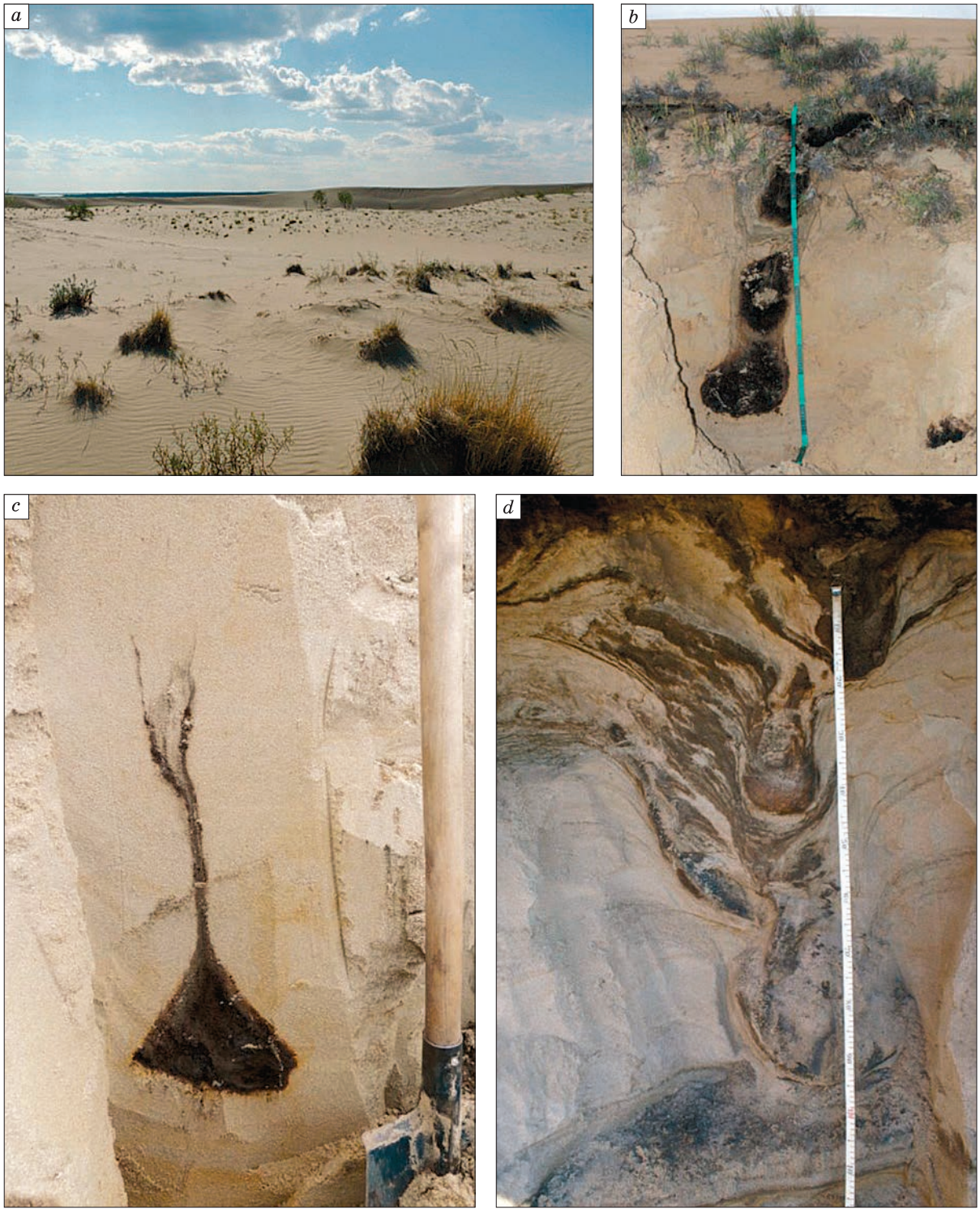

Fig. 11. Holocene biogenic-aeolian humus veins and nodules in D'olkuminskaya Series dune deposits (Kysyl-Syr outcrop in the basin of the lower course of the Vilyuy River, Central Yakutia).

a – stage of partial fixing of dunes by herbaceous tussocks; *b* – "migrating" humus nodules under a modern tussock; *c* – fully humified herbaceous tussock in dune sands; *d* – ice humus-sandy vein in frozen dune sands. A.A. Galanin's photo from July, 2015.

tense freezing, and an increased permafrost aquitard. Signs of cryoturbational processes in the form of microfolding are often seen in the same horizons.

Peschanaya Gora facies composition and age

Bestyakh Series pebble-gravel-sand deposits (units Ia, Ib) lying at the very base of the Kerdyom 25-meter terrace and categorized as Middle Neopleistocene "periglacial alluvium" by predecessors (bs Q_{II}) [*Alekseev et al., 1990; Kamaletdinov, Minuk, 1991*] are among the oldest formations. As of yet there are no absolute dates for the Bestyakh Series. The series' reverse magnetization identified in the Peschanaya Gora outcrop has been juxtaposed to the Matuyama Chron, the upper boundary of which is 780 ka [*Kamaletdinov, Minuk, 1991; Minuk, 2004*]. At the same time, the age of the alluvium at the bottom of Peschnaya Gora can be juxtaposed to the Blake or Seroglazka magnetic events (100 and 120 ka), especially considering that these events have already been identified in the sections of some terraces of Central Yakutia [*Minuk, 2004*].

The author of the present study has established a small-thickness sand unit (unit II) above the Bestyakh Series, possibly linked by predecessors to the "periglacial alluvium" of the Middle Pleistocene-aged Mavrinskaya Series (mv $Q_{II–III}$) [*Alekseev et al., 1990; Kamaletdinov, Minuk, 1991; Spektor et al., 2017*].

Because of a significant structural non-homogeneity, for convenience of research in the present article unit II has been divided into four nominal units (IIa–IId), which differ significantly in their sedimentary stratification and lamination features. The bottom unit IIa has clear signs of alluvial origin in the form of oblique series of submarine dunes and riffles.

The overlaying unit IIb is composed predominantly of humid aeolian deposit structures: wavy adhesion stratification and lamination types, as well as niveo-aeolian and denivation structures. The given facies set is typical for vast point bars, sandspits, and low basins with a rather sparse grass-subshrub cover, which are flooded rarely and for short periods of time during the spring snowmelt. The date obtained for the root of unit IIb (at a depth of 20 m from the brink of the terrace and 5 meters above the Lena Rive edge) – 22.10–19.60 ka (MPI-759) [*Alekseev et al., 1990*] – indicates deposit formation during the thermal minimum of MIS-2.

Unit IIc contains structures of dry aeolian deposition represented by translatent stratification and climbing ripple lamination, as well as deflational horizons with fine gravel and fragments of poorly developed paleosols. The age of the latter (unit IId) is characterized by two dates: 18.39–16.70 ka (MPI-901) at a depth of 15 m [*Kamaletdinov, Minuk, 1991*] and 18.33–15.68 ka (MPI-760) at a depth of 14 m [*Alekseev et al., 1990*].

Overall, the stratigraphic sequence of the facies of units IIa–IIc indicates a continuous decrease in the amount of atmospheric precipitation, a decrease in surface runoff, and an increase in aeolian process activity in the first half of MIS-2.

A wide distribution of deflational horizons in unit IIc and thin horizontal paleosol interlayers (unit IId) indicates that during this period the valley of the Lena River was a long deflational basin from which alluvial sediments were carried by wind in a southeast direction and partially deposited within the Kerdyom terrace. The bottom of the Paleo-Lena basin during this period was possibly a cold sand-gravel semidesert discontinuously covered with grass-subshrub vegetation. Secondary sand veins and wedges indicate an intense freezing of aeolian sand deposits under conditions of severe dehydration. Paleo-Lena runoff and the volume of annual river loads in this period were very insignificant.

Unit IIIa deposits differ drastically from underlying deposits. Structures of fast accumulation of aeolian deposits under dry conditions formed by gently sloping windward and steep dune slip face and crest facies dominate here. The former are represented by translatent climbing ripple stratification, the latter by steeply inclined grain-fall dune slip face structures. Sediment bedding and lamination indicate aeolian transport in a southeast direction, opposite the modern flow of the Lena River.

11 m below the terrace brink (14 m above the Lena's water level) a date of 14.07–13.40 ka (GIN-2461) [*Kamaletdinov, Minuk, 1991*] was obtained from a paleosol fragment (unit IIIb), which matches the Belling–Allerød warming. Due to this it can be assumed that the formation of unit IIIa took place during the interval 17.00–14.00 ka. The Lena's valley bottom in this period was covered with parabolic and spear-shaped dunes of a southeast orientation. The absence of adhesion, niveo-aeolian, and denivation structures in unit IIIa indicates hyperarid conditions, an extremely small amount of atmospheric precipitation, a lack of a snow cover or its insignificant role. At the same time, fading deflation and an increase in the rate of aeolian accumulation within the Kerdyom terrace and Central Yakutia in general indirectly indicates an influx of new aeolian loads and an increase in river runoff in the interval of 15–14 ka. An increase in runoff and the volume of river loads may be related to the beginning of the degradation of the last mountain glaciation in the Paleo-Lena basin.

The Unit IIIc, overlapping the Belling–Allerød paleosol, is similar to unit IIIa in terms of facies. Swift dry aeolian deposition structures (translatent climbing ripple lamination, grain-fall lamination) are predominant here. Horizontal and wavy types of aeolian stratification are spread through the top portion of the unit, biogenic stratification in the form of tiers of thin divot interlayers appears. Adhesion and niveo-

aeolian stratification types and denivation structures appear near depressions of the unit top, which indicates an increase in the influence of the snow cover. The formation of unit IIIc is related to the last pulse of the Younger Dryas global cooling, which is clearly reconstructed in all Late Neopleistocene aeolian covers of Northern Eurasia [*Kasse, 2002; Zieliński, 2015; Zykina et al., 2017; Kasse, Aalbersberg, 2019; Konstantinov et al., 2019*].

Unit IV deposits form a gently sloping depression on the top of the D'olkuminskaya Series, which is filled with lake and swamp deposits. In the bottom portion (unit IVa) there are facies of a small body of water which appeared in an enclosed interdune basin on the border of the Neopleistocene and Holocene. Contrasting interchange of greyish lake loamy sands and well sorted white aeolian sands (unit IVb) indicate a periodic drying out of the lake. Clearly, the lake existed at this site for a very short time and quickly filled with deposits, of which there was an abundant influx from nearby unvegetated dunes.

During the Early Holocene a peat bog (unit IVc) appeared in place of the lake and persisted through the Middle Holocene. Several radiocarbon dates indicate the age of the peat bog. At a depth of 2.4 m from the surface (unit IVc) a date of 8.99–8.60 ka (GIN-2462) was obtained [*Alekseev et al., 1990*]. The author of the present article obtained four more dates for unit IVc from depths of 2.5, 2.0, 1.5, and 1.0 m: 9.89–8.58 ka (MPI-121), 8.06–6.72 ka (MPI-118), 12.03–9.89 ka (MPI-119), and 7.86–6.65 ka (MPI-120), respectively. The obtained dates have a certain inversion, but definitely indicate a fast accumulation of the peat bog over the course of the first half of the Holocene in the interval from 10 to 6 ka.

The author has established numerous freshwater mollusk and ostracod shells from 1 to 4 mm in size in the top of the lake deposits. According to the data of V.A. Kamaletdinov and P.S. Minuk [*1991*], they are represented by a set of species which are widely distributed in modern shallow brackish lakes of Central Yakutia.

It is imperative to note that systematic interlayers of well-sorted white quartz sand are present in the bottom layers of the peat unit, and they are completely absent in the top layers. This indicates that during the beginning period of its formation this and other peat bogs were small vegetation oases within a wide field of unvegetated U-shaped dunes of the Kerdyom terrace. Complete stabilization of the latter with vegetation had clearly finished by the beginning of the Boreal optimum of the Holocene, since the middle and top parts of the peat layers have no mineral interlayers.

Pollen and paleontological composition of aeolian sand covers of Central Yakutia

The spore-pollen composition of the D'olkuminskaya Series is known by individual samples and is rather scant. According to the data of V.V. Spektor and colleagues [*2017*], spores and pollen in the Peschanaya Gora outcrop are predominantly represented by herbaceous taxa and contain a significant amount of mineralized, mechanically damaged, and redeposited grains. The pollen composition indicates formation of the D'olkuminskaya Series under conditions of a discontinuous soil-vegetation cover of impoverished steppes where xerophytic taxa dominated: Artemisia, Poaceae, sedges, Caryophyllaceae, and Chenopodioideae (Artemisia, Cyperaceae, Asteraceae, Chenopodiaceae, Poaceae, Ranunculaceae, Fabaceae, Brassicaceae). A small presence of tree, shrub and subshrub pollen (*Pinus*, *Larix*, *Betula*, *Alnaster*, *Ericales*, *Selaginella* sp.), as well as moss spores (*Sphagnum*) and seaweed (*Botryococcus*), indicates a mosaic landscape in which small bodies of water and possible wood-shrub vegetation oases persisted.

Similar pollen spectrums are established in D'olkuminskaya Series sections in a 45-meter (Bestyakh) terrace of the Lena River near the small town of Nizhny Bestyakh [*Pravkin et al., 2018*], 120 km south of Peschanaya Gora, in a 12-meter terrace of the Suola River (right-bank tributary of the Lena River [*Potapova et al., 2016*], as well as in a 35-meter terrace of the Vilyuy River [*Pavlova et al., 2017; Galanin, Pavlova, 2019*]. An additional feature of the series is the vastitude of *Glomus* and *Sordaria* spores, which live on the excrements of large herbivores and are typical for dry landscapes with discontinuous soil-vegetation cover [*Potapova et al., 2016*].

The paleontological composition of the D'olkuminskaya Series can be described using the example of the Suullar Myraan outcrop (62°33.54′ N; 129°59.49′ E) on the right bank of the Lena River, 20 km downstream of the Kangalassky cape, as well as in the Megin mammoth fauna location in the river cliff of a 12-meter terrace of the Suola River (62°05.14′ N; 130°11.18′ E), situated within the dune cover distribution of the D'olkuminskaya Series (Fig. 4). *Mammuthus primigenius*, *Bison priscus*, *Coelodonta antiquitatis*, *Equus lenensis*, *Saiga tatarica* remains are identified in the Suullar Myraan outcrop (Kerdyom terrace of the Lena River) [*Spektor et al., 2017*]. A date of 23.79–21.86 ka (GIN-14410) [*Spektor et al., 2017*] has been obtained for the bone of a woolly rhinoceros, which corresponds to the beginning of MIS-2.

60 fauna and 25 vegetation taxa were identified in the peat bog of the Megin outcrop based on carpological analysis [*Potapova et al., 2016*]. The remains of several *Bison priscus*, *Ovibos moschatus*, *Equus lenensis* individuals and an almost complete skeleton of an archaic form of *Mammuthus primigenius (Megin Mammoth)* were identified, the calibrated age of the latter of which – 23.86–22.65 ka (MPI-80) – is also associated with the beginning of MIS-2. A paleoecological reconstruction of the flora and fauna of the

peat bog has revealed that during its formation the average temperature in July was no less than +12 °C. The vegetation cover was formed by a mosaic combination of impoverished steppes, meadows, islands of larch forests and vast unvegetated landscapes [*Potapova et al., 2016*]. Remains of aquatic vegetation together with xerophytes indicate significant seasonal fluctuations in the level of bodies of water and the domination of evaporative environments.

It must be noted that all the numerous discoveries of large herbivores of the mammoth biome in Central Yakutia date to the Kargin thermochrone (MIS-3) [*Boeskorov et al., 2016*]. Currently all discoveries of later representatives of the mammoth biome of Central Yakutia (Megin mammoth – 23.86–22.65 ka; Suolsky mammoth – 22.06–21.45 ka; woolly rhinoceros from the Suullar Myraan section – 23.79–21.86 ka) are limited to the beginning of MIS-2. All the aforementioned discoveries are associated with the bottom of the D'olkuminskaya Series; they are not found within the series itself. Results of studies of the D'olkuminskaya Series key sections have demonstrated that a catastrophic drought and desertification of Central Yakutia started at the beginning of MIS-2 and peaked in the interval of 18–13 ka. The maximum expansion of dune cover areas happened specifically during this time, and likely a sharp decline in the areas and productivity of meadow steppes – the main feed base of the mammoth biome.

It is curious that later and seemingly already disappearing Suolsky and Meginsky mammoths are associated with the archaic form, which is morphologically cognate with the steppe mammoth [*Boeskorov, Mashchenko, 2014*]. It is possible that these forms were the last micropopulations which inhabited small oases of vegetation among surrounding D'olkuminskaya Series dune covers and attempted to adapt to the conditions of extreme drought and desertification. Indeed, the disappearance of the larger representatives of the mammoth biome of Central Yakutia 10–12 thousand years earlier, compared to more northern and eastern regions, is difficult to relate to warming climate in the Holocene. But it can be explained by desertification, expansion of the area of dune massifs, a decrease in Yedoma meadow steppe areas and productivity – the main feed base of the mammoth biome. Of course, this assumption requires additional factual justification.

CONCLUSION

The results of the additional study of the Peschanaya Gora key outcrop and other sections of Central Yakutia indicate a subaerial origin of D'olkuminskaya Series cover sands in cold and dry conditions of the final Neopleistocene. The majority of its facies features are typical for contemporary and Late Quaternary dune massifs which are widely distributed in the cold regions of North America, Europe, Western Siberia.

A revision of radiocarbon datings of all key sections of Central Yakutia shows that the main portion of the D'olkuminskaya Series within the Kerdyom 25-meter terrace formed in the interval from 22 to 12 ka. In the interval of 22–17 ka (thermic minimum of MIS-2), because of a catastrophic decrease in the amount of precipitation and river runoff, a deflational basin partially fixed by curtain herbaceous vegetation formed within the bottom of the valley of Paleo-Lena. The majority of river channel and basin deposits was carried away beyond the basin in a southeast direction and deposited within the Kerdyom and Bestyakh terraces.

In the interval of 17–14 ka deflation was replaced by intense aeolian accumulation, as a result of which a sand dune desert with islands of tundra-steppe vegetation formed within the Kerdyom and Bestyakh terraces of the Lena River.

In the interval of 14–13 ka dune relief stabilization of the Kerdyom and Bestyakh terraces by grass-subshrub xeryophytic groups and islands of wood vegetation was taking place under conditions of climate softening (Belling-Allerød warming).

In the interval of 12.8–11.8 ka there was abrupt Younger Dryas desertification, which was accompanied by the expansion of dune massifs within the Kerdyom and Bestyakh terraces of the Lena River.

During the beginning of the Holocene in the interval of 11–10 ka, as a result of a significant increase in atmospheric precipitation and climate softening, the surface of the dunes began to gradually become colonized by vegetation. At the initial stage many shallow lakes were formed in enclosed interdune depressions, the smaller of which became swamps with abundant peat accumulation by the beginning of the Boreal optimum of the Holocene. The final stabilization of the Kerdyom terrace dune relief by vegetation ended approximately 9–8 ka.

The mineralogical similarities between dune (D'olkuminskaya Series), loess-ice (Yedoma Series), and alluvial deposits in the basin of the middle course of the Lena River indicate a common source of terrigenous material (Jurassic greywacke-quartz sandstone). An important indicator of the aeolian origin of D'olkuminskaya Series dune deposits is an almost threefold increase in the content of the heavy fraction and magnetite to 3.1 % in comparison to the underlying alluvium of the Bestyakh (1 %) and Mavrinskaya (1.1 %) series. Another important mineralogical indicator is the presence of secondary carbonate and metal hydroxide in dune deposits, which form specific cementing films and interlayers called calcretes.

The features of the granulometric composition and mineralogical similarities of the D'olkuminskaya and Yedoma series indicate that they are two separate granulometric derivatives which appeared as a result

of aeolian differentiation of a single source – Quaternary alluvium of the Bestyakh and Mavrinskaya series. The first derivative (dune sands) consists predominantly of sand fractions, and the latter (loess) of dusty fractions. This conclusion proves the zonal character of the spatial distribution of dune massifs and loess-like deposits in relation to the east-southeast direction of wind transfer in the region. As such, the D'olkuminskaya Series dune deposits compose predominantly the 18–25-meter (Kerdyom) and 45–75-meter (Bestyakh) terraces of the Lena River, while the main area of the ice-loess covers of the Yedoma Series is located eastward and linked to higher elements of the Lena-Amga interfluve relief (Tyungulu, Abalakh, and Magan surfaces).

The sedimentational structure of the D'olkuminskaya Series deposits is represented by a wide set of specific types of stratification and lamination, some of which are typical only for aeolian deposits. They include translatent climbing ripple stratification and lamination, grain-fall cross-stratification and lamination of steep dune slip faces and others.

The formation of the D'olkuminskaya Series in cold arid conditions is emphasized by the wide distribution of primary sandy veins and wedges and other structures of dry aeolian deposition. Additionally, adhesion, niveo-aeolian and denivation structures formed under conditions of seasonal snow cover and contrasting humidification are widespread in the composition of its individual units in the bottom and top.

An analysis of pollen and paleontological data shows that the cooling and desertification of the last cryochrone (MIS-2), which took place in the interval of 22–17 ka, was catastrophic in Central Yakutia and could have been the cause of the early extinction of some of the larger representatives of the mammoth biome.

Acknowledgements. *The author would like to thank the staff of MPI SB RAS I.V. Klimova, G.I. Shaposhnikova, A.L. Lobanova, N.N. Remizova, A.N. Vasilieva, and A.M. Safina for their help in the completion of analyses.*

The study was conducted with support from RFBR No. 17-05-00954-a, RFBR-RS(Y) No. 15-45-05129, No. 18-45-140012.

References

Alekseev, M.N., 1961. Stratigraphy of continental Neogene and Quaternary deposits of the Vilyuy depression and the valley of the lower reaches of the Lena River. USSR Academy of Sciences, Moscow, 120 pp. (in Russian).

Alekseev, M.N., Grinenko, O.V., Kamaletdinov, V. A., et al., 1990. Neogene and Quaternary deposits of the Lower Aldan depression and the Middle Lena (Central Yakutia). Geological excursion guide. YSC SO AN SSSR, Yakutsk, 42 pp. (in Russian).

Alekseev, M.N., Kamaletdinov, V.A., Grinenko, O.V., 1984. Cenozoic deposits of the Lena and Aldan. In: 27th International Geological Congress. Yakut ASSR, Siberian platform. Generalized guide of excursions 052, 053, 054, 055. Nauka, Novosibirsk, pp. 21–42 (in Russian and in English).

Astakhov, V.I., Svensen, J.I., 2011. Covering formation of the Final Pleistocene in the extreme north-east of European Russia. Regional'naya geologiya i metallogeniya [Regional Geology and Metallogeny], No. 47, 12–27 (in Russian).

Ayling, B.F., McGowan, H.A., 2006. Niveo-eolian Sediment Deposits in Coastal South Victoria Land, Antarctica: Indicators of Regional Variability in Weather and Climate. Arctic, Antarctic, and Alpine Research 38 (3), 313–324.

Black, R.F., 1951. Eolian deposits of Alaska. Arctic 4 (2), 89–111.

Blott, S.J., Pye, K., 2001. Gradistat: a grain size distribution and statistics package for the analysis of unconsolidated sediments. Earth Surface Processes and Landforms, vol. 26, 1237–1248.

Boeskorov, G.G., Mashchenko, E.N., 2014. The systematic position of the "Suolsky" mammoth (Mammuthus, Proboscidea). Nauka i obrazovanie [Science and Education], No. 2, 48–54 (in Russian).

Boeskorov, G.G., Nogovitsyn, P.R., Mashchenko, E.N., et al., 2016. New data on mammals of the mammoth fauna of the Middle Lena Basin (Yakutia; the national natural park "Lena Pillars" and adjacent territories). Doklady Akademii Nauk [Reports of the Academy of Sciences], 469 (2), 190–194, DOI: 10.7868/S0869565216200147.

Boggs, Jr.S., 2009. Sedimentary structures. In: Petrology of Sedimentary Rocks. Cambridge University Press, Cambridge, pp. 63–110.

Bolshiyanov, D.Yu., Makarov, A.S., Schneider, V., et al., 2013. Origin and Development of the Lena River Delta. AARI, St. Petersburg, 268 pp. (in Russian).

Bolshiyanov, D.Yu., Tide, Y, Savelieva, L.A., et al., 2016. To the study of the stages of development of the river valley Lena. In: Proceedings of the All-Russian Scientific and Practical Conference "Geology and mineral resources of the North-East of Russia" (Yakutsk, April 6–8, 2016). NEFU, Yakutsk, pp. 469–472 (in Russian).

Botvinkina, L.N., 1962. Layering of sedimentary rocks. In: Proceedings of the Geological Institute of the USSR Academy of Sciences. USSR Academy of Sciences, Moscow, vol. 51, 542 pp. (in Russian).

Bronk, R.C., 2009. Bayesian analysis of radiocarbon dates. Radiocarbon, No. 51 (1), 337–360.

Brookfield, M.E., 2011. Aeolian processes and features in cool climates. Geological Society London Special Publications, pp. 241–258.

Cailleux, A., 1974. Formes précoces et albédos du nivéo-éolien. Z. Geomorphology, No. 18, 437–459.

Calkin, R.E., Rutford, R.H., 1974. The Sand Dunes of Victoria Valley, Antarctica. Geographical Review 64 (2), 189–216.

Caputo, M., 2020. Adhesion Ripple Structures in Quaternary Carbonate Eolianites, San Salvador Island, the Bahamas. Preprint, 13 pp.

Carter, L.D., 1981. A Pleistocene Sand Sea on the Alaskan Arctic Coastal Plain. USGS Staff Published Research 924.

Derbyshire, E., Owen, L.A., 2017. Glacioaeolian processes, sediments, and landforms. In: Past Glacial Environments. J. Menzies, J. van der Meer (Eds.). Elsevier, N.Y., pp. 273–308.

Dijkmans, J.W.A., Galloway, J.P., Koster, E.A., 1988. Grain-size and mineralogy of eolian and fluvial sediments in the central Kobuk valley, northwestern Alaska. Department of the interior United States Geological Survey. Open-file report No. 88-369, 21 pp.

Dijkmans, J.W.A., Koster, E.A., Galloway, J.P., et al., 1986. Characteristics and origin of calcretes in a subarctic environment. Great Kobuk Sand Dunes, northwestern Alaska, USA. Arctic and Alpine Research 18, 377–387.

Dinwiddie, C.L., McGinnis, R.N., Stillman, D.E., et al., 2012. Internal sedimentary structure and aqueous-phase distribution of the Great Kobuk Sand Dunes, northwestern Alaska: Insights from an arctic aeolian analog site. In: Third International Planetary Dunes Workshop: Remote Sensing and Image Analysis of Planetary Dunes. USA, Arizona, Flagstaff, 2012 June 12–15, abstract #7034. – https://www.lpi.usra.edu/meetings/dunes2012/pdf/7034.pdf

Ershov, E.D., 1989. Geocryology of USSR. Middle Siberia. Nedra, Moscow, 414 pp. (in Russian).

Fedorovich, B.A., 1983. Zonality of aeolian relief formation. In: Dynamics and patterns of relief formation of deserts. Nauka, Moscow, 236 pp. (in Russian).

Fenton, L.K., Hayward, R.K., Horgan, B.H.N., et al., 2013. Summary of the Third International Planetary Dunes Workshop: Remote Sensing and Image Analysis of Planetary Dunes, Flagstaff, Arizona, USA, June 12–15, 2012. Aeolian Research, No. 8, 29–38.

Filippov, V.Ye., Vasiliev, I.S., 2006. Periglacial relief of the Lena-Vilyuy interfluve. Geografiya i prirodnye resursy [Geography and Natural Resources], No. 4, 82–86.

Folk, R.L., 1980. Petrology of sedimentary rocks. Texas, Hemphill Publishing Company Austin, 350 p.

Galanin, A.A., Pavlova, M.R., Klimova, I.V., 2018. Late Quaternary dune formations (D'olkuminskaya Series) in Central Yakutia (Part 1). Earth's Cryosphere, XXII (6), 3–14.

Galanin, A.A., Pavlova, M.R., 2019. Late Quaternary dune formations (D'olkuminskaya Series) in Central Yakutia (Part 2). Earth's Cryosphere, XXIII (1), 3–15.

Galanin, A.A., Pavlova, M.R., Shaposhnikov, G.I., Lytkin, V.M., 2016. Tukulans: sand deserts of Yakutia. Priroda [Nature], No. 11, 44–55.

GOST 12536-2014. Soils. Methods of laboratory determination of granulometric (granural) and microaggregate composition, 2015. Staidartinform, Moscow, 18 p. – http://docs.cntd.ru/document/1200116022

Huissteden, J.V., Vandenberghe, J., Van der Hammen, T., Laana, W., 2000. Fluvial and aeolian interaction under permafrost conditions: Weichselian Late Pleniglacial, Twente, eastern Netherlands. Catena 40 (3), 307–321.

Hunter, R.E., 1977. Basic types of stratification in small eolian dunes. Sedimentology 24, 361–387.

Ivanov, A.D., 1966. Aeolian sands of Western Transbaikalia and the Baikal region. Buryat. Book Publishing House, Ulan-Ude, 232 pp. (in Russian).

Ivanov, M.S., 1984. Cryogenic structure of the Quaternary deposits of the Lena-Aldan depression. Nauka, Novosibirsk, 126 pp. (in Russian).

Kamaletdinov, V.A., Minuk, P.S., 1991. Structure and characteristics of sediments of the Bestyakh terrace of the Middle Lena River. Byulleten' Komissii po izucheniyu chetvertichnogo perioda AN SSSR [Bulletin of the Commission of Quaternary Research of AS USSR], No. 60, 68–78 (in Russian).

Kasse, C., 2002. Sandy aeolian deposits and environments and their relation to climate during the Last Glacial Maximum and Lateglacial in northwest and central Europe. Progress in Physical Geography: Earth and Environment, No. 26 (4), 507–532.

Kasse, C., Aalbersberg, G., 2019. A complete Late Weichselian and Holocene record of aeolian coversands, drift sands and soils forced by climate change and human impact, Ossendrecht, the Netherlands. Netherlands Journal of Geosciences 98, e4-1–e4-22.

Kolpakov, V.V., 1983. Aeolian Quaternary deposits in the Lena area of Yakutia. Byulleten' Komissii po izucheniyu chetvertichnogo perioda AN SSSR [Bulletin of the Commission of Quaternary Research of AS USSR], No. 52, 123–131.

Konstantinov, A., Loiko, S., Kurasova, A., et al., 2019. First Findings of Buried Late-Glacial Paleosols within the Dune Fields of the Tomsk Priobye Region (SE Western Siberia, Russia). Geosciences 9(82), 1–18.

Kossovskaya, A.G., 1962. Mineralogy of the terrigenous complex of the Vilyuy Depression and Western Verkhoyansk. Tr. Geological Institute of the USSR Academy of Sciences. Issue 63. USSR Academy of Sciences, Moscow, 190 pp. (in Russian).

Koster, E.A., Dijkmans, J.W.A., 1988. Niveo-aeolian deposits and denivation forms, with special reference to the Great Kobuk Sand Dunes, northwestern Alaska. Earth Surface Processes and Landforms, No. 13, 153–170.

Kulik, N.A., 1928. About the sands of the Pechora region. Doklady Akademii Nauk [Reports of the Academy of Sciences]. Ser. A, No. 9, 156–158.

Kutyrev, E.I., 1968. Formation conditions and interpretation of oblique bedding. Nedra, Leningrad, 128 pp. (in Russian).

Kuznetsova, L.V., Zakharova, V.I., Sosina, N.K., et al., 2010. Flora of Yakutia: geographical and ecological aspects. Nauka, Novosibirsk, 192 pp. (in Russian).

Lea, P.D., 1996. Vertebrate tracks in Pleistocene eolian sandsheet deposits of Alaska. Quaternary Research 45 (2), 226–240.

Map of Quaternary formations of the territory of the Russian Federation. Scale 1:2 500 000, 2014. VSEGEI. Moscow. Electronic resource on 1 sheet.

Map of Quaternary Deposits of the USSR, 1959. VSEGEI. Moscow. Electronic resource on 1 sheet. – http://neotec.ginras.ru/neomaps/M050_Union_1959_Quatern-depos.jpg

Map of Quaternary Deposits of the USSR. Scale 1:16 000 000. 1983. In: Atlas of the USSR. Main Directorate of Geodesy and Cartography under the Council of Ministers of the USSR, Moscow, pp. 90–91.

Minuk, P.S., 2004. Magnetostratigraphy of the Cenozoic of northeastern Russia. SVKNII FEB RAS, Magadan, 198 pp. (in Russian).

Okhotin, V. V., 1933. Granulometric classification of soils based on their physical and mechanical properties. Lengostransizdat, Leningrad, 70 pp. (in Russian).

Pavlova, M.R., Rudaya, N.A., Galanin, A.A., et al., 2017. The structure and dynamics of the development of dune massifs of the Vilyuy basin in the Late Quaternary (on the example of the Makhatta and Kysyl-Syr tukulans). Contemporary Problems of Ecology 10 (4), 411–422.

Pewe, T.L., 1975. Quaternary Geology of Alaska. United States Government printing office, Washington, 144 pp.

Pewe, T.L., Journaux, A., 1983. Origin and character of loess-like silt in unglaciated south-central Yakutia, Siberia, U.S.S.R. Geological survey. Professional paper 1262. United States Government Printing Office, Washington, 46 pp.

Pomortsev, O.A., Bolshiyanov, D.Yu., Popov, V.B., et al., 2017. On the problem of marine transgressions and sedimentary environments in Central and Northern Yakutia in the Neopleistocene. Vestnik SVFU. Seriya Nauki o Zemle [Bulletin SVFU. Earth Sciences series], No. 4 (08), 5–13.

Potapova, O., Maschenko, E.N., Protopopov, A., et al., 2016. The sartanian biodiversity of Central Yakutia, Russia: the analyses of the new Late Pleistocene Megin Site. Society of Vertebrate Paleontology – 76th Annual Meeting, October 26–29, 2016, Salt Lake City, Utah, USA. Journal of Vertebrate Paleontology, Program and Abstracts, 208 pp.

Pravkin, S.A., Bolshiyanov, D.Yu., Pomortsev, O.A., et al., 2018. Relief, structure and age of Quaternary sediments of the river valley. Lena in the Yakutsk bend. Vestnik Sankt-Peterburgskogo universiteta. Nauki o Zemle [Bulletin of St. Petersburg University. Earth Sciences], No. 63 (2), 209–229.

Schwan, J., 1986. The origin of horizontal alternating bedding in Weichselian aeolian sands in Northwestern Europe. Sedimentary Geology, No. 49, 73–108.

Schwan, J., 1988. The structure and genesis of Weichselian to Early Holocene Aeolian sand sheets in western Europe. Sedimentary Geology 55, 197–232.

Siegert, K., Staukh, G., Lemkul, F., et al., 2007. Development of glaciation of the Verkhoyansk ridge and its foothills in the Pleistocene: results of new research. Regional geology and metallogeny [Regional Geology and Metallogeny], No. 30–31, 222–228.

Sizov, O.S., 2015. Geoecological aspects of modern aeolian processes in the northern taiga subzone of Western Siberia. Electronic resource. Academic Publishing House "Geo", Novosibirsk, 124 pp. (in Russian).

Sizov, O., Konstantinov, A., Volvakh, A., Molodkov, A., 2020. Timing and Sedimentary Record of Late Quaternary Fluvio-Aeolian Successions of the Tura-Pyshma Interfluve (SW Western Siberia, Russia). Geosciences 10 (396), 1–19.

Soloviev, P.A., 1959. Cryolithozone of the northern part of the Lena-Amga interfluve. USSR Academy of Sciences, Moscow, 144 pp. (in Russian).

Spektor, V.B., Spektor, V.V., Bakulina, N.T., 2011. Buried snowfields on the Lena-Amga plain. Earth's Cryosphere XV (4), 16–21.

Spektor, V.B., Spektor, V.V., Torgovkin, Ya.I., et al., 2016. Areal hydrogenic forms and associated floodstreams on the territory of the Central Yakut Plain at the turn of the Pleistocene and Holocene. In: Geography Issues. Vol. 142 Geography of the polar regions. Kodeks, Moscow, pp. 291–315 (in Russian).

Spektor, V.V., Spektor, V.B., Boeskorov, G.G., et al., 2017. Periglacial alluvium of the Central Yakut Plain according to the study of the reference outcrop Sand Hill. Vestnik ZabGU [Bulletin of Trans-Baikal State University], 23 (5), 45–59.

Ufimtsev, G.F., Dzhanotta, A., Perevalov, A.V., et al., 1997. Aeolian landscapes of the Tunkinskaya depression. Geografiya i prirodnye resursy [Geography and Natural Resources], No. 1, 65–70.

Velichko, A.A., Timireva, S.N., 2005. Western Siberia – the great late glacial desert. Priroda [Nature], No. 5, 54–62.

Volkov, I.A., 1971. Late Quaternary subaerial formation. Nauka, Moscow, 274 pp. (in Russian).

Vyrkin, V.B., 2010. Aeolian relief formation in the Baikal and Transbaikal regions. Geografiya i prirodnye resursy [Geography and Natural Resources], No. 3, 25–32.

Waters, M.R., Forman, S.L., Pierson, J.M., 1999. Late quaternary geology and geochronology of Diring an early Paleolithic site in Central Siberia. Quaternary Research, No. 51, 195–211.

Wolfe, S., Bond, J., Lamothe, M., 2011. Dune stabilization in central and southern Yukon in relation to early Holocene environmental change, northwestern North America. Quarternary Science Reviews, No. 30 (3–4), 324–334.

Zieliński, P., Sokołowski, R., Woronko, B., Jankowski, M., Fedorowicz, S., Zaleski, I., Molodkov, A., Weckwerth, P., 2015. The depositional conditions of the fluvio-aeolian succession during the last climate minimum based on the examples from Poland and NW Ukraine. Quaternary International 386, 30–41.

Zykina, V.S., Zykin, V.S., Volvach, A.O., et al., 2017. Upper quaternary deposits of the Nadym Ob area: stratigraphy, cryogenic formations, and deposition environments. Earth's Cryosphere XXI (6), 12–20.

Received June 4, 2020
Revised version received August 2, 2020
Accepted November 25, 2020

EARTH'S CRYOSPHERE
SCIENTIFIC JOURNAL

Kriosfera Zemli, 2021, vol. XXV, No. 1, pp. 31–39

PHYSICAL AND CHEMICAL PROCESSES IN FROZEN GROUND AND ICE

ESTIMATION OF THE FREEZING INTENSITY OF THE SALT WATER DROPS IN THE COURSE OF WINTER SPRINKLING

A.V. Sosnovsky, N.I. Osokin

Institute of Geography, Russian Academy of Sciences,
Staromonetniy lane 29, Moscow, 119017, Russia; alexandr_sosnovskiy@mail.ru

The simplified dependencies for estimation the fraction of the ice formed in a drop of fresh water when falling in the atmospheric air have been obtained. Based on mathematical modeling, the intensity of the freezing of salt-water droplets with various variants of salt rejection from the freezing boundary has been determined. An estimate of the increase in air temperature in a droplet plume consisting of drops of salt water has been given. The fraction of ice in a drop of salt water falling in atmospheric air and in a droplet plume has been calculated depending on the air temperature and the size of the drops.

Key words: *freezing drops, winter sprinkling, intensity of freezing-up, mathematical modeling, salt water.*

INTRODUCTION

In recent years, the winter sprinkler method has been used increasingly to freeze up ice. It is based on the use of long-range sprinkler systems to spray water and create a droplet plume. Such sprinklers are widely used in agriculture to irrigate crops. Based on the serial sprinkler DDN-70 (long-range mounted sprinkler with a jet range of 70 m), the Grad-1 sprinkler was developed for sprinkling in winter conditions [*Design..., 1991*]. When the sprinkler is operating, the stream of water rises to a height of 20 m, and then breaks up into small drops, which fall to the ground. The droplet diameter is generally 1–2 mm. The dimensions of the droplet plume (the volume of the space in which the drops fall) are 15–20 m in height, 30–40 m in length and 5–10 m in width. The size of the plume depends on the wind speed. With increasing wind speed, the height of the plume decreases and its width increases. The sprinkler can operate by moving both in a circle and in a sector or with a fixed position of the sprinkler barrel.

An ice shell forms on the surface of the freshwater drops falling in frosty air. When more than 55 % of the volume of a water droplet freezes, the ice shell (in that time the shell thickness is 0.23 of the droplet radius) does not break when it hits the underlying surface. Experiments on winter sprinkling in Yakutia [*Gordeichik, Sosnovsky, 1982*] have demonstrated that more than 60 % of the drop volume freezes at an ambient temperature below –50 °C. At the same time, dry granular ice is formed, consisting of partially or completely frozen water droplets, that ice is not suitable for the construction of an ice crossing.

When the ice shell of the drop breaks, unfrozen water flows out of the drop and a water-ice mixture forms on the surface of the earth. After its freezing, the monolithic ice with the density of 800–850 kg/m^3 is formed. At present, winter sprinkling is widely used for the construction of ice crossings and winter roads [*Design..., 1991*]. The foreign experience in creating artificial ice islands demonstrates that the ice freezing-up by means of sprinkling provides the best effect [*Kubyshkin et al., 2018*]. The method has a great advantage over others in the speed of creating large masses of frozen ice, and it is accepted as the main method for creating artificial ice islands in the international standard ISO 19906.

With continuous sprinkling and removal of unfrozen water outside the freezing zone, the porous ice with a density of 400–600 kg/m^3 is formed. With sprinkling during the day, the height of the porous ice massif can exceed seven meters [*Sosnovsky, Khodakov, 1995*]. The studies carried out to date have revealed that one of the most economical methods of desalination and purification of large volumes of saline water is the drip freezing-out method, which is implemented during winter sprinkling [*Sosnovsky, Khodakov, 1995; Gao et al., 2004; Biggar et al., 2005*]. So, with the mineralization of frozen water up to 10 g/L, the mineralization of porous ice does not exceed 1 g/L.

The freezing of salt water has a number of features. The freezing point of salt water and the temperature of its highest density depend on its salinity. The salinity of the frozen ice is several times lower than that of the original water. Those features entail

differences in convection, the mechanism of ice formation, and the thermal regime of waters of different salinity during freezing.

One of the factors affecting the intensity of ice formation during winter sprinkling is the supercooling of water droplets. A detailed review of that problem is presented in [*Smorygin, 1988*]. The supercooling of water droplets is investigated to prevent the icing of aircrafts in flight and the icing of sea vessels [*Kulyakhtin, Tsarau, 2014; Alekseenko et al., 2016*], as well as for the assessment of the ice-cover deposits and the possibility of ice-rain formation [*Vilfand, Golubev, 2011; Smorodin et al., 2014*]. When studying the phenomenon of supercooling, the distilled water purified from impurities is used to obtain significant supercooling. When supercooling stops, ice grows rapidly in a drop of water. The possible mechanisms of branching of needle-shaped ice crystals in supercooled water have been experimentally investigated in the [*Shibkov et al., 2013*]. The growth of branched crystals also occurs when salt-water droplets freeze [*Adams et al., 1963*]. The supercooling of the fresh-water and salt-water droplets in the open air has not been studied enough. Thus, the dependence of the time and magnitude of supercooling on the size of the droplets, the rate of cooling and the salinity of water is not clear. However, it is possible to assess the effect of possible supercooling of water droplets on the intensity of ice formation.

In the [*Sosnovsky, 1993*], on the basis of experiments and mathematical modeling, an assessment of the effect of supercooling of fresh water drops on the intensity of ice formation during winter sprinkling is given. The results of calculations have demonstrated that at the air temperature of –20 °C, and a supercooling of –8...–6 °C, the productivity of ice formation decreases by 5 % for water droplets with a diameter of 1–2 mm. The experiments in the open air with the use of fresh water have revealed that the supercooling of water droplets is about –1...–3 °C. Unfrozen drops have not been observed in the droplet plume, which mainly consisted of water droplets 1–2 mm in diameter. Perhaps that is due to the presence of a large number of tiny ice crystals in the plume, which serve as crystallization centers for falling water drops. Therefore, at the air temperatures below –10...–15 °C, the effect of supercooling of water on the intensity of ice formation during winter sprinkling can be neglected.

The aim of the research is to assess the intensity of ice formation in a drop of salt water and in a droplet plume during winter sprinkling.

FREEZING OF FRESH-WATER DROPS

The freezing intensity of salt-water drops must be compared to that of fresh-water drops. Therefore, let us first consider the freezing of fresh-water drops. During operation of the Grad-1 sprinkler, the height of the droplet plume is 18 m at a wind speed of 5 m/s and a jet range of 70 m. The water discharge with a nozzle diameter of 55 mm is 240 m^3/h. The falling time of water droplets with a diameter of 1.5 mm from a height of 18 m is 3.3 seconds at a vertical drop speed of 5.4 m/s [*Mason, 1961*].

When fresh-water droplets freeze, an ice shell forms on their surface, being thickened during the droplet's fall, and reducing the radius of the liquid part.

In the [*Sosnovsky, 1980*], the problem of freezing of the water-drop falling in frosty air has been considered. As a result of solving the heat conduction equation with the Stefan condition at the freezing boundary (phase boundary), and the condition of heat transfer at the droplet boundary using the known criterion dependences to determine the heat and mass transfer coefficients of the falling water-drops, a dependence has been obtained for determining the freezing time of a fresh-water drop (τ) on the position of crystallization front (ξ) (origin of coordinate is at the center of the drop) in the form of:

$$\tau = \frac{264R^2}{M}\left[\frac{109}{3\mathrm{Nu}}\left(1-\frac{\xi^3}{R^3}\right)+M_1\right], \qquad (1)$$

where $\mathrm{Nu} = 2 + 17.2R^{0.815}$ is the Nusselt number; R is the radius of the drop, mm; $M = T_0 - T_a + 2.3(4.8 - fe_a)$; $T_0 = 273$ K; T_a is an ambient air temperature, K; e_a – water vapor pressure, kg/m^3; f – air humidity, in fractions of unit; $M_1 = (1 - \xi^2/R^2)/2 - (1 - \xi^3/R^3)/3$.

The fraction of ice in a drop (P) is calculated from the dependence of $P=1- \xi^3/R^3$.Then equation (1) can be transformed to the form, taking into account that $\tau = h/v_f$,

$$P = \frac{3\mathrm{Nu}}{109}\left[\frac{hM}{264v_fR^2}+M_1(P)\right],$$

where h is the drop-fall height; v_f is the drop-fall rate.

When the proportion of ice in a water droplet is $P < 0.6$, the contribution of the second term on the right-hand side of M_1 to P does not exceed 2.4 %.

For express-assessments, the resulting dependence has been simplified as much as possible. Thus, to calculate the fraction of ice (P) in a drop of fresh-water with a diameter of d = 1–2 mm, a simplified dependence has been obtained in the form of [*Sosnovsky, 1983*]

$$P = h\,|t_a|/(500d^2)$$

and taking into account that $h = \tau v_f$, we obtain

$$P = \tau v_f |t_a|/(500d^2), \qquad (2)$$

where t_a is the air temperature, °C; d is the droplet diameter, mm.

The calculations using the formulas (1) and (2) with an air temperatures of above –10 °C coincide

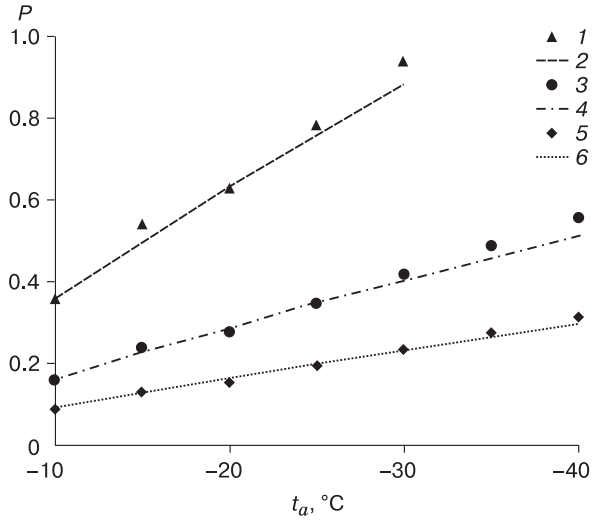

Fig. 1. Proportion of ice (*P*) in the drop of fresh water falling from a height of 18 m.

1, *3*, *5* – calculation by the simplified formula (2); *2*, *4*, *6* – calculation by the model dependence (1). Drop radius: *1*, *2* – 0.5 mm; *3*, *4* – 0.75 mm; *5*, *6* – 1 mm.

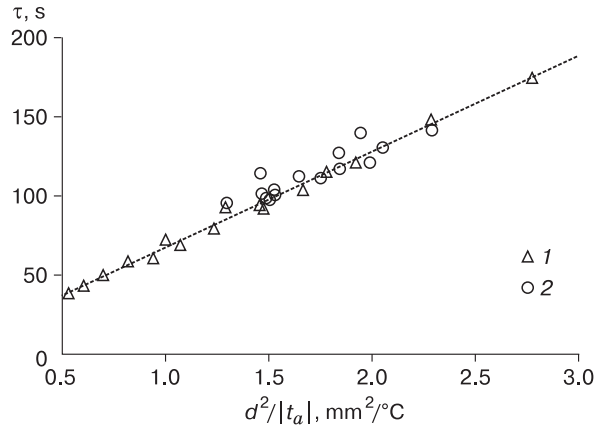

Fig. 2. Dependence of the time of complete freezing of fresh-water drops (τ) on the value of $d^2/|t_a|$:

1 – by the formula (2) for drops with a diameter of d = 3, 4 and 5 mm; *2* – by the data of the [*Balkarova et al., 2011*].

with an accuracy of 8 %. At lower air temperatures, the contribution of evaporation to heat transfer decreases; therefore, the calculations using the formula (2) overestimate the share of ice in a drop. To maintain an 8 % accuracy of calculations with an air temperature of –10...–40 °C, a correction factor is introduced: the results of calculations using the formula (2) are multiplied by 0.87. Because of that correction, the calculations by the formula (2) of the ice fraction for droplets with a diameter of 1–2 mm coincide with an accuracy of 8 % with the results of calculations by the formula (1) within the air temperature range of from –10 to –40 °C (Fig. 1).

The processing of the experimental data of the [*Mason, 1961*], carried out by the authors, has revealed that the droplet falling can be taken as $v_f = 6.42R^{0.63}$ m/s, where R is the radius in mm. In that case, the approximation confidence factor is $R^2 = 0.995$.

Let us compare the calculations by the formula (2) with the experimental data of other authors. In the [*Balkarova et al., 2011*], the results of measuring the time of complete freezing of fresh water droplets with a diameter of d = 3.8–5.2 mm with an air temperature t_a from –8 to –17.2 °C, floating freely in the air flow, are presented. The dependence of the time of complete freezing of a drop of fresh water τ according to the data of that work on the value of $d^2/|t_a|$ as well as the calculations by formula (2) of the value of τ at P = 1 (the proportion of ice in a drop of water when it is completely frozen) can be seen in Figure 2. It follows from Fig. 2 that the results of calculations of the time of complete freezing of a water drop according to the theoretical formula (2) and the measurements presented in the [*Balkarova et al., 2011*] have a good match.

FREEZING OF THE SALT-WATER DROPS IN THE COURSE OF WINTER SPRINKLING

The freezing of salt water occurs as a result of the selective growth of ice crystals, accompanied by the formation of cells and interbeds of brine between them [*Adams et al., 1963*]. As the temperature drops, new fresh-ice crystals fall out of the brine. Therefore, the salinity of the brine increases until a state of thermodynamic equilibrium is established at a given temperature. Thus, a certain phase composition corresponds to each value of the temperature of the ice formed from salt water.

When the drops of fresh water or slightly mineralized water (up to 10 g/L) freeze, an ice shell forms on the surface of the drop and thickens, reducing the radius of the liquid part. When water droplets with a higher salinity freeze, the branched crystals can grow deep into the liquid part of the droplet and penetrate into the brine. However, it is difficult to predict the growth of branched crystals. Moreover, as the drop freezes, the volume of its liquid part decreases, its mineralization increases, and its freezing temperature decreases. The amount of brine in the ice shell decreases as the ice cools because of the advance of the crystallization front.

The phase composition of salty ice depends on temperature and salinity. With a salt ice temperature

of above –8...–10 °C, in the first approximation, a linear relationship between the concentration of brine S_b (kg/m^3) in ice and the ice temperature t_i can be assumed [*Doronin, 1969*]:

$$S_b = \sigma t_i, \quad (3)$$

where $t_i = T_i - 273$; T_i is the ice temperature, K; the values of the σ coefficient depend on the freezing point of various salts, for sea water σ = –18.2 kg/(m^3·K). That dependence can be used to estimate the temperature of the beginning of freezing of the brine. As the salinity of the brine S_b increases, its freezing temperature t_i decreases in accordance with the formula (3).

Thermophysical calculations take into account the effective heat capacity of salted ice c_{ie}, which is equal to the weighted average value of the sum of the heat capacities of the crystalline ice c_i and the brine c_b, with taking into account the melting heat of ice L. The value of c_{ie} is determined by the formula [*Doronin, 1969*], with taking into account the salinity of ice S_i

$$c_{ie}(T_i) = c_i + (c_b - c_i)\frac{S_i}{\sigma(T_i - 273)} - \frac{LS_i}{\sigma(T_i - 273)^2}. \quad (4)$$

The problem of determining the dynamics of freezing of a drop of salt water is the uncertainty at the phase boundary, since it is not clear what part of the salts is rejected into the liquid part of the drop, lowering the freezing point of salt water at the phase front. Therefore, the extreme variants of the rejection of salt ions from the freezing boundary into the liquid part of the drop have been chosen:

1 – salt ions are not rejected into the liquid part of the drop, the salinity of the ice shell and of the liquid core are equal, while the effective heat capacity of ice is determined by formula (4);

2 – salt ions during the freezing are completely rejected into the liquid part of the drop, while the heat capacity of the ice shell is equal to the heat capacity of the crystalline ice c_i; the salinity of the liquid part of the drop increases with the increasing of the thickness of the ice shell of the drop, and the temperature of the onset of freezing (the phase transition temperature t_i) is recalculated at the known salinity of the brine (a liquid part of the drop) according to the formula (3).

For the first option, the empirical formula of V.L. Tsurikov determining the salinity of the sea ice depending on the rate of its growth can serve as some justification [*Nazintsev, Panov, 2000*]:

$$S_i/S_w = 7w^{0.5}/(7w^{0.5} + 10.3),$$

where S_i is the ice salinity, ‰; S_w is the salinity of sea water, ‰; w is the rate of ice growth, mm/h.

At a high growth rate of salted ice up to 20 mm/h (at low negative air temperatures and significant wind), the salinity of ice according to V.L. Tsurikov will be 75 % of the initial one. When a drop with a diameter of 1.5 mm freezes, even at a small negative air temperature of –10 °C, the freezing rate is 55 mm/h. In that case S_i/S_w = 0.83. At lower air temperatures the S_i/S_w rises to 0.9.

The rationale for the second option is as follows. The moisture content of the porous ice frozen from fresh water in the first few days is 10–12 %, and the water is located on the surface of ice crystals in the form of film moisture [*Sosnovsky, Khodakov, 1995*]. The experiments of the authors have demonstrated that when using the water with a salinity of up to 10 g/L, the salinity of the formed porous ice decreases by an order of magnitude, which corresponds to the preservation of about 10 % of unfrozen water in porous ice. Since part of the water remains on the surface of ice crystals, it can be assumed that when salt water freezes, almost all brine will also be concentrated in the film moisture on the surface of ice crystals, and the presence of brine cells inside the ice is insignificant. Such a scenario can occur if during the formation of ice shells of droplets, the capture of salt ions by growing ice crystals is insignificant, and most of them are rejected into the central unfrozen part of the droplet and flow out of the mass of porous ice when the ice shell breaks after falling.

The first option solves the problem of ice formation within the entire range of negative temperatures without isolating a freezing front. The problem is entirely due to the dynamics of heat exchange between a drop of water and the surrounding air, to the dependence of the effective thermal conductivity of salted ice and the dependence of the content of unfrozen water on temperature. When calculating the freezing of seawater in the [*Bogorodsky et al., 2009*], an extended section of the ice-unfrozen liquid mixture – a two-phase zone – is used, in the volume of which a phase transition occurs, and the liquidus condition is used (the line of complete melting of solid phases in the phase diagrams, above which there is only liquid). For an object of millimeter dimensions, it is advisable to apply the heat balance model for the entire volume of a drop, considered in the [*Sosnovsky, 1988*]. In that case, the change in the heat content of the drop

$$dQ_1 = -c_{ie}(T_i)\rho_w V_d\, dT_i$$

is determined by the heat flux at the drop boundary

$$dQ_2 = \alpha_{eff}(T_i(\tau) - T_{eff})F_d\, d\tau_s,$$

where α_{eff} and T_{eff} are the effective heat transfer coefficient and the reduced air temperature, respectively; F_d is the surface area of the drop; T_i is the temperature of the freezing drop; ρ_w and V_d are the water density and drop volume, respectively.

Equating dQ_1 and dQ_2, and solving the differential equation to determine the freezing time of salt water (τ_s), we obtain the following dependences:

$$\tau_s = -\frac{\rho_w V_d L}{\alpha_{eff} t_{eff} F_d}(f_i + \Delta f_i + A_i + A_b), \quad (5)$$

where

$$\Delta f_i = \frac{t_{i0}}{t_{eff}} \ln t_1, \; A_i = \frac{c_i t_{eff}}{L} \left(\Delta f_i - \ln \frac{1 - t_{i0} t_{eff}^{-1}}{1 - t_i t_{eff}^{-1}} \right),$$

$$A_b = \frac{-c_b t_{i0}}{L} \ln t_1, \; t_1 = \frac{1 - t_{eff} t_{i0}^{-1}}{1 - t_{eff} t_i^{-1}}, \; t_{eff} = T_{eff} - T_0,$$

where $t_i = T_{i0} - T_0$; T_{i0} is freezing point of salt water, K; $T_0 = 273$ K; $S_i = \sigma t_{i0}$; $f_i = 1 - t_{i0}/t_i$.

For water droplets 0.5–4.0 mm in diameter, the dependences can be used to determine α_{eff} (W/(m^2·K)) and T_{eff} (K) [*Sosnovsky, 1988*]:

$$\alpha_{eff} = 44.8 R^{-0.3},$$

$$T_{eff} = 61.06 \cdot 10^{-2} [T_a + 2.325(70.08 + 10^3 f_a e(T_a)],$$

where T_a, f_a are the temperature and relative humidity of air; $e(T_a)$ is density of saturated water vapor (kg/m^3) at air temperature T_a (K).

Since droplets with a radius $R \leqslant 1$ mm can be considered spherical, then $V_d/F_d = R/3$. The A_i and A_b values demonstrate the contribution to the intensity of freezing-up of the heat capacity of ice crystals and brine. The dependence of the heat capacity of fresh ice (c_i) and brine (c_b) on temperature and salinity is determined by the following empirical expressions [*Doronin, 1978*]:

$$c_i = 2.12 + 0.0078 t_i, \text{ kJ/(kg·K)},$$

$$c_b = 4.19 - 4.55 \cdot 10^{-3} S_b, \text{ kJ/(kg·K)}.$$

With the ice temperatures above –10 °C, the value of c_i can be taken equal to 2.08 kJ/(kg·K) with an accuracy of 2 %, while for $c_b = 3.73$ kJ/(kg·K) within the range of salinity of brine from 35 to 200 kg/m^3, the error is no more than 13 %. The authors' calculations reveal that taking into account the contribution of the values A_i and A_b to the intensity of freezing-up, the error in the application of the considered values of c_i and c_b does not exceed 0.2 and 0.4 %, respectively.

Let us assume that in the process of freezing of a water drop with an initial salinity S_0 at the time τ, the ice fraction will be $f_i(\tau)$. Then, taking into account that the precipitation of crystals of the main components of salts occurs at lower temperatures, we obtain the brine concentration $S_b = S_0/(1 - f_i)$ and $f_i = 1 - S_0/S_b$. Taking into account the equitation (3), we obtain $f_i = 1 - f_b$, where $f_b = S_0/(\sigma t_i)$. Thus, we get a relationship between the proportion of ice in a drop of water and its temperature.

The results of calculations of the ice fraction (f_i) in a freezing water droplet with a diameter of 1.5 mm depending on the fall time (τ) according to the first option (with the initial water mineralization of 35 g/L and the air temperatures of –10 °C, –20 °C and –40 °C) are demonstrated in Fig. 3. The time of

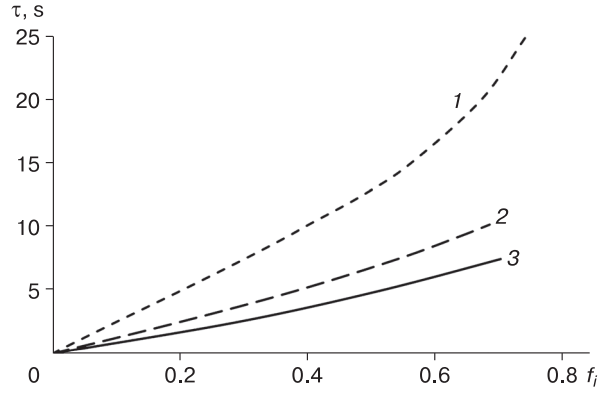

Fig. 3. Dependence of the proportion of ice (f_i) in a freezing drop on the time of falling (τ) according to the first option with the mineralization of the initial water of 35 g/L and air temperature of –10 °C (*1*), –20 °C (*2*), –40 °C (*3*).

falling of a water drop 1.5 mm in diameter from a height of 18 m is 3.3 s. At a water salinity of 35 g/L and the air temperature of –20 °C the water drops with a diameter of 1.5 mm, falling from a height of 18 m, will freeze by 27 % of their volume (Fig. 3). Whereas if the water is fresh, under the same initial conditions, the proportion of frozen water in the drop will increase by 11 %, reaching 30 % of its volume (Fig. 1). In that case, the temperature of the freezing drop of salt water will be –2.7 °C. At an air temperature of –10...–30 °C, the temperature of the drop of salt water falling from a height of 18 m will be –2.3 and –3.5 °C at the end of the fall, respectively.

Let us consider the second option, i.e. the complete rejection of salt ions from the freezing boundary into the liquid part of the drop. For mathematical modeling and calculations, we will accept (as in the case of a fresh water drop) a freezing scheme with the formation of an ice shell symmetrical advancing towards the center of the drop. The modeling assumes that the initial droplet temperature is equal to the freezing point at the initial salinity. In that case, the internal circulation of liquid in a freezing drop is not considered [*Sultana et al., 2017*].

In the presence of a phase boundary in a freezing water drop, the heat transfer and the freezing of water are described by the boundary-value problem of thermal conductivity provided that in the ice shell $\xi(\tau) < r < R$ and in the liquid part of the drop $0 < r < \xi(\tau)$, where r is the coordinate along the drop's radius:

$$\frac{\partial T_i}{\partial \tau} = a_i \left(\frac{\partial^2 T_i}{\partial r^2} + \frac{2}{r} \frac{\partial T_i}{\partial r} \right), \; \xi(\tau) < r < R,$$

$$\frac{\partial T_w}{\partial \tau} = a_w \left(\frac{\partial^2 T_w}{\partial r^2} + \frac{2}{r} \frac{\partial T_w}{\partial r} \right), \; 0 < r < \xi(\tau), \quad (6)$$

where T_w is the temperature of the liquid central part of the water drop.

The heat transfer condition on the droplet surface is

$$-\lambda_i \left.\frac{\partial T_i}{\partial r}\right|_{r=R} = \alpha_{eff}\left(T_i(R) - T_{eff}\right). \quad (7)$$

Stefan's condition at the freezing boundary provided $r = \xi(\tau)$ is

$$\lambda_i \frac{\partial T_i}{\partial r} - \lambda_w \frac{\partial T_w}{\partial r} = -L\rho_i k_i \frac{d\xi}{d\tau}. \quad (8)$$

At the freezing boundary, the temperature equality condition of the liquid and solid parts of the drop is applied.

In the central part of the drop with $r = 0$, the following condition is assumed:

$$\frac{\partial T_w}{\partial r} = 0. \quad (9)$$

In the initial period, the water temperature is taken equal to the freezing point of salt water (T_0): $T_w = T_0$, $\xi = R$ at $\tau = 0$.

Here the following designations are accepted: $a_i = \lambda_i/(c_i\rho_i)$ is the thermal diffusivity coefficient of ice, m^2/s; $a_w = \lambda_w/(c_w\rho_w)$ is the thermal diffusivity coefficient of water, m^2/s; λ_i is the thermal conductivity coefficient of ice, W/(m·K); c_i is the heat capacity of ice, kJ/(kg·K); ρ_i is ice density, kg/m^3; λ_w is the thermal conductivity coefficient of water, W/(m·K); c_w is the heat capacity of water, kJ/(kg·K); ρ_w is the density of water, kg/m^3; L is the heat of melting of ice, kJ/kg; k_i is the coefficient of influence, fraction of unit.

The k_i coefficient takes into account the influence of the spherical surface of the phase boundary on the freezing time of the next layer. When a water drop freezes, the time required to move the phase front to one spatial node of the computational grid decreases as the front shrinks to the center. Heat losses for the phase transition from a layer with radius ξ to a layer with radius $(\xi - \Delta\xi)$ are $(4/3) \times \times \pi\rho L(\xi^3 - (\xi - \Delta\xi)^3)$, where $\Delta\xi$ is the spacing of the spatial grid. The value of the heat flux through the phase surface during the time $\Delta\tau$ is equal to $4\pi\xi^2 Q_\xi \Delta\tau$, where Q_ξ is the left side of equation (8). Equating the heat loss to the value of the heat flux and neglecting the value of $\Delta\xi^3$, we obtain $k_i = 1 - \Delta\xi/\xi$.

INTENSITY OF WATER-DROP FREEZING

In the [*Sosnovsky, Glazovsky, 2018*], when solving the system of equations (6)–(9) and calculating the freezing intensity of a drop of salt water, the different variants of the growth of mineralization of the unfrozen part of the drop have been considered. Calculations have shown that the freezing time of a drop of salt water increases in comparison with the time of freezing of a drop of fresh water. That difference grows with an increase of the frozen part of the droplet and is most significant at low negative air temperatures. The freezing time of the droplet's half-volume for drops with the diameter of 1.5 mm (the water salinity is 35 g/L and the air temperature is –10 °C) is 25 % longer than that for fresh water, and 17 % longer at the air temperature of –20 °C. It has been assumed that 1/3 of the salt is retained in the ice shell of the drop when it freezes.

The system of equations (6)–(9) is solved for the water with a salinity of 35 g/L and the freezing point of –1.8 °C, providing the completely rejection of the salt ions from the freezing boundary into the liquid part of the drop and the formation of the fresh-ice shell. The droplet diameters of 1.0 mm, 1.5 mm, and 2.0 mm are taken for calculations. The intensity of water-drop freezing depends on the magnitude of the temperature difference between the air and the surface of the ice shell. According to the calculations by second option, the surface temperature of a drop of 1.5 mm in diameter is –3.8 °C at the moment when the half-volume of the droplet have been frozen. With complete rejection of salt from the freezing boundary, the salinity of the liquid core reaches 70 g/L.

An important parameter for heat transfer between air and a drop of water falling in a droplet plume is the time-weighted mean of the droplet surface temperature. As a result of solving the system of equations (6)–(9), the dependence of the temperature of droplet surface on the dynamics of droplet freezing has been calculated. Thus, at the moment when the half-volume of the drop with a radius of 1.5 mm has been frozen up, the time-weighted mean surface temperature is –2.8 °C for an air temperature of –20 °C. At that, the surface temperature depends mainly on the percentage of the frozen droplet volume and, to a lesser extent, on the air temperature. So, for a drop with a diameter of 1.5 mm the surface temperature at the moment when half-volume of the droplet has been frozen up (according to the second option of calculation) is –3.7, –3.9 and –4.1 °C for the air temperatures –10, –20 and –40 °C, respectively.

The results of calculating of the freezing time of a water drop 1.5 mm in diameter depending on the ice percentage according to the second option for different air temperatures are demonstrated in Fig. 4. During the fall of a drop from a height of 18 m, 0.14, 0.20, 0.24 and 0.39 of the droplet's volume has time to freeze up at the air temperatures of –10, –15, –20 and –40 °C, respectively.

The calculations by the formula (1) have revealed that for the air temperature of –20 °C, it takes 5.6 seconds to freeze the half-volume of a drop of fresh water with a diameter of 1.5 mm. For salt water, according to the 1st option of calculations, the freezing of the droplet's half-volume takes 21 % more time,

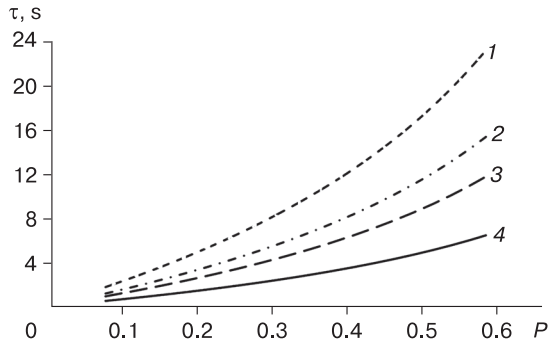

Fig. 4. Dependence of the freezing time of a drop with a diameter of 1.5 mm (τ) on the volume proportion of ice (*P*) with complete rejection of salt for air temperature of –10 °C (*1*), –15 °C (*2*), –20 °C (*3*), –40 °C (*4*).

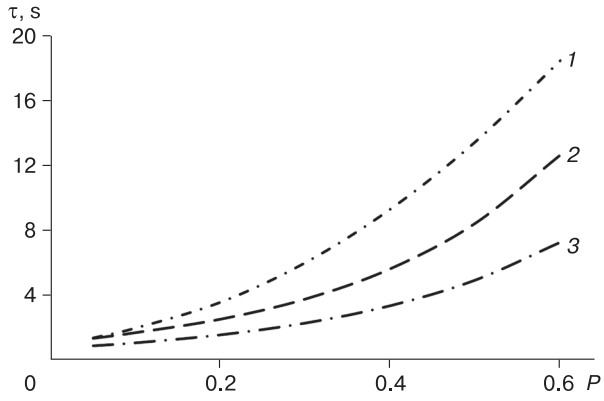

Fig. 5. Dependence of the freezing time of a water drop (τ) on the proportion of ice volume (*P*) according to the second option of calculations for an air temperature of –20 °C for drops with a diameter of 2.0 mm (*1*), 1.5 mm (*2*), 1.0 mm (*3*).

i.e. 6.8 seconds (Fig. 3); and according to the 2nd option, the same takes 8.4 seconds (Fig. 4). During the fall of a drop from a height of 18 m for an air temperature of –20 °C, 24 % of the ice volume freezes according to the 2nd variant of calculations (Fig. 4). That is 8 % less than by the 1st option of calculation and 25 % less than for fresh water.

For low negative air temperatures in order to increase the freezing-up performance the droplet size is reduced by using the nozzles of a smaller diameter. The influence of the droplet's size (diameters of drops are 1.0, 1.5 and 2.0 mm) on the intensity of freezing-up according to the 2nd option of calculations is demonstrated in Fig. 5. It reveals that for an air temperature of –20 °C, the freezing time of the droplet's half-volume according to the second variant of calculations are 4.9, 8.4 and 13.4 seconds for drops with diameters of 1.0, 1.5 and 2.0 mm, respectively.

HEAT EXCHANGE IN DROPLET PLUME

In the droplet plume, the air is heated due to the heat exchange of the falling water drop with the air and the release of the latent heat of ice formation. The intensity of heat release depends, among other things, on the temperature difference between the surface of the freezing water drop and the air in the plume. With an increase in the salinity of the initial water and an increase in the proportion of ice in the drop, the drop temperature and, as a consequence, the heat exchange rate decreases, reducing as a result the heating of air in the plume. The authors' calculations have demonstrated that during the fall of a drop (1.5 mm in diameter) its average temperature is –2.0 and –2.7 °C for salt frozen water (salinity of 35 g/L) and about –0.3 and –0.4 °C for fresh water at the air temperature of –10 and –40 °C, respectively.

For an assessment of the increase in air temperature in the droplet plume, in the [*Sosnovsky, 1983*], the dependence has been obtained in the form of:

$$\Delta T = \frac{T_i - T_a}{1 + 0.0121 v_1 R^{1.93} S_l G^{-1}}, \qquad (10)$$

where T_a is the temperature of the atmospheric air, K; T_i is the temperature of ice in a drop, K; v_1 is the speed of ventilation of the plume by the wind (the speed of blowing-off a drop of water by the wind is the difference between the speed of the wind and the horizontal speed of movement of the drop under the influence of wind force), m/s; R is the radius of drops, mm; S_l is plume length, m; G is water flow rate of the sprinkler, m^3/s.

The ventilation speed v_1 of a drop with a diameter of d = 1.5 mm is about 1.3 m/s for a wind speed of 5 m/s [*Sosnovsky, 1983*]. For $G/S_l = 18 \cdot 10^{-4}$ m^2/s (G = 0.065 m^3/s, S_l = 40 m), using the formula (10), we obtain the air temperatures of –8.7 and –33.9 °C for the ambient air temperature of –10 and –40 °C, respectively, in the plume for the water droplets with a diameter of 1.5 mm and a salinity of 35 g/L. For fresh water, the air temperatures in the plume are –8.3 and –33.6 °C for the ambient air temperature of –10 and –40 °C, respectively. As a result, the temperature of falling-in-air water droplets are higher than the temperature of the ambient air, and the proportion of the ice frozen-up in the plume is lower. The air temperatures in the droplet plume of fresh water differ slightly from those of salt one. Therefore, the main difference between the freezing of fresh water and salt one in the droplet plume is due to the peculiarities of salt-water-drops freezing.

To calculate the productivity of freezing salt water during winter sprinkling, we use the formula for the volumetric freezing of a drop (5) and the formula (10) for calculating the air temperature in a droplet

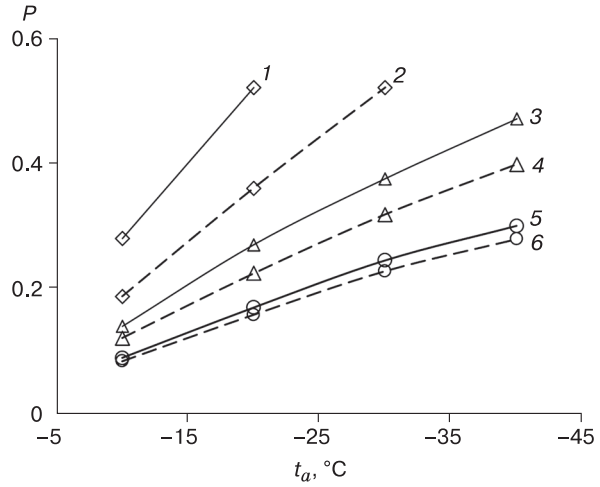

Fig. 6. Dependence of the proportion of ice (*P*) on the temperature (*1*, *3*, *5*) in a drop of water with a salinity of 35 g/L and in a droplet plume (*2*, *4*, *6*) 18 m high for drops with a diameter of:

1, *2* – 1.0 mm; *3*, *4* – 1.5 mm; *5*, *6* – 2.0 mm.

plume. The results of calculations of the dependence of the ice proportion in the water droplet with a salinity of 35 g/L and a diameter of 1.0, 1.5, and 2.0 mm as well as in the droplet plume on the air temperature are demonstrated in Fig. 6. For water droplets with a diameter of 1.5 mm, the difference in the ice proportion in an individual droplet and in a droplet plume is 15–18 %, whereas for the drops with a diameter of 2 mm, that difference is 6–8 %, and for those with a diameter of 1 mm, it is more than 44 %.

CONCLUSION

An assessment of the intensity of freezing of salt-water drops during winter sprinkling has been accomplished . A simplified relationship which makes it possible to estimate the proportion of ice in a drop of fresh water for an ambient temperature below –10 °C has been obtained. According to the data of independent studies, the model of freezing of fresh-water drops has been verified. The freezing of water droplets with increased mineralization, in particular, sea-water droplets, has been considered. When salt-water droplets freeze during the rapid ice formation process, both the growth of branched crystals permeating the entire volume of the droplet and, possibly, the formation of a phase front (as in a drop of fresh water or slightly mineralized one) can occur.

When solving the phase problem of freezing of a salt-water drop, the main problem is the uncertainty in determining the amount of the salts captured by the growing ice, and accordingly, in the increase of the salinity of the liquid part of the drop. To assess the influence of that uncertainty, the extreme variants of salt rejection are considered: 1) salt ions are not rejected into the liquid part and their uniform distribution over the droplet volume is maintained; 2) salt ions are completely rejected into the liquid part of the freezing droplet. At that, different models of freezing of a drop of water were applied: in the first case, it was a previously developed model of volumetric freezing, in the second case, the front problem of freezing of a drop of salt water was solved with the Stefan condition at the phase boundary. After a series of calculations, for the first time, a comparison of the intensity of ice formation has been made for the considered freezing models. The results of calculations for an air temperature of –20 °C have revealed that according to those models the difference in the proportion of ice in a drop of salt water is about 8 %. Due to the slight difference in the intensity of freezing-up of a drop of water, it is advisable to use a simpler scenario of volumetric freezing for the calculations.

For the first time, the calculations of the increase in air temperature in a droplet plume of salt water are given. On their basis, the proportion of ice in a drop of salty water falling in the atmospheric air and in the droplet plume has been determined, depending on the air temperature and the size of the drops. Calculations have shown that for water droplets with a diameter of 1.5 mm, the difference in the proportion of ice in an individual droplet and in a droplet plume is 15–18 %.

Acknowledgements. *Mathematical modeling and analysis of archival materials have been carried out within the framework of the State Assignment No. 0148-2019-0004. Calculations, processing and analysis of experimental data have been carried out with the support of the program of the Presidium of the Russian Academy of Sciences No. 22 "Perspective physicochemical technologies for special purposes". Expeditionary research on the Svalbard archipelago has been carried out with the financial support of the State Assignment (No. 0127-2019-0009) and logistic assistance from the Russian Scientific Center on Svalbard (RSCS).*

References

Adams, C.M., French, D.N., Kingery, W.D., 1963. Field solidification and désalinisation of sea ice. In: Ice and Snow. Cambridge, M.I.T. Press, pp. 277–288.

Alekseenko, S.V., Mendig, C., Schulz, M., Sinapius, M., Prihod'ko, A.A., 2016. An experimental study of the freezing process of a supercooled surface drop. Pis'ma v zhurnal tekhnicheskoj fiziki [Letters to the Journal of Technical Physics], No. 10 (42), 54–61.

Balkarova, S.B., Shogenova, M.M., Dugarlieva, M.K., 2011. Experimental and theoretical study of the patterns of crystallization of water droplets in an air stream. In: Applied aspects of geology, geophysics and geoecology using modern information technologies. Materials of the International Scientific-Practical Conference. "Magarin Oleg Grigor'evich", Maykop, pp. 5–9 (in Russian).

Biggar, K.W., Donahue, R., Sego, D., Johnson, M., Birch, S., 2005. Spray freezing decontamination of tailings water at the Colomac Mine. Cold Regions Sci. and Technol., No. 42, 106–119.

Bogorodsky, P.V., Makshtas, A.P., Pnyushkov, A.V., 2009. Ice accumulation under conditions of non-stationary characteristics of the energy exchange of the ocean and atmosphere. Okeanologiya [Oceanology], No. 3 (49), 359–367.

Doronin, Yu.P., 1969. Thermal interaction of the atmosphere and hydrosphere in the Arctic. Gidrometeoizdat, Leningrad, 300 pp. (in Russian).

Doronin, Yu.P., 1978. Ocean Physics. Gidrometeoizdat, Leningrad, 295 pp. (in Russian).

Gao, W., Smith, D.W., Sego, D.C., 2004. Release of Contaminants from Melting Spray Ice of Industrial Wastewaters. J. Cold Regions Engineering, No. 18, 35–51.

Gordeichik, A.V., Sosnovsky, A.V., 1982. The application of spray-cone freezing of ice for construction of ice-crossing over the river Lena River. Materialy Glyatsiologicheskikh Issledovaniy [Data of Glaciological Studies], No. 45, 159–162.

Kubyshkin, N.V., Buzin, I.V., Golovin, N.V., Gudoshnikov, Yu.P., Zamarin, G.A., Skutin, A.A., 2018. Aspects of ice engineering for the aims of construction of the transport infrastructure and reconnaissance drilling in the Arctic. Problemy Arktiki i Antarktiki [Problems of Arctic and Antarctic], No. 4 (64), 407–426.

Kulyakhtin, A., Tsarau, A., 2014. A time-dependent model of marine icing with application of computational fluid dynamics. J. Cold Regions Science and Technology 104–105, 33–44.

Mason, B.J., 1961. The physics of Clouds. Gidrometeoizdat, Leningrad, 542 pp. (in Russian).

Nazintsev, Yu.L., Panov, V.V., 2000. Phase Composition and Thermophysical Characteristics of Sea Ice. Gidrometeoizdat, St. Petersburg, 84 pp. (in Russian).

Design, Construction, and Maintenance of Winter Motor Roads under Conditions of Siberia and the North-East of the USSR, 1991. VSN (All-Russia Construction Rules) 137–89. Moscow, Mintransstroy, 177 pp. (in Russian).

Shibkov, A.A., Zheltov, M.A., Zolotov, A.E., Denisov, A.A., Gasanov, M.F., Grebenkov, O.V., 2013. Morphological transitions between Euclidean and fractal forms of ice growth in strongly supercooled water. Vestnik Tomskogo gosudarstvennogo universiteta [Bulletin of the Tomsk State University], 18 (5), 2804–2809.

Smorodin, B.L., Kalinin, N.A., Davydov, D.V., 2014. Modeling the process of changes in droplet temperature during freezing precipitation. Meteorologiya i gidrologiya [Meteorology and Hydrology], No. 9, 34–40.

Smorygin, G.I., 1988. Theory and Methods of Artificial Ice Production. Nauka, Novosibirsk, 282 pp. (in Russian).

Sosnovsky, A.V., 1980. Freezing of drops of the artificial rain. Materialy Glyatsiologicheskikh Issledovaniy [Data of Glaciological Studies], No. 38, 54–59.

Sosnovsky, A.V., 1983. Computations of the ice formation efficiency under spray-cone freezing. Materialy Glyatsiologicheskikh Issledovaniy [Data of Glaciological Studies], No. 47, 228–232.

Sosnovsky, A.V., 1988. Estimation of the rate of spray-cone freezing of ice from saline water. Materialy Glyatsiologicheskikh Issledovaniy [Data of Glaciological Studies], No. 61, 149–154.

Sosnovsky, A.V., 1993. On the impact of supercooled dropes of water on the rate of spray-cone freezing of ice. Materialy Glyatsiologicheskikh Issledovaniy [Data of Glaciological Studies], No. 77, 165–168.

Sosnovsky, A.V., Glazovsky, A.F., 2018. Freezing of mineralized water droplets in winter sprinkling. In: IOP Conf. Series: Earth and Environmental Science, No. 193, 012063. Polar Mechanics. IOP Publishing, DOI: 10.1088/1755-1315/193/1/012063.

Sosnovsky, A.V., Khodakov, V.G., 1995. Artificial ice formation in natural conditions for handling environmental problems. Materialy Glyatsiologicheskikh Issledovaniy [Data of Glaciological Studies], No. 79, 3–6.

Sultana, K.R., Pope, K., Lam, L.S., Muzychka, Y.S., 2017. Phase change and droplet dynamics for a free falling water droplet. Intern. J. Heat and Mass Transfer 115, 461–470.

Vilfand, R.M., Golubev, A.D., 2011. Meteorological conditions of freezing rain December 25–26, 2010 over the center of the European part of Russia. Led i Sneg [Ice and Snow], No. 3 (115), 119–124.

Received December 10, 2019
Revised version received November 11, 2020
Accepted November 17, 2020

EARTH'S CRYOSPHERE
SCIENTIFIC JOURNAL

Kriosfera Zemli, 2021, vol. XXV, No. 1, pp. 40–47

METHODS OF CRYOSPHERIC RESEARCH

MODELING THE WAYS OF THE MORPHOLOGICAL PATTERN DEVELOPMENT FOR THERMOKARST PLAINS WITH FLUVIAL EROSION

A.S. Victorov, T.V. Orlov, V.N. Kapralova, O.N. Trapeznikova

Sergeev Institute of Environmental Geoscience, Russian Academy of Sciences, Ulansky lane 13, buld. 2, Moscow, 101000, Russia; vic_as@mail.ru

The research deals with four different hypotheses on the development of thermokarst plains with fluvial erosion based on the mathematical modeling of their morphological pattern. The models result from the mathematical morphology of landscapes, which broadly uses the random processes theory. The analysis revealed that each way of the development is characterized by a specific probabilistic distribution of sizes, areas of thermokarst lakes first of all. The empirical testing was done for 17 key sites with different environmental and permafrost conditions in Western and Eastern Siberia, and Canada. Our analysis revealed that in the majority of cases the areas of the thermokarst lakes within the homogenous sections of the thermokarst plains with fluvial erosion obey the integral exponential distribution. Hence, the model of the morphological pattern corresponding to the asynchronous start of thermokarst process is valid, and the increase in the size of the lakes is proportional to the heat loss density through the side surface. Thus, the morphological pattern of the vast areas of thermokarst plains with fluvial erosion is in a state of dynamic equilibrium, which should be taken into account when predicting its development and assessing natural risks.

Key words: *mathematical morphology of the landscapes, thermokarst plains with fluvial erosion, morphological pattern.*

INTRODUCTION

One of the most interesting objects in permafrost studies is the dynamics of landscapes developed in it [*Kirpotin et al., 2008; Kravtsova, Bystrova, 2009; Polishchuk, Polishchuk, 2013; Grosse et al., 2016*]. It is especially important to analyze the development of permafrost landscapes over a long time period. In recent studies, an attempt to solve a similar problem in relation to lacustrine-thermokarst plains was made [*Victorov et al., 2015*], but the dynamics of thermokarst plains with fluvial erosion has not been studied in detail.

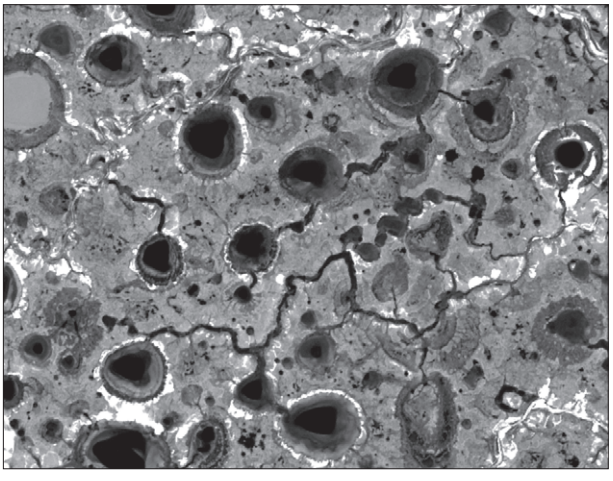

Fig. 1. A typical image of a site of thermokarst plain with fluvial erosion on a satellite image.

The purpose of the work is to study the regularities of changes in the morphological structure of thermokarst plains with fluvial erosion under different ways of its development.

The landscape of thermokarst plain with fluvial erosion is a slightly undulating flat surface with tundra or forest-tundra vegetation (cotton grass tundra, sedge-cotton grass tundra, etc.), with lakes, khasyreys and sparce erosion network (Fig. 1). The lakes are often rounded and scattered around the plain. Khasyreys are flat-bottomed peaty depressions with gentle slopes, also of isometric shape, occupied by grassland or swamp vegetation and, similarly to lakes, are disorderly located on the plain. Small residual lakes along the periphery and large lakes in the central part can remain inside the khasyrey. Secondary permafrost aggradation and development of frost mounds are possible within the khasyrey. It is generally accepted that khasyreys are formed as a result of drainage of thermokarst lakes, most often as a result of erosion.

The landscape of considered plains is under the complex influence of thermokarst, thermal abrasion

and thermal erosion processes, which are manifested in the following elements:

– new primary thermokarst depressions appear;

– thermokarst depressions grow independently of each other like lakes due to thermal abrasion;

– at a random moment, the lake can be drained by erosion and turns into a khasyrey, while the growth of the basin stops due to the lack of water body.

Thus, the authors believe that the main reason for the lateral lake growth is the process of thermal abrasion. In particular, commonly rounded lake shape indicates this.

In the study, various versions of hypotheses for the development of the thermokarst plains with fluvial erosion on the basis of mathematical modeling of their morphological structure have been considered. Four hypotheses have been considered, each with its own mathematical model of development (models 1.0, 1.1, 2.0, 2.1). Hypotheses differs in the initial assumptions, which are analyzed in detail below (Table 1). The main differences between the initial assumptions are the ideas about the appearance of primary thermokarst depressions (synchronous or extended in time) and about the rate of growth (constant or changeable over time).

The model creation is based on the approaches of the mathematical morphology of landscapes [*Victorov, 2006; Kapralova, 2014*] using the theory of random processes.

METHODS OF THERMOKARST PLAINS DEVELOPMENT STUDYING

The model of the morphological structure of thermokarst plains with fluvial erosion describes an area with homogeneous environmental and permafrost conditions, under the modern climate. The model does not assume absolute homogeneity, but only statistical one. Model 1.0 is based on the following assumptions:

1. The process of thermokarst initiation occurred in a short period of time ("synchronous start"); it was probabilistic and went independently on non-overlapping sites, while the probability of depression formation on the test site depended only on the area of the test site[1].

2. The change in the radius of the resulting thermokarst depression is a random process; it occurs independently of other lakes, and its rate is proportional to the density of heat losses through the lateral submerged surface of the lake basin.

3. Growing lake can turn into a khasyrey in case of its drainage. The probability of that does not depend on other lakes. The growth of the lake stops after drinage.

Table 1. **Versions of considered models of the morphological pattern development**

Model	Assumptions	
	Start	Size growth
1.0	Synchronous	Proportional to the heat loss density
1.1	Asynchronous	Same
2.0	Synchronous	Quasi-uniform
2.1	Asynchronous	Same

4. The inception of erosional forms on non-intersecting areas are independent random events; the probability of the presence of initial erosional forms on the test site depends only on its area[2].

Let us clarify the second assumption. During the thermoabrasional interaction of the lake water mass with the edges not only the mechanical effect, but also the thermal effect of water on the edge plays an important role. Permafrost degrades while ground ice inside it melts out. The thermal effect works mainly on the underwater part of the lake. It seems natural to assume that the more heat of the lake's water mass is spent on ground ice melting at 1 square meter of the underwater side of the basin (in the article this value is conditionally named "density of heat losses"), the faster, other things being equal, the degradation of permafrost proceeds increasing the size of the lake. This simplified view was the basis for the second assumption.

For the case of a synchronous start, the following initial dependences obtained earlier in the mathematical morphology of the landscape remain to be valid [*Victorov, 2006*]:

– distribution of the radius of growing thermokarst lake in time t after the emergence of a given lake (logarithmically normal distribution)

$$f_0(x,t) = \frac{1}{\sqrt{2\pi}\sigma x\sqrt{t}} \exp\left(-\frac{\left(\ln x - at\right)^2}{2\sigma^2 t}\right), \quad (1)$$

where a, σ are parameters, t is time elapsed from the beginning of the process;

– distribution of the distance from the center of the growing lake to the head of nearest erosional form which could stop the lake growth with transformation into a khasyrey (Rayleigh distribution)

$$F(x) = 1 - \exp\left(-\pi\gamma x^2\right), \quad (2)$$

where γ is average density of the heads of erosional forms[3]; $P(k) = \frac{\lambda^k}{k!}\exp(-\lambda)$ – distribution of number

[1] In that case, the probability of formation of more than one depression is infinitely small value of a higher order than the probability of formation of one depression.

[2] In that case, the probability of occurrence of more than one initial erosional form is infinitely small of a higher order than the probability of occurrence of one initial erosional form.

[3] The average density of the heads of erosional forms is the average number of heads per the area unit (km^{-2}).

of primary depressions on the test site occurred at the beginning of thermokarst process (Poisson distribution).

Subsequently, the average density of the lakes decreases in accordance with the possibility of their transformation into khasyreys. Since the probability of lake's turning into a khasyrey does not depend on the location of the lake, it is easy to demonstrate that the distribution of the number of lakes and the number of khasyreys on the test site at any time remains to be Poissonian.

The distribution of the radii of khasyreys at an arbitrary moment is determined by the distance to the nearest head of the erosional form which will stop the growth, and, hence, the distribution of the area of the khasyreys under a long-term development corresponds to an exponential distribution [*Victorov et al., 2016*].

The distribution of the radii of thermokarst lakes at an arbitrary point in time is determined by the distribution of the corresponding radius under conditions of free growth, but given that the lake will not become a khasyrey, that is, the distance to the head of erosional form will be greater than the lake radius

$$f_l(x,t)=\frac{f_0(x,t)\exp\left(-\pi\gamma x^2\right)}{\int\limits_0^{+\infty} f_0(u,t)\exp\left(-\pi\gamma u^2\right)du}. \qquad (3)$$

Using the expression for free lake growth (1) and simplifying it due to the identical terms in the numerator and denominator, which depend only on time, we find that under long-term development ($t\to+\infty$) the density of the lake radius distribution tends to the limiting distribution

$$f_l(x,\infty)=\frac{x^{a/\sigma^2-1}\exp\left(-\pi\gamma x^2\right)}{\int\limits_0^{+\infty} x^{a/\sigma^2-1}\exp\left(-\pi\gamma x^2\right)dx},$$

which is χ distribution. Hence, taking into account the circular shape of the lake, we obtain that the limiting distribution for the lake area is the gamma distribution

$$f_{sl}(x,\infty)=\frac{\gamma^{a/2\sigma^2}}{\Gamma\left(a/\left(2\sigma^2\right)\right)}x^{a/2\sigma^2-1}\exp\left(-\gamma x\right),$$

where $\Gamma(x)$ is the gamma function.

Thus, based on the assumptions of the model, the main expressions describing the features of the morphological structure of the thermokarst plains with fluvial erosion and its dynamics have been obtained in the version 1.0 of the model.

The second version of the model (1.1) differs from the first in the assumption 1a ("asynchronous start"):

1a. Emergence of the primary thermokarst depressions (initial point) for non-intersecting time intervals and at non-overlapping areas is independent random events; the probability of depression formation depends only on the duration of the time interval and the size of the site[4].

Model 1.1 introduces an additional fifth assumption:

5. The emergence of primary thermokarst depressions does not occur in the area of existing thermokarst lakes.

For the case of asynchronous start, two initial dependences obtained earlier ((1) and (2)) also remain valid.

Analysis of the model's assumptions allows one to obtain significant conclusions about the process dynamics. The formation of primary thermokarst depressions in a lake-free area without erosion is described by a Poisson process, as has been demonstrated earlier (for example, [*Victorov 2006; Victorov et al., 2016*]). However, if we take into account the second assumption of the model (primary depressions are formed only outside the lakes area), then the density of primary depressions formation is variable

$$\lambda_1(t)=\lambda\left[1-P_l(t)\right],$$

where $P_l(t)$ is the area percentage. The function $P_l(t)$, as shown earlier (for example, [*Victorov, 2006*]), is related with the process parameters through the dependence:

$$P_l(t)=1-\exp\left[-\tau(t)s(t)\right], \qquad (4)$$

where $s(t)$ is average lake area at a point of time t; $\tau(t)$ is average number of lakes per unit area at a time t.

The distribution of the number of lakes, as well as khasyreys, remains Poissonian, since the probability of turning into khasyreys does not depend on the location of the lake.

The distribution density of the lake radii at the moment of time t will be equal to the ratio of the number of lakes with a given radius (taking into account the different times of their initiation and the probability of preservation without turning into khasyreys) to the total number of lakes, and after simplification it will be:

$$f(x,t)=\exp\left(-\pi\gamma x^2\right)\int\limits_0^t\left[1-P_l(u)\right]f_0\left(x,t-u\right)du\times$$

$$\times\left[\int\limits_0^t\left[1-P_l(u)\right]\int\limits_0^{+\infty}\exp\left(-\pi\gamma x^2\right)f_0\left(x,t-u\right)dxdu\right]^{-1}. \qquad (5)$$

[4] In that case, for the small areas and short time intervals, the probability of formation of several depressions is much less than of a single one.

The model allows one to obtain an expression describing the dynamics of the lake area percentage. Using the above-mentioned law of the lake radius distribution to determine the value of the average area of the lake, and the expression for the average density of the lake location and the expression (4), after simplification and taking the logarithm, we can obtain the integral equation [*Victorov, 2006*]:

$$\ln\left[1-P_l(t)\right]=-\pi\lambda\int_0^t\left[1-P_l(u)\right]\times$$

$$\times\int_0^{+\infty}x^2\exp\left(-\pi\gamma x^2\right)f_0\left(x,t-u\right)dxdu, \qquad (6)$$

the solution of which is the function of lake area percentage.

Of particular interest is *long-term behavior of each process*, since quite often the researcher is faced-up with longstanding processes. Using the integral equation (6), it can be demonstrated that if the integral of lake area percentage

$$I=\int_0^{+\infty}\int_0^{+\infty}x^2\exp\left(-\pi\gamma x^2\right)f_0(x,u)dxdu,$$

converges and solution of the equation[5]

$$\ln\left[1-P_l^*\right]=-\lambda\pi\left[1-P_l^*\right]I$$

does not exceed $(1-e^{-1})$, that is 0.63, then there exists a limit of the function $P_l(t)$ with $t\to+\infty$, and it is equal to the solution of that equation $\left(P_l^*\right)$. The proof is based on the construction of a pair of step functions bounding the function $P_l(t)$ from above and below. Using the equation (6), it can be demonstrated that under the above condition, both step functions converge to a single limit. According to the well-known theorem, the function $P_l(t)$ must also have the same limit.

Under those conditions, ensuring the existence of the limiting value of the lake area $\left(P_l^*\right)$, there is also a limiting distribution of the radii of the lakes with $t\to+\infty$. Using the expression (1) for the distribution density of the lake radius under free growth and calculating the upper integral of the expression (5) at $t\to+\infty$ as the value of the Laplace transformation [*Victorov, 2006*], we obtain that the distribution of the lake area with the area of the primary depression ε will correspond to the expression

$$f_{sl}(x,\infty)=-\frac{2}{x\mathrm{Ei}(-\gamma\varepsilon)}\exp\left(-\gamma x\right),\quad x\geq\varepsilon,$$

where $\mathrm{Ei}(-x)$ is an integral exponential function. Lake area distribution can be called "integral-exponential". Finally, it follows from the obtained result [*Victorov, 2005*] that in that case there is a limiting value for the average number of lakes per unit area.

Thus, according to the model 1.1, after a long $(t\to+\infty)$ time, a dynamic equilibrium is established in the processes of generation of the thermokarst lakes (initial formation of primary thermokarst lakes) and their transformation into khasyreys.

The third version of the model (model 2.0) is based on the assumption of a synchronous start, as well as on the assumption that the lake growth occurs quasi-uniformly. The basis for that assumption is empirical data [*Burn, Smith, 1990; Smith et al., 2005*]. In that case, the second assumption is changed:

2a. The change in the radius of the resulting thermokarst depression is a random process; the change per unit of time is an independent, equally distributed random variable.

For that option, the first initial dependence is altered [*Victorov et al., 2015*], i.e. the radius distribution of a freely growing thermokarst lakes obeys the normal distribution

$$f_0\,(x,t)=\frac{1}{\sqrt{2\pi}\sigma\sqrt{t}}\exp\left(-\frac{(x-at)^2}{2\sigma^2t}\right), \qquad (7)$$

where a, σ are the distribution parameters, t is time elapsed since the beginning of the process.

The distribution of lake radii is determined by the expression (3), but with a free growth function corresponding to quasi-uniform growth (7). Calculating the integral and simplifying, we find that at any moment of time the lake radii must obey the normal law with following density of distribution:

$$f_l\,(x,t)=\frac{1}{\sqrt{2\pi}\sigma_l(t)}\exp\left(-\frac{\left[x-a_l(t)\right]^2}{2\sigma_l^2(t)}\right),$$

were $a_l(t)=\dfrac{at}{2\pi\gamma\sigma^2t+1}$, $\sigma_l(t)=\sigma\sqrt{\dfrac{t}{2\pi\gamma\sigma^2t+1}}$.

Passing to the limit, we find that with $t\to\infty$ the distribution of lake radii in model 2.0 is also close to the normal one.

In the fourth version of the model (2.1) the first assumption is replaced by 1a (asynchronous start), and, as in model 1.1, an additional fifth assumption appears about the impossibility of new thermokarst depressions generation within existing lakes. For that option, two initial dependencies are preserved: the distribution of the radius of a freely growing thermokarst lake in time t after the emergence of that lake, which obeys a normal distribution, and the Rayleigh distribution of the distance to the heads of erosional forms.

Analysis of the model 2.1, as in the model 1.1, leads to the conclusion about the Poisson distribu-

[5] It can be demonstrated that the equation always has a solution, and a sole one.

Table 2. **Pattern of lake size distribution for different models**

Model	The type of statistical distribution of lake sizes
1.0	Gamma distribution
1.1	Integral-exponential distribution
2.0	Normal distribution (average radius)
2.1	Gamma distribution

tion of both lakes and khasyreys. Performing similar analysis under longer development time, we also find that under general conditions, a dynamic equilibrium is established between the processes of generation of the thermokarst lakes and their transformation into khasyreys, and we also find that the exponential distribution of the areas of khasyreys is valid.

The distribution density of the radius of lakes under long-term development can be determined using the expression for the limiting distribution of the radius in the model 1.1, if we replace the density function of the radius distribution with free growth by (7)

$$f_l\ (x,\infty) = \sqrt{\gamma}\exp\left(-\pi\gamma x^2\right), \quad x \geq 0,$$

and, therefore, the area of lakes obeys the gamma distribution in that model, but with a fixed value of the shape parameter equal to 0.5

$$f_{sl}(x,\infty) = \sqrt{\frac{\gamma}{\pi}}\frac{\exp\left(-\gamma x\right)}{\sqrt{x}}.$$

Analysis of hypotheses about the development of thermokarst plains with fluvial erosion reveal that the ways differ in the distribution patterns of the lake areas (Table 2).

EMPIRICAL VERIFICATION AND RESULTS OF RESEARCH OF THERMOKARST PLAINS DEVELOPMENT

Empirical verification included analysis of the correspondence of thermokarst lakes areas distribution to different types of distribution. The results of comparing the correspondence of the distribution of the number of centers of lakes and khasyreys on a randomly selected site to Poisson's law have already been published and there is a good agreement [*Victorov et al., 2019a*], the same applies to the distribution of areas of khasyreys [*Victorov et al., 2019b*].

For empirical verification of thermokarst lakes areas distribution the sites with different environmental and permafrost conditions have been selected (Fig. 2, Table 3). The following satellite imagery were used: Corona (2–10 m/pix, 1965–1976); medium resolution Sentinel 2A images 2018–2019, 10 m/pix; high resolution images 0.5–1.5 m/pix (SPOT 6, 7, WorldView 2, June–August 2013–2019), both specially ordered and obtained from open sources (Google, Bing, Yandex mosaics). The latest surveys from 2013–2019 are named *term 2*, and the data from Corona imagery is named *term 1*.

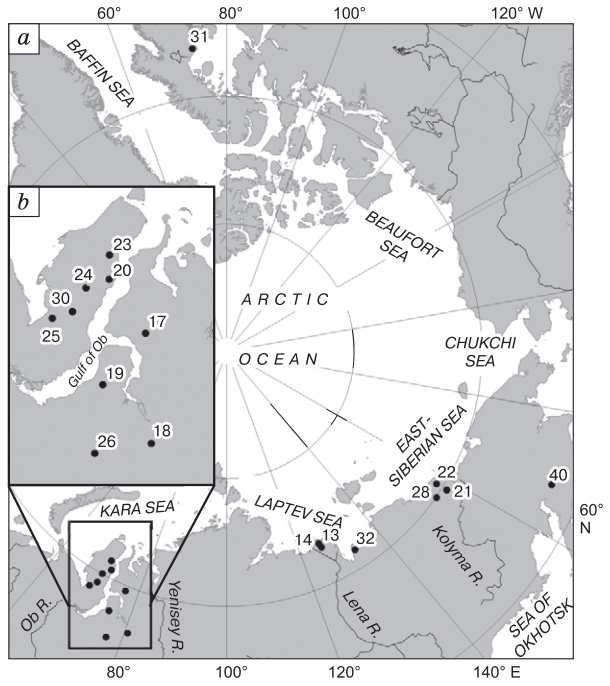

Fig. 2. Layout of key sites of thermokarst plains with fluvial erosion:

a – general scheme, *b* – enlarged scheme of the Yamal-Gydan region.

The boundaries of thermokarst depressions were identified both by an automated method – based on the ArcGIS and QGIS software modules according to the spectral brightness of the image, – and in the expert mode.

The verification of the correspondence of the theoretically obtained distributions to the empirical data was carried out for most distributions by means of a software package for statistical analysis using the Pearson test based on a well-known technique (see, for example, [*Kramer, 1970*]), in compliance with the conditions of its application. For the integral-exponential distribution, a special module to calculate the value of the Pearson criterion has been created (by P.V. Berezin). In that case, the minimum value of the sample was taken as estimate of the ε-parameter, and the γ-value was found by the method of moments by numerical solution within the framework of the same program module of the equation

$$-\frac{1}{\gamma \mathrm{Ei}(-\gamma\varepsilon)}\exp\left(-\gamma\varepsilon\right) = \overline{s_l},$$

where $\overline{s_l}$ is the average area of a lake.

Empirical verification for the model of thermokarst plains with fluvial erosion has given the following main results. The empirical data obtained for the areas of thermokarst lakes for the key sites of thermokarst plains with fluvial erosion included samples from 62 to 598 elements (Table 4).

Table 3. **Characteristics of test sites (fragment)**

Site number (see Fig. 2)	Site characteristics	Mean annual permafrost temperature, °C	Permafrost thickness, m
13	Accumulative type of relief, flat or gently sloping alluvial-marine plain of the Q_{III}–H age with sections of lacustrine boggy plains of the Late Holocene age, with numerous thermokarst and talik lakes, pingos, boggy depressions, water tracks. Sediments: sandy loams with interlayers of sands, plant detritus and peat at the areas of thermokarst lakes, lacustrine and boggy clayey silts. Outside the areas of lake distribution – alluvial-marine deposits represented by sands with interlayers of sandy loam and peat. Continuous permafrost distribution	–9...–11	300–400
22	Accumulative relief type. Flat lacustrine boggy (alas) plain, created by the joint activity of thermokarst and lacustrine-paludal processes, corresponds to the final stage of destruction of the Yedoma plain by thermokarst. Extensive confluent lacustrine basins of different stages of alas formation. The time of the formation of the relief is from the Late Pleistocene to early Holocene. Sediments: loess-like lacustrine-alluvial gray clayey silts, less often sandy silts with peat interlayers and lenses. Continuous permafrost distribution	–9...–11	300–500
23	Accumulative relief type. II alluvial-marine terrace of the Ob Bay of the Q_{III} age. Flat, swampy plain with numerous lakes. Sediments: sands with thin layers of sandy loam and loam. Continuous permafrost distribution	–7...–9	200–300
26	Erosion-accumulative relief type, the third lacustrine-alluvial terrace of the Pur River of the Q_{III} age. A flat plain, partly swampy with numerous drained lake basins. Frost mounds and thermokarst subsidence are widely developed. Sediments: the basal part is dominated by fine and medium-grained sands with inclusions of pebbles and gravel with oblique bedding. The middle part of the section (floodplain facies) is represented by silty sands and fine sands, often peaty with interlayers of sandy loam and loam. The lacustrine facies are composed of loams, less often clays and silts with interlayers of fine sand. Sporadic permafrost distribution	– 2...–0.5	0–15

For term 2, in 10 sites out of 17 (59 %), the empirical distributions correspond to the integral-exponential one (Fig. 3), which corresponds to the asynchronous start model 1.1. For term 1, the compliance is observed in 5 out of 11 sites (45 %). At the same time, in 8 out of 17 sites, the distribution of lake areas corresponds to the lognormal distribution, typical for lacustrine-thermokarst plains. In 3 out of 17 sites, the empirical distributions correspond to the gamma distribution; all the same samples correspond to the lognormal distribution, which corresponds to the synchronous start model [*Victorov, 2006; Victorov et al., 2016, 2019b*]. The closeness to the lognormal distribution, as in the case of the khasyreys, is fully explained by two factors:

– the thermokarst plains with fluvial erosion at the initial stages were lacustrine-thermokarst plains, since the probability of the drainage of lakes with their initially limited sizes was small, and those plains are characterized by a lognormal distribution of lake areas;

– integral-exponential distribution is the limiting distribution with $t \to +\infty$, and the time elapsed since the beginning of the thermokarst process is, although long, but finite one.

Interestingly, for typical lacustrine-thermokarst plains, only the lognormal distribution is valid, and no correspondence with the gamma distribution is observed. The distribution of the average radii of the lakes does not correspond to the normal one in any area. Finally, in 5 sites for term 2, the distributions do not correspond to any of the studied species.

Thus, on the whole, the empirical verification forces us to conclude that the situation of asynchronous start described by the model 1.1 for thermokarst plains with fluvial erosion is realized in nature over a sufficient number of territories. The theoretically obtained patterns – the integral-exponential distribution of lake areas – are confirmed empirically on a significant number of key areas.

At the same time, signs of a synchronous start described by the model 1.0 present only in 17 % of the sites (they have a gamma distribution of lake areas), while in 11 % a similarity with the integral-exponential distribution simultaneously is observed.

Analysis of the data reveals that the hypothesis about the possibility of the development of erosional-thermokarst plains with a synchronous start apparently does not correspond to reality, since no sites was found with the distribution of the average radii of the lakes close to the normal. At the same time, signs of the development of the considered plains with the validity of the hypothesis of quasi-uniform growth and asynchronous start (model 2.1), are observed in the form of a gamma distribution of the area of lakes with a shape parameter value equal to 0.5 only in 1 site out of 17.

Table 4. **Correspondence of empirical and theoretical distributions of thermokarst lakes areas**

Site	Term*	Sample size	Distribution			
			Lognormal	Gamma	Normal**	Integral-exponential
13	2	581	0.000	0.000	0.000	0.000
13	1	598	0.000	0.000	0.000	0.000
14	2	209	**0.014**	**0.017**	0.000	**0.022**
17	2	232	0.005	0.000	0.000	0.002
18	2	62	**0.160**	**0.018**	0.000	**0.086**
19	2	161	**0.017**	0.000	0.000	**0.213**
19	1	160	**0.091**	0.000	0.000	**0.394**
20	2	318	0.007	0.000	0.000	0.000
20	1	359	0.000	0.000	0.000	0.000
21	2	405	0.000	0.000	0.000	**0.109**
21	1	339	**0.010**	0.000	0.000	0.004
22	2	244	0.000	0.000	0.000	**0.014**
22	1	337	0.000	0.000	0.000	**0.641**
23	2	257	**0.044**	0.000	0.000	**0.220**
24	2	346	0.004	0.000	0.000	**0.663**
24	1	376	0.001	0.000	0.000	**0.024**
25	2	278	**0.225**	0.000	0.000	0.000
25	1	281	**0.265**	0.000	0.000	0.000
26	2	500	0.008	0.000	0.000	0.001
28	2	264	**0.310**	0.000	0.000	**0.053**
28	1	267	**0.122**	0.000	0.000	**0.085**
30	2	519	**0.322**	0.000	0.000	**0.245**
30	1	519	**0.710**	0.000	0.000	**0.023**
31	2	74	0.000	**0.015**	0.000	0.005
31	1	70	0.000	0.000	**0.018**	0.001
32	2	430	0.000	0.000	0.000	0.000
32	1	439	0.000	0.000	0.000	0.000
40	2	535	0.001	0.000	0.000	**0.122**

Note: the table presents *p*-values (the probability of exceeding the actual value of the chi-squared criterion); empirical data do not contradict theoretical ones at the significance level of 0.99, if $p > 0.01$ (in bold).

* Term 1 – 1965–1976 (Corona imagery); term 2 – 2013–2019.

** For mean radii of lakes.

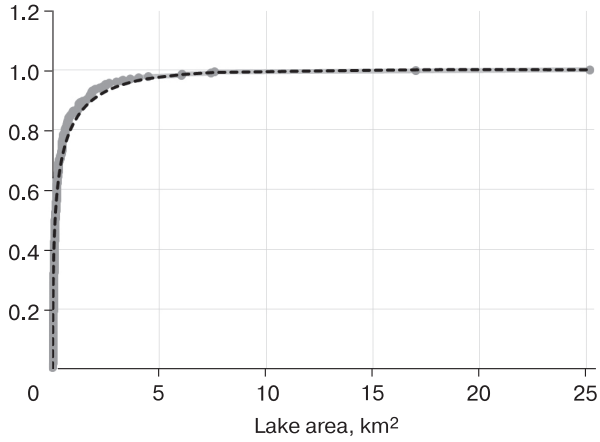

Fig. 3. An example of the correspondence of the empirical distribution of lake areas (solid line) to the cumulative-exponential distribution (dashed line), Site 28.

Thus, the analysis of the data allows us to reveal that most of the distributions can be explained using the hypothesis of lake growth, although determined by the influence of many random factors, but proportional to the density of heat losses through the lateral surface of the lake (models 1.0 and 1.1). That is consistent with the results of the analysis of lacustrine-thermokarst plains [*Victorov, 2006; Victorov et al., 2015, 2016*]. At the same time, at first glance, there is inconsistency in other obtained results, – the analysis of lacustrine-thermokarst plains indicated the hypothesis of synchronous start. In more than a half of the cases there are signs of an asynchronous start (model 1.1). This can be partly explained by the favorableness of the khasyreys area for the development of a large number of secondary lakes.

Let us emphasize that the determination of the lake area percentage indicates the fulfillment of the above-mentioned condition, for which the tendency

of the parameters to the limiting values in the model 1.1 has been proved. For all areas, the lake area percentage is within the range of 0.01–0.50, reaching a value of 0.66 only in site 24.

Inconsistency with any distributions in 5 sites can be caused by the transient processes under climatic changes. The study has demonstrated that exactly in 2 out of 3 of those sites, which are part of the five and at the same time have two survey dates, the distribution of lake areas for term 1 and term 2 differs significantly (according to Smirnov's criterion). At the same time, such differences are observed in 4 areas among all investigated.

This analysis certainly does not claim to be exhaustively reliable, and it will be clarified. The performed analysis is limited primarily due to the assumption of insignificant climate changes. At the same time, such analysis should have been carried out primarily as an analysis of the situation with the simplest conditions.

CONCLUSIONS

1. In homogeneous areas of thermokarst plains with fluvial erosion in a variety of environmental and permafrost conditions, the model of the development of the morphological structure is valid in most cases. It corresponds to an asynchronous start and growth of lakes size proportional to the density of heat losses through the lateral surface.

2. In homogeneous areas of thermokarst plains with fluvial erosion under different environmental and permafrost conditions the integral-exponential law of thermokarst lakes areas distribution is valid in most cases.

3. Analysis of the development of thermokarst plains with fluvial erosion for the period from 1965 to 2019 demonstrated that with all the observed changes, the plain's structure does not change in a significant number of areas, but is in a state of dynamic equilibrium, despite the widely discussed impact of climate change. That should be taken into account when forecasting lake development and assessing natural risks.

The study has been carried out with the financial support of the Russian Science Foundation, project No. 18-17-00226.

References

Burn, C.R., Smith, M.W., 1990. Development of thermokarst lakes during the Holocene at sites Near Mayo, Yukon Territory. Permafrost and Periglacial Processes I, 161–176.

Grosse, G., Jones, B.M., Nitze, I., et al., 2016. Massive thermokarst lake area loss in continuous ice-rich permafrost of the northern Seward Peninsula, Northwestern Alaska, 1949–2015. In: XI International Conference on Permafrost: Abstracts (Potsdam, 20–24 June 2016). Potsdam, Germany, pp. 739–740.

Kapralova, V.N., 2014. Regularities of the development of thermokarst processes within the lake-thermokarst plains (based on the approaches of the mathematical morphology of landscapes). Abstract of PhD thesis. Moscow, 24 pp. (in Russian).

Kirpotin, S.N., Polishchuk, Yu.M., Bryksina, N.A., 2008. The dynamics of the areas of thermokarst lakes in continuous and discontinuous permafrost zones of Western Siberia under global warming. Vestnik TSU [Bulletin of TSU], No. 311, 185–189.

Kramer, G., 1970. Mathematical Methods of Statistics. Mir, Moscow, 648 pp. (in Russian).

Kravtsova, V.I., Bystrova, A.G., 2009. Changes in thermokarst lake size in different regions of Russia for the last 30 years. Kriosfera Zemli [Earth's Cryosphere], XIII (2), 16–26.

Polishchuk, V.Yu., Polishchuk, Yu.M., 2013. Geosimulation modeling of fields of thermokarst lakes in permafrost zones. Ural State University, Khanty-Mansiysk, 129 pp. (in Russian).

Smith, L.C., Sheng, Y., Macdonald, G.M., Hinzman, L.D., 2005. Disappearing Arctic Lakes. Science 308 (3), p. 14.

Victorov, A.S., 2005. Mathematical models of thermokarst erosion plains. In: GIS and Spatial Analysis. Proc. of IAMG, Toronto, Canada, printed by China University of Geosciences Printing House, vol. I, pp. 62–67.

Victorov, A.S., 2006. The main problems of the mathematical morphology of the landscape. Nauka, Moscow, 252 pp. (in Russian).

Victorov, A.S., Kapralova, V.N., Orlov, T.V., et al., 2015. An analysis of the morphological structure development of the thermokarst-lake plains on the base of the mathematical model. Geomorfologiya [Geomorphology], No. 3, 3–13.

Victorov, A.S., Kapralova, V.N., Orlovm, T.V., et al., 2016. Mathematical morphology of cryolithozone landscapes. RUDN, Moscow, 232 pp. (in Russian).

Victorov, A.S., Orlov, T.V., Sadkov, S.A., Trapeznikova, O.N., 2019a. Remote assessment of natural hazards on the base of the mathematical morphology of landscape. Geoekologiya. Inzhenernaya geologiya. Gidrogeologiya. Geokriologiya [Geoecology. Engineering geology. Hydrogeology. Geocryology], No. 5, 61–73.

Victorov, A.S., Orlov, T.V., Arkhipova, M.V., 2019b. Laws for size distribution of khasyreis. Doklady Earth Sciences, 488 (2), 1253–1255.

Received March 13, 2020
Revised version received November 4, 2020
Accepted November 22, 2020

EARTH'S CRYOSPHERE
SCIENTIFIC JOURNAL

Kriosfera Zemli, 2021, vol. XXV, No. 1, pp. 48–60

CHRONICLE

THE MELNIKOV PERMAFROST INSTITUTE, SIBERIAN BRANCH, RUSSIAN ACADEMY OF SCIENCES AT THE TURN OF ITS 60th ANNIVERSARY

M.N. Zheleznyak, R.V. Zhang, V.V. Shepelev, M.N. Grigoriev, A.N. Fedorov, O.I. Alekseeva

Melnikov Permafrost Institute, Siberian Branch of the Russian Academy of Sciences, Merzlotnaya str. 36, Yakutsk, 677010, Russia; o.i.alekseeva@mpi.ysn.ru

2020 marked the 60th anniversary of the Melnikov Permafrost Institute SB RAS. This paper presents a brief history of its foundation and describes the major research achievements and outputs over the last decade. Promising avenues and projects for further geocryological research are outlined. In view of intensive industrial development of the permafrost regions, the authors believe that the Melnikov Permafrost Institute should be accorded a National Research Institute status with relevant government support.

Key words: *permafrost, geocryology, permafrost engineering, buildings and structures, cryogenic processes, climate change, frozen ground.*

THE HISTORICAL BACKGROUND

In 2020 it was 60 years since the foundation of the Melnikov Permafrost Institute SB RAS (hereinafter – Institute) (Fig. 1).

The Institute has been established on the basis of the Yakutsk Scientific Research Geocryology Station that has existed since 1941(since 1956 Northeast Department) of the Obruchev Institute of Geocryology, Academy of Sciences of USSR (INMERO, Moscow).

The principal decision to establish the Institute in Yakutsk was made by the Decree of the Presidium

Fig. 1. The Melnikov Permafrost Institute, SB RAS. Yakutsk, 2020.

of the Academy of Sciences of the USSR No. 899 of September 16, 1960. Council of Ministers of the RSFSR recommended to establish the Institute within the structure of the Siberian Branch of the USSR Academy of Sciences in the letter No. 2.5897-350 of November 2, 1960 to the Presidium of the USSR Academy of Sciences. On December 9 of the same year, the Presidium of the USSR Academy of Sciences decided to create the Institute "with the purpose of the development of regional studies of permafrost soils of Siberia, necessary to meet the needs of the national economy" and approved a structure of the Institute by the decree No. 1043, which was signed by the President of the USSR Academy of Sciences A.N. Nesmeyanov. The formation of the Institute was very successful in all basic fields of geocryological science, including, certainly, engineering-applied studies. In 1969, the Institute was awarded the Order of the Red Banner of Labor for major achievements in the development of national geocryology. In 1995, the Institute was named after Academician Pavel Ivanovich Melnikov, the founder and first Director of the Institute, by the Decree of the President of the Republic of Sakha (Yakutia) M.E. Nikolaev. According to the statute of the Institute, its basic activities are the fundamental research and applied developments in the following scientific areas: the evolution of the cryolithozone under the impact of natural and anthropogenic factors; thermal and mechanical interaction of engineering structures with permafrost soils. The Institute was referred to the Ministry of Science and Higher Education of the Russian Federation according to the Decree of the President of the Russian Federation of 15.05.2018 No. 215 "On the structure of federal executive bodies" and the Order of the Government of the Russian Federation of 30.05.2018 No. 1055-r.

Academician Melnikov Pavel Ivanovich (1908–1994), one of the founders of the geocryological science, was the founder and permanent head of the Institute from 1960 to 1987 (Fig. 2).

Rostislav Mikhailovich Kamenskii (1936–2008), Doctor of Technical Sciences (post-doctorate degree in Russia) was Director of the Institute from 1988 to 2003. Zhang Rudolf Vladimirovich, Doctor of Technical Sciences, was Director of the Institute from 2004 to 2012. Since 2012, Mikhail Nikolayevich Zheleznyak, Doctor of Geological and Mineralogical Sciences, has been Director of the Institute.

The Institute develops geocryology (permafrost science), which is the research area of national importance for Russia and monitors the cryolithozone, which occupies 65 % of Russia's territory. In addition to six research units in Yakutsk, the institute has a number of regional research units (stations, laboratories, observation sites) located in certain regions of the Russian Federation and abroad (Kazakhstan), has

Fig. 2. Pavel Ivanovich Melnikov (1908–1994), the founder and the first director of the Institute, the first president of the International Permafrost Association, the full member of the USSR Academy of Sciences and Russian Academy of Sciences, Hero of Socialist Labor.

a strong material and technical base [*Shepelev, Zheleznyak, 2019, 2020*].

The staff members of the Institute have published about 400 monographs, methodological guidelines, and manuals, have received about 150 patents, and have issued more than 500 scientific and technical developments to industrial partners. In 2012, the Institute with the participation of other scientific institutions has established the world-class research station "Island Samoilovskii" (Fig. 3), which currently operates successfully. The unique engineering structure, the repository of federal importance for cryopreservation and long-term storage of the seed gene pool in permafrost soils, has been put into operation (Fig. 4).

The Institute currently employs 207 people, including 83 Researchers, 17 Doctors and 40 Candidates of science (PhD equivalent in Russia). The Institute offers the graduate study program and includes the branch of the Geocryological Department at the Ammosov North-Eastern Federal University and the Doctoral Dissertation Council. The Institute is the founder of the scientific journal "Earth's Cryosphere" and publishes the popular science journal

Fig. 3. The Arctic research station "Island Samoilovskii", 2015.

Fig. 4. A group of participants at the opening session of the Federal Permafrost Seed Repository against the background of an above-mine structure. Territory of the Institute, 2012.

Fig. 5. The Integrated Geocryological Expedition «Main Pipeline "Power of Siberia"».

"Science and Technology in Yakutia". The Institute has three recognized geocryological scientific schools ("Hydrogeology and Engineering Geocryology", "Permafrost-Climatic Studies', "Geothermics of the Frozen Zone of the Lithosphere"). In 2010, the Institute was licensed to conduct educational activities on a specialty 25.00.08 "Engineering geology, geocryology and soil science". The Institute is a member of the self-regulatory organization (SRO) "Russian Geotechnical Association" (AIIS) to promote the engineering survey. The institute has a Certificate of Conformity to the requirements of GOST ISO 9001-2008. Since 2020, the Institute has been granted the rights to perform the survey with respect to highly hazardous, technically complex and unique objects. The staff members of the Institute have carried out the geocryological studies for the scientific support of the following megaprojects: the South Yakutia Hydropower Complex; the Talakan Oil and gas condensate field; the Elkon uranium deposit; iron ore and coal deposits of South Yakutia; "Mir", "Aikhal", and "Udachnyi" diamond-bearing mines; "Eastern Siberia–Pacific Ocean" oil pipeline; "Power of Siberia" gas pipeline; Vankor gas condensate field; Evenkiya Hydropower Plant; railroads of the Baikal–Amur Mainline (BAM), "Ulak–Elga – Tommot–Kerdem–Yakutsk", "Amur–Yakutia Rail Mainline"; "Vilyui", "Amur", "Kolyma" highways; the high voltage Power Transmission Line st. Khani–Tarynnakh Mining and Processing Plant, and others (Fig. 5).

Acquiring of new knowledge and confirmation of theoretical concepts in the geocryological science is impossible without field studies. The fieldworks have been carried out on an annual basis from 2011 to 2020 by 11 integrated expeditions and 15–20 field teams of the Institute. The geography of the expeditions is as follows: Eastern Siberia (Verkhoyanye, Lena River delta, Novosibirsk Islands); Northern Tian Shan; Altai Mountains; Tibet Mountains. The monitoring of the thermal state of frozen soils are conducted at the research stations and test sites in Yakutia, northern Krasnoyarsk Krai, Magadan Region, and Chukotka. The expedition works are supported by the Russian Foundation for Basic Research, contract-based works, and subsidies from the budget of the Russian Federation.

MAIN RESULTS OF THE GEOCRYOLOGICAL RESEARCH OF THE INSTITUTE IN 2010–2020

A role of the geocryological science at the present stage of the development of our country is determined by expansion and intensification the economic development of the northern and eastern territories located in the distribution area of permafrost (cryolithozone) [*Alekseeva, Zhang, 2011*]. Current climate warming, that is observed almost all over the globe, is particularly evident in the circumpolar regions of our planet. The territory of Yakutia as well as all the Arc-

tic and subarctic regions of the country belong to the zone of the greatest impact of global warming. These conditions require a special approach to the impact on the permafrost according to the law on permafrost protection in the Republic of Sakha (Yakutia) adopted in 2019. This low differentiates between the sparing development in unstable permafrost areas and the intensive development in the stable ones.

The Institute has heavily worked and continues to work with various national and federal committees to prepare the federal law "On the Protection and Rational Use of Permafrost". This enactment is very relevant and well-timed, because overwise, the adoption of the republican law will be complicated.

In the modern world, the issues of global climate warming and its impact on the natural environment are more important than ever. In this aspect, the staff members of the Institute carry out the fundamental geothermophysical and geochemical research, study a structure, cryogenesis of ice-bearing formations, and assess risks of their exploration, as well as research dynamics of cryogenic landscapes and hydrogeological conditions of North Asia. The assessment of reliability of engineering structure bases under conditions of climate change and anthropogenic impacts play an important role [*Alekseeva, Zhang, 2011*].

The most important results of these studies are:

1. A rate of degradation of the subsea permafrost has been determined instrumentally for the first time in the shallow shelf of the Laptev Sea. It has been established, that over 30 years, the submarine permafrost table has been lowered at the average rate of 14, 18.5, 13.5, and 6 cm per year at the distances of 0.3, 0.6, 0.85, and 2.5 km from the shoreline, respectively (Fig. 6) [*Grigoriev, 2017; Shakhova et al., 2017*].

2. A mathematical model of the evolution of the cryolithozone of the East Siberian Sea shelf has been developed to estimate the distribution, transformation rates, and morphological parameters of subaquatic permafrost in the Late Cenozoic. The sedimentary deposits, which occur on the shelf of the central sector of the East Siberian Sea, currently include, presumably, six horizons of relict permafrost. On the inner shelf, thermal degradation of the upper permafrost horizons prevails at the estimated rate of 2 to 20 cm/year. On the middle and outer shelf, the permafrost degrades at the rate of 0.2 to 0.5 cm/year due to diffusion of sea salts. This new knowledge makes it possible to take the permafrost boundaries into consideration during the exploration of the shelf zone of the Eastern sector of the Russian Arctic.

3. The permafrost-landscape and engineering-geocryological maps of Yakutia of 1:1 500 000 scale have been prepared. These maps demonstrate the main patterns of natural and engineering-geocryological conditions and serve as a basis for assessing the sustainability of natural and technical systems in the cryolithozone (Fig. 7) [*Shestakova et al., 2016; Fedorov et al., 2018*].

These maps are currently used in the projects on the assessment and forecast of geocryological settings with the recommendations for the construction of the "Power of Siberia" gas pipeline and for the planning of the socio-economic development of settlements of the Republic of Sakha (Yakutia) for the periods up to 2030 and 2050.

4. The specific features of the unsteady permafrost occurrence in the oil-and-gas bearing regions of the Siberian Platform have been identified and characterized. The maps of the distribution and depths of

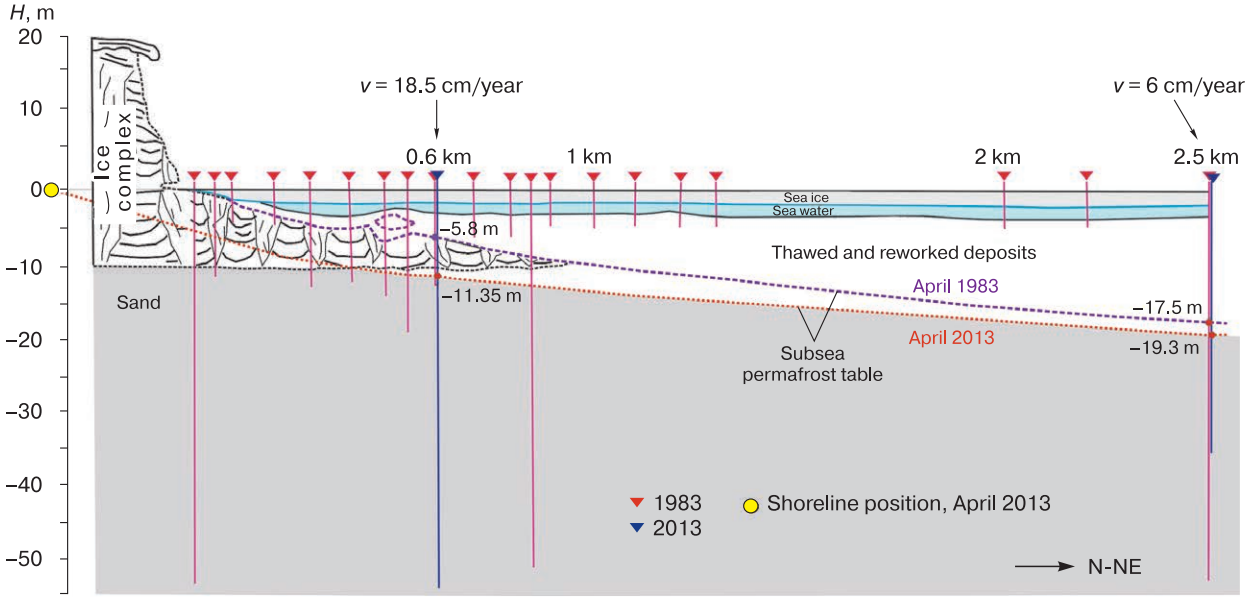

Fig. 6. The drilling profiles in Buor-Khaya Gulf (Laptev Sea) to the north of Muostakh Island, demonstrating the rate of the lowering of the subsea permafrost table (v) over 30 years (from April 1983 to April 2013).

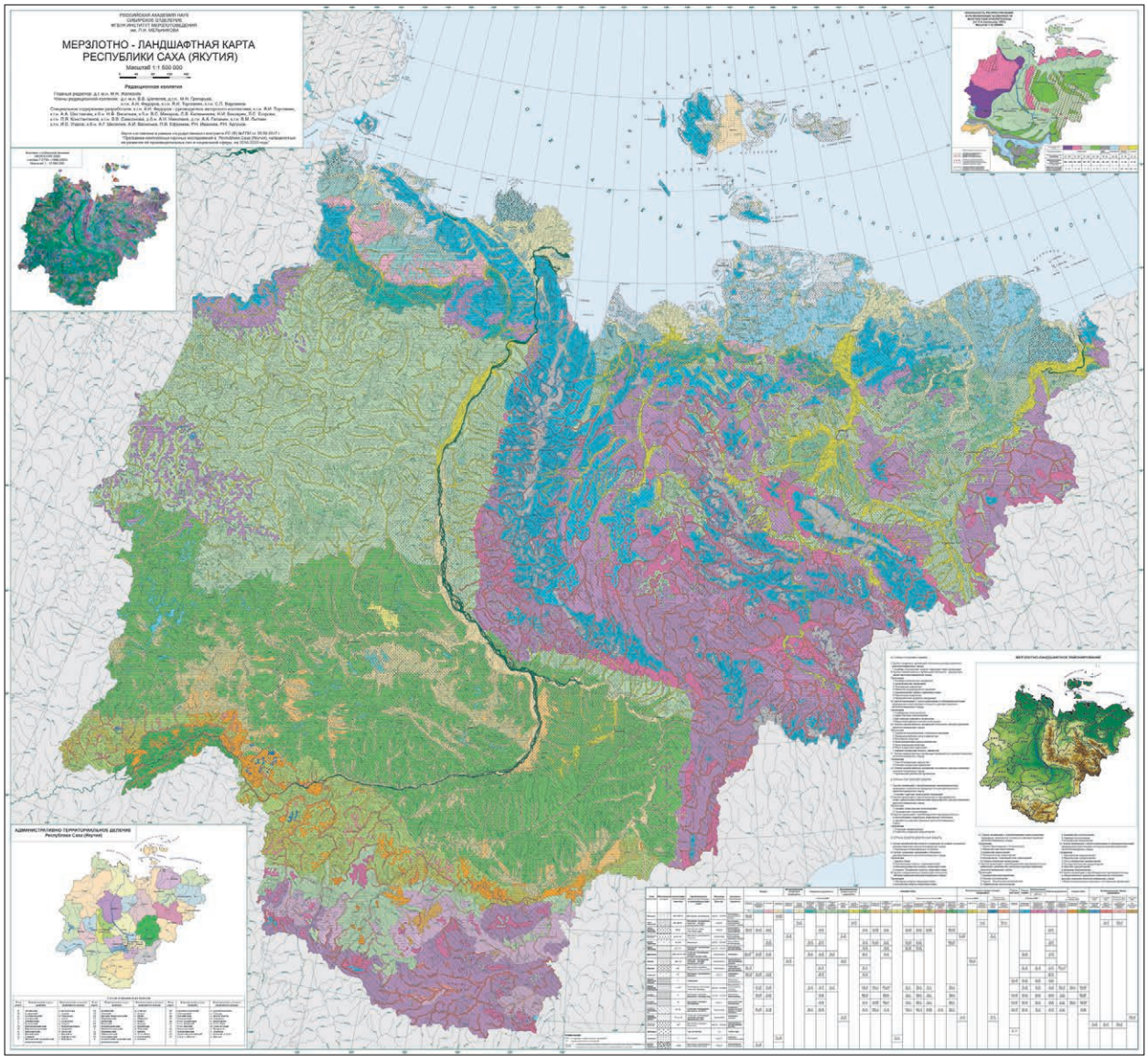

Fig. 7. The permafrost-landscape map of the Republic of Sakha (Yakutia) at a scale of 1:1 500 000 (http://mpi.ysn.ru/images/mlk20182.pdf).

the lower boundary of the permafrost with a series of the permafrost-geothermal sections have been compiled (Fig. 8). The permafrost thickness has been characterized for individual fields, tectonic structures, and within the Vilyui syneclise as a whole. The geocryological databases of the Vilyui syneclise and the Aldan anteclise have been created [*Zheleznyak, Semenov, 2020*].

5. It has been established that during more than 50 years of the operation of the Vilyui HPP, which had been built in the zone of the continuous permafrost, the thermal regime of the cryogenic environment of this hydraulic facility has not reached the stationary regime. The engineering and geophysical monitoring has revealed the changes in the temperature-cryogenic and temperature-moisture regime of the geocryological environment (Fig. 9), as well as the role of rockfill in the heat- and mass-exchange (cryogenic) processes of the artificially created complex natural-technical system. The degradation rate of the cryogenic environment in the areas of the bank adjacencies of the dam and the reservoir bed has been assessed [*Shepelev, Zheleznyak, 2019*].

6. The basic features of the distribution and composition of modern and relict permafrost phenomena in the vast plains and lowlands of Kazakhstan and adjacent regions of Central Asia have been revealed. The basic facies factors of arid (desert) and cryogenic

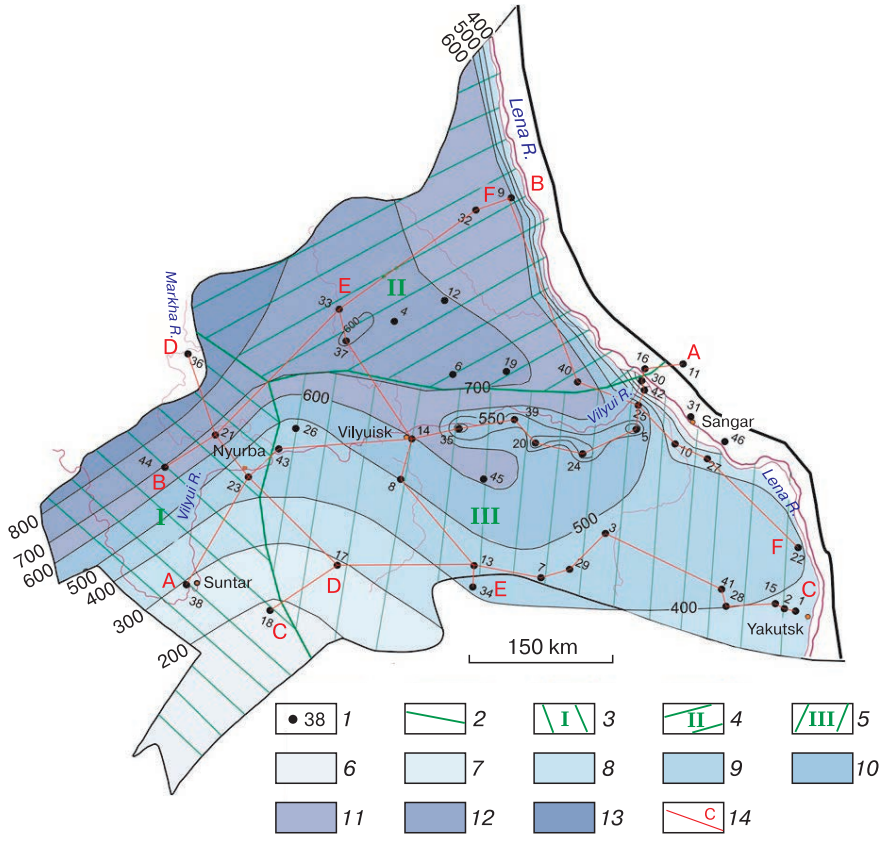

Fig. 8. The map of the depth of the permafrost lower boundary in the Vilyui syneclise:

1 – the exploration area, its number; *2* – the boundaries of the permafrost distribution areas; *3* – I permafrost distribution area; *4* – II permafrost distribution area; *5* – III permafrost distribution area; *6–13* – the thickness of permafrost: *6* – up to 200 m, *7* – from 200 to 300 m, *8* – from 300 to 400 m, *9* – from 400 to 500 m, *10* – from 500 to 600 m, *11* – from 600 to 700 m, *12* – from 700 to 800 m, *13* – over 800 m; *14* – lines of the geocryological-geothermal cross sections.

formations have been identified. The maximum depths, to which zero temperatures have spread, have been established for different types of cryolithogenic deposits [*Shepelev, Zheleznyak, 2020*]. Volumes of ground ice in the mountain regions of the Northern Tian Shan have been estimated for the first time. Dynamics of high-mountain ground ice is being studied.

7. The specific features of the structure, isotopic composition, and age of the glaciers of the Suntar-Khayata Ridge (Northeast Yakutia) have been revealed, and the sizes of the glaciers have been reconstructed for different periods of their degradation.

8. The paleogeography of the formation of the cover dune deposits in Central Yakutia under the conditions of severe desiccating and desert invasion have been reconstructed for the period from the end of the Karginsky thermochron to the beginning of the Holocene. The modern blown dune massifs (tukulans) started to form not more than 1 ka BP. This phenomenon is associated with the climatic events of the Little Ice Age of the 13th–19th centuries. The main types of the Late Quaternary and Holocene dune relief and the areas of its distribution (Dyolkumin Formation) in Central Yakutia have been characterized [*Shepelev, Zheleznyak, 2019, 2020*].

9. The thermal response of the upper horizons of the cryolithozone of Central Yakutia to anthropogenic impacts has been quantitatively evaluated. The 30-year dynamics of the thermal regime of soils has been studied on the basis of a thickness of an active layer and a temperature in an annual heat-turn layer for more than 40 disturbed landscapes in 9 types of terrain patterns.

The monitoring has revealed that climate warming causes the significant increase in the temperature of permafrost at the depth of the annual heat-turn. Thus, the temperature of permafrost in the territory of Yakutsk has increased by 3 °C over the past 80 years. The geocryological and hydrogeological conditions in the near-surface permafrost have been transformed against this background. The formation of multilevel zones of cryopegs (saline waters with negative temperature) has been revealed in the area

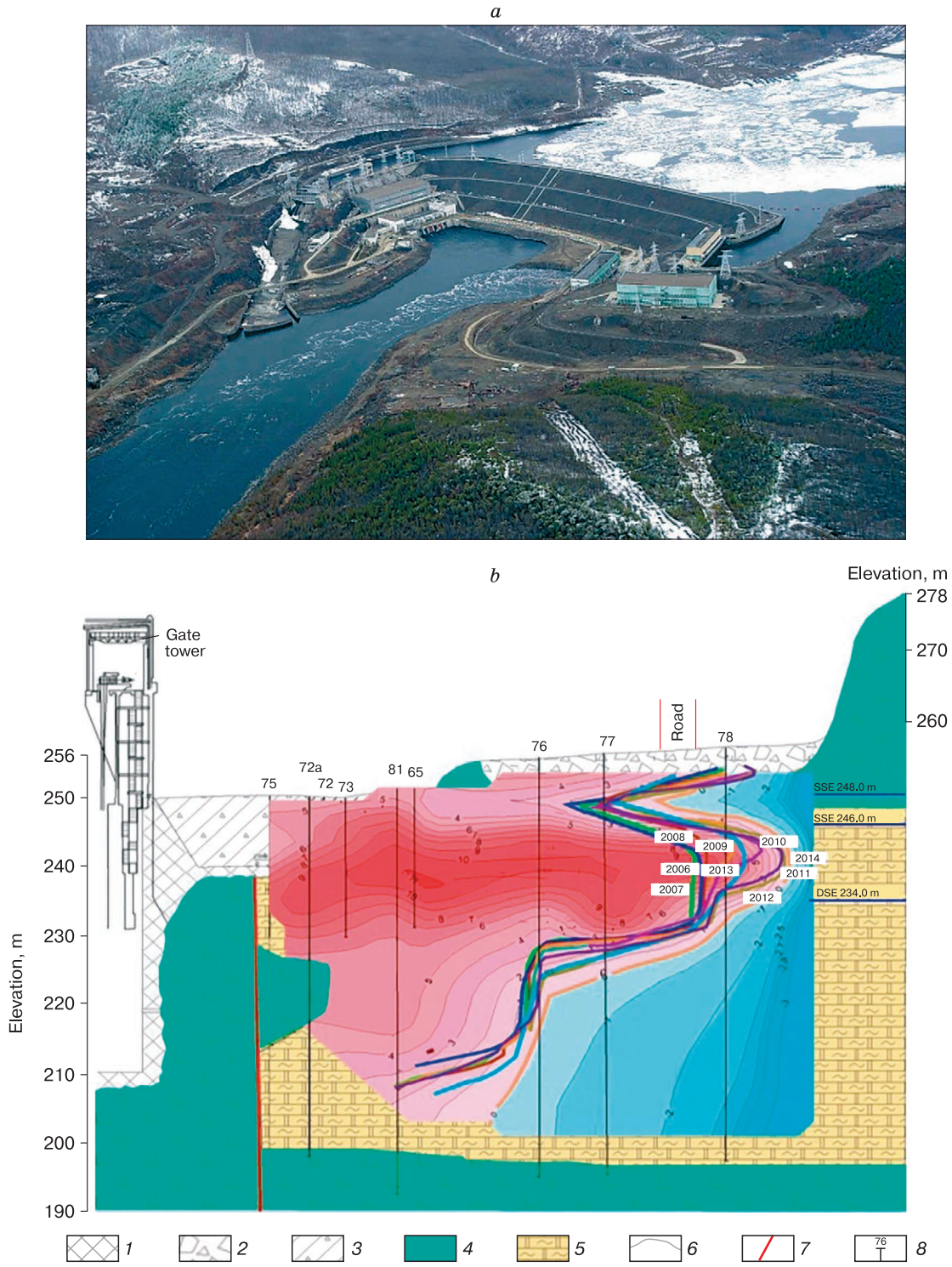

Fig. 9. The general view of the hydraulic facilities of Vilyui HPP-1, 2 (*a*) and dynamics of talik along the transverse profile of boreholes 75–78 for 2006–2014 at the right-bank adjacency of the dam to the mountain frame (*b*).

The talik profile is highlighted in red, shades of red demonstrate dynamics of talik, lines of different colors demonstrate the talik boundary in different years, shades of blue are perennially frozen rocks. *1* – concrete; *2* – blocks, rubble, gruss with sandy loam filler; *3* – gruss soil with loamy filler; *4* – diabase; *5* – xenoliths of carbonate rocks; *6* – geological boundaries; *7* – tectonic contacts of sedimentary rocks and intrusions; *8* – thermometric borehole.

of Yakutsk. The dynamics of their level and variability in their chemical composition indicate that the permafrost, which separate individual horizons of cryopegs, have transitioned into a thaw state [*Shepelev, 2011; Shepelev, Zhang, 2011; Anisimova, Pavlova, 2014*]. Such transformation of the geocryological settings in the northern Russian cities significantly reduces the bearing capacity of frozen bases of buildings and structures, increasing their deformability and accident rate.

The cities of Yakutsk, Mirny, Norilsk, Murmansk, Vorkuta, Apatity, Monchegorsk, Kandalaksha, Kirovsk, Naryan-Mar, and Salekhard are situated in the cryolithozone. The problem of construction of buildings on the frozen bases existed, exists and will continue to exist. It is almost impossible to foresee all the negative features of the thermal and mechanical interaction of buildings and structures with frozen soils in the process of urbanization, but it is a feasible task to minimize them. In this regard, the Institute has developed the techniques, which can provide the reliable operation of the engineering structures under the conditions of climate change and intense anthropogenic impact. The most important of these techniques should include the following:

– the creation of the hardware-methodological complex and the technology of geophysical monitoring to prevent natural and human-induced disasters at large hydrotechnical structures operated in the permafrost zone;

– the creation and implementation of the effective methods for soil stabilization to strengthen the foundation bases in the cryolithozone using nanotechnologies and cryogenic resources;

– the development and implementation of the effective methods for drainage of waterlogged territories in the cryolithozone on the basis of innovative design solutions;

– the development of the territorial construction standards for bases and foundations in the high-temperature cryolithozone;

– the creation of the modern systems to control and manage the stability of headframes in the permafrost zone, etc. [*Velikin, 2012; Alekseeva, 2017*].

Over the period of 2010–2020, the staff members of the Institute analyzed and forecasted reliability of the low-pressure hydraulic facilities in the cryolithozone and developed the design schemes for dams and canals included in them. The comprehensive summary of the dam engineering in the Russian cryolithozone has been made. Results of field studies of the cryogenic-temperature regime of the power and water management structures have been obtained. The temperature regime of the hydraulic facilities is the basis for their static and filtration sustainability. The results of the studies have been applied in design, construction, and operation of many hydraulic facilities, as well as have been included in the regulatory documents. Recommendations for the low-pressure hydraulic facilities on frozen bases have been made. They can be used in construction of new hydraulic and land reclamation facilities in the cryolithozone and reconstruction of the existing ones [*Zhang et al., 2012, 2019*].

Roads and railroads are important objects of the permafrost engineering. Sustainability of road beds remains a crucial scientific and practical challenge. The main ways to prevent their deformations are the lowering of an average annual temperature of the base soils and the keeping them frozen (by means of snow-clearing and painting, with the use of a sun-and-precipitation awning, horizontal (GET) and vertical (VET) systems of soil temperature stabilization, and a film screen) or the preventive removing of ice-rich soils (ice lenses) from the base with subsequent filling of the cavities by non-subsiding soils.

Trunk gas and oil pipelines, as well as roads, are linear structures, the routes of which are laid in the most diverse engineering-geological and geocryological conditions. This requires the acceptance of different schemes for the pipeline laying in certain areas. The underground laying is the most reliable in terms of the impact of external factors on a pipeline. However, even here cryogenic processes (thawing, frost heave) are activated resulting in a loss of sustainability and continuity of the pipe. Therefore, the engineering-geocryological monitoring is very important during the operation of the linear objects [*Alekseeva, 2017*].

The staff of the Institute improve various technologies, which provide the reliable operation of engineering structures under conditions of climate change and intense anthropogenic impact on the territory of their location. This involves the development of the hardware and methodological complex and technologies of the geophysical monitoring on the large hydraulic and mining structures operated in the permafrost zone (Vilyui HPP cascade, “Mir”, “Internationalnaya”, “Udachnaya” diamond pipes, etc.) [*Velikin, 2012; Zhang et al., 2019*].

The Institute has also obtained significant results in the development of the fundamental principles of the use of the cryogenic construction resources of the cryolithozone. The developments in the field of energy-saving technologies are particularly prominent [*Kuzmin et al., 2012a,b; Kuzmin, Kuvaev, 2019*]. During the creation of the seed cryobank in Yakutsk, the new patent developments have been implemented to use the resources of natural cold. This technique is characterized by enhanced sustainability and economic efficiency (minimal energy consumption during operation), providing the stability of the temperature-humidity regime in underground galleries for a long period of time. The uniqueness of the seed cryo-

bank is that it is the first underground facility in Russia, which has been specially built for the long-term storage of plant seeds in the permafrost.

The Institute has also built an experimental garage using the technology of heating based on heat, which is released during phase transitions of water. This technique is effective for the heating of certain types of premises (ice rinks, parking garages, hangars, recreational and sports facilities at children's institutions, various storage facilities, etc.) and for the maintaining of near-zero negative temperatures in the cold season almost all over Russia.

The development of the guidelines for design, construction and operation of structures for various purposes is an important result of the work of the Institute staff members. The guidelines for the design and construction of pile foundations, constructed under conditions of sporadic, discontinuous, and continuous permafrost, with the assumption of their thawing during operation, have been made for the thawing and thaw soils of Magadan Oblast [*Vlasov et al., 2012*].

The guidelines for the design of buildings and structures on spatial ventilated foundations on an intermediate layer (fill) in the areas of perennial frozen soils have been compiled. The guidelines are intended for the calculation of the temperature regime of permafrost soils of the bases, preserved in the frozen state during construction and during the entire specified period of the operation, as well as for the design and technology of the arrangement of the spatial ventilated foundations [*Goncharov, Popovich, 2012; Goncharov, 2016*].

DEVELOPMENT OF INTERNATIONAL SCIENTIFIC RELATIONS

> Close international scientific cooperation in the field of the geocryology is of the utmost importance for the full realization of the modern scientific potential of geocryologists and for the providing of the environmentally safe existence of the modern world.
>
> *Academician P.I. Melnikov*
> [*Klimovskiy, 2008*]

The geocryologists of Yakutia established the first scientific contacts with foreign colleagues in 1963 during the First International Conference on Permafrost (ICP) in Lafayette, Indiana, USA. The Second International Conference on Permafrost was held in 1973 in Yakutsk, Russia, where there were decided to hold ICP every five years. Director of the Institute P.I. Melnikov was the chairman of the founding committee of this major international forum of geocryologists. In the decision of the Second ICP, which was composed and signed by the representatives of the USSR (P.I. Melnikov), the USA (T. Peve), and Canada (R. McKay) it was written: "To consider it expedient to conduct the international integrated studies related to the preservation of the environment in the areas of the distribution of permafrost. They include the exchange of scientific information, reciprocal visits by specialists, effective control over environmental disturbances, and improvement of the methods of the use of natural resources" [*Klimovskiy, 2008*]. Thus, the study of the problems of the environmental protection in the areas of the distribution of permafrost have been launched, especially in relation to the exploration of oil and gas fields and the projects for their development.

In 1983, the International Permafrost Association (IPA) was founded in Fairbanks, Alaska, USA. P.I. Melnikov was elected its first president. All this contributed to the international reputation of the Institute and the growth of the scientific authority of the Yakutia geocryological school. Over the past 37 years, IPA has demonstrated the need of its existence.

Over the subsequent years, the directors of the Institute R.M. Kamensky, R.V. Zhang, and M.N. Zheleznyak have supported and developed the international scientific activities of the Institute staff, achieving success in various fields. Since the 1990s, the international conferences on geocryology have amplified their subjects and increasingly included the cryosphere and other topics in their programs. These are the conferences, which have been annually held in Pushchino, Tyumen, Salekhard, etc. together with the International Associations of geomorphologists, cryosphere sciences, etc.

The Congress of Geocryologists of Russia has been established in parallel with the international conferences at the initiative of geocryologists of Moscow State University and has been held every five years. The Melnikov Permafrost Institute SB RAS has actively participated in these conferences, sending the delegations for presentations in various subforums.

In 1993, R.M. Kamensky, R.V. Zhang, and D.M. Shesternev, together with the Heilongjiang Institute in Cold Region Engineering (Harbin, China), founded and held the First International Symposium on Permafrost Engineering Issues in Chita. It became a complementary event to ICP in the field of engineering. Such symposiums are held every three years in parallel with the Main International Forum of Geocryologists under the aegis of the Council of the Earth Cryology, Russian Academy of Sciences and IPA [*Alekseeva, 2015*].

The Institute maintains mutually beneficial cooperation with many scientists from foreign countries. Research is conducted under contracts, agreements, memorandums of the joint cooperation with institutes and universities in China, Mongolia, Germany, Canada, USA, South Korea, Finland, Japan,

France and other countries. The Institute is the permanent representative in the Arctic Coastal Dynamics (ACD) program of the International Arctic Scientific Committee (IASC), as well as the participant in other international Arctic programs.

Foreign specialists continue to demonstrate great interest in studying permafrost in Siberia. Many institutions actively collaborate with Yakutia geocryologists, in particular:

– The Alfred Wegener Institute (AWI) for Polar and Marine Research (Germany) – the joint studies of the material composition and the history of accumulation of coastal-marine, and frozen alluvial, lacustrine and other continental sediments, their transformation processes in an active layer and taliks of the coastal zone of the Arctic seas, monitoring of the interaction processes in the land-sea-atmosphere system;

– The Swedish Museum of Natural History (Sweden), British University, Oxford (UK) – the joint biogeochemical research in the watershed of the Lena River and its tributaries; the identification of the changes in the transfer of carbon and trace metals in the rivers of the Siberian region due to global climate change;

– The Laboratory of the environment-surface interaction and dynamics, the Paris-Saclay University, Orsay (France) – the study of geomorphological, thermal, and hydrological changes during permafrost degradation, the reactions of the thermal regime of permafrost at depth in response to its degradation;

– The Swedish Meteorological and Hydrological Institute (Sweden) – the study of hydrological processes under conditions of changes in the natural environment of the cryolithozone;

– The Japan Agency for Marine-Earth Science and Technology (JAMSTEC) (Japan) – monitoring of the meteorological, water and heat balance observations, the integrated geocryological and landscape studies at the Tiksi test sites;

– The Institute of Geography, the Ministry of Education of the Republic of Kazakhstan, Almaty, Kazakhstan – the scientific and technical cooperation in glaciology, geocryology, landscape science, geoinformation systems, geomorphology, exogenic and endogenic processes and phenomena, climatology.

The staff of the Institute annually participate in the international conferences abroad: Potsdam, Hamburg (Germany), San Francisco, New Orleans (USA), Frascati (Italy), Brest (France), Brussels (Belgium), Zurich (Switzerland), Fairbanks (USA), etc. (Fig. 10). The Institute, in turn, officially invites from 60 to 100 foreign scientists every year to work under various joint contracts.

The Russian-German expedition "Lena" has been working in the poorly explored East Siberian region of the Arctic for over 20 years. The International Forum "20 Years of the Lena Expedition" was held in St. Petersburg in 2018. The forum was founded by the Arctic and Antarctic Research Institute (AARI), St. Petersburg; the Melnikov Permafrost Institute (MPI) SB RAS, Yakutsk; Helmholtz Center for Polar and Marine Research, AWI (Germany); the German House for Research and Innovation (DWIH, Moscow). Hundreds of articles and tens of monographs, which have explained the current and historical state of the Earth's geosphere and climate change in the Arctic, have been published on the basis of the results of this expedition. The scientific and material and technical base of the Lena expedition, located on Samoilovskii Island, is one of the best Arctic research stations in the world.

In 2018–2019, the Institute established two new analytical laboratories: the Russian–German isotope laboratory to analyze the isotopic composition of water together with the Stable Isotope Laboratory at AWI Potsdam (Germany); the laboratory to determine carbon and water content in soil samples with the use of the LECO RC612 multiphase determinator (USA).

In recent years, the scientific cooperation with the Chinese institutions has been very active. In 2017, the International Research Center for Asian Cold Regions Environment and Engineering (IRC-AACEE) was officially founded in Lanzhou (Gansu Province). The agreement on the establishment of this center was signed between the Northwestern Institute of Eco-environment and Resources (NIEER), the Chinese Academy of Sciences (CAS) and the Melnikov Permafrost Institute, SB RAS. The center focuses on the development the joint research projects in the priority fields including general geocryology, engineering geocryology, and material engineering of cold regions.

Fig. 10. Delegation of the Melnikov Permafrost Institute SB RAS at the XI International Conference on Permafrost, June 20–24, 2016 (Potsdam, Germany).

The International Cooperation Program with the CAS has entered into force. The program includes the following topics: the assessment of the impact of the changing cryolithozone in China, Russia and Mongolia on large engineering structures; the educational exchange of the State Departments of Education and Culture with the People's Republic of China (PRC); the scientific and technical support and preliminary consultations on the Beijing–Moscow high-speed railroad link as part of the project "One Belt and One Road"; the joint studies of the cryolithozone of the Central Asian mountain regions in Altai, Stanovoy Range and Tibet.

The experience of the international cooperation, accumulated by the Institute, demonstrates that it is possible to perform the studies jointly with foreign scientists, including a great deal of field work, laboratory and field experiments, which are related to the study of composition, structure, state of the cryolithozone and the processes of its interaction with other components of the environment, as well as the rapid publication of results obtained in Russia and abroad.

PROSPECTS FOR THE DEVELOPMENT OF THE GEOCRYOLOGICAL STUDIES

To develop the human resources, material-technical and instrumental base of the Institute, as well as the fundamental geocryological study for the future, the application was sent to the Federal Agency for Scientific Organizations (FASO) of Russia in 2016 in order to restructure the Institute and give it the status of the National Research Institute (NRI). The key task of the NRI is to lay the necessary groundwork for new fundamental knowledge in science, providing new opportunities for the implementation of the applied studies and experimental design works in the future. This initiative of the Institute has been supported by the leadership of the Siberian Branch of the Russian Academy of Sciences, the Republic of Sakha (Yakutia), and the Federation Council of the Russian Federation.

The Scientific Council of the Institute has set up the Concept for the Program of the Development of NRI Melnikov Permafrost Institute SB RAS of the Order of the Red Banner of Labor. The strategic goals of the Institute are as follows:

– to achieve a qualitatively new level of scientific knowledge on the distribution, composition, structure of permafrost and the processes of their interaction with the atmosphere, hydrosphere, biosphere and noosphere of the Earth;

– to develop the more technologically advanced and ecologically safe methods of construction of buildings and engineering structures in the northern and Arctic regions of the country;

– to provide the priority development of geocryological studies, taking into consideration the global trends in the scientific development and with active cooperation with scientific institutions-partners;

– to create the support program for the geocryological scientific school to engage talented young people in science, etc.

Current climate change and the increasing industrial development of the cryolithozone put forward new theoretical, scientific, and technical challenges to the geocryological science. They include the identification of zonal and regional patterns of the response of the permafrost upper horizons to climate change and technogenic impacts and the forecast of the development of cryogenic processes, the activation of which significantly increases the ecological hazard of environmental management in the cryolithozone.

Solution of geocryological issues under these conditions is possible with the appropriate support from the State in the course of the reorganization of the Institute into the National Research Institute [*Alekseeva, 2017*].

Unfortunately, the modern scientometric approach of the Federal Agency for Scientific Organizations, and later, of the Ministry of Education and Science of Russia, to the assessment of the efficiency of research institutes does not allow the Melnikov Permafrost Institute SB RAS to achieve the necessary numerical rating of publications to get the NRI status. Although the results of the geocryological studies are primarily needed in Russia for the use of new knowledge in training the specialists in geocryology and for the implementation of the recent innovations in the institutions engaged in the development of the Russian cryolithozone.

In terms of the applied science, the Institute has developed and is ready to carry out the following important initiative projects, subject to availability of funds:

1) sustainability of engineering structures and ecological safety of the northern cities;

2) sustainability of roads in the permafrost zone;

3) optimization of the use of farmlands in the cryolithozone to provide the population with agricultural products;

4) the use of agro-geophysics to control farmlands of the cryolithozone in terms of the increase in soil fertility;

5) dynamics of the continental and subaquatic cryolithozone of the Russian Arctic;

6) the response of cryogenic ecosystems in the Arctic zone of Russia to global climate warming (on the example of the Kolyma Lowland);

7) the development and implementation of the modern engineering-geocryological monitoring of

hydraulic structures (ground dams and dikes) in the cryolithozone of Russia;

8) the cryogenic resources of Russia;

9) the assessment of the prospective use of subpermafrost waters of the cryolithozone as an alternative source of water supply;

10) the building of Akademic town in Yakutsk on the territory of the Melnikov Permafrost Institute SB RAS.

The All-Russian Conference with international participation "Sustainability of Natural and Technical Systems in Cryolithozone" was held in Yakutsk on September 28–30, 2020 to the 60th anniversary of the Melnikov Permafrost Institute SB RAS [*Zheleznyak et al., 2020*].

The conference program included the following sections:

– the problems of general geocryology; sustainability of natural systems under conditions of climate change and anthropogenic impacts;

– the interaction between surface and ground waters; their role in the formation and dynamics of cryogenic landscapes; geochemical evaluation of cryogenic landscapes;

– the problems of engineering geocryology; sustainability of engineering systems under conditions of climate change and anthropogenic impacts;

– the youth sub-forum "Modern Climate and Permafrost".

Definitely, the results of the geocryological studies have been regularly discussed at various conferences and symposiums, which have been held both in Russia and abroad. However, this conference is significant and relevant because it has been held in Yakutsk, which has been called "the cradle of geocryology" by M.I. Sumgin, the founder of the geocryology.

Over 150 people from Russia (Yakutsk, Moscow, Khabarovsk, Perm, Irkutsk, Novosibirsk, Tyumen, Nizhny Novgorod, Chita, Vladivostok, St. Petersburg) and also from China, Sweden, Kazakhstan and other countries have applied for participation in the conference.

References

Alekseeva, O.I., 2015. X International Symposium on Permafrost Engineering. Kriosfera Zemli [Earth's Cryosphere], XIX (1), 114–118.

Alekseeva, O.I., 2017. Permafrost engineering in Yakutia geocryological research. Earth's Cryosphere XXI (4), 3–9.

Alekseeva, O.I., Zhang, R.V., 2011. Leader of geocryology. Kriosfera Zemli [Earth's Cryosphere], XV (3), 82–88.

Anisimova, N.P., Pavlova, N.A., 2014. Hydrogeochemical studies of permafrost in Central Yakutia. Acad. Publ. House "Geo", Novosibirsk, 189 pp. (in Russian).

Fedorov, A.N., Vasilyev, N.F., Torgovkin, Y.I., et al., 2018. Permafrost-landscape map of the Republic of Sakha (Yakutia) at scale 1:1,500,000. Geosciences, 8 (465), DOI: 10.3390/geosciences8120465. – http://mpi.ysn.ru/images/mlk20182.pdf

Goncharov, Yu.M., 2016. Foundations in permafrost. Melnikov Permafrost Institute SB RAS, Yakutsk, 578 pp. (in Russian).

Goncharov, Yu.M., Popovich, A.P., 2012. Guidelines for design and construction of surface spatial ventilated foundations on fill in permafrost areas. Melnikov Permafrost Institute SB RAS, Yakutsk, 60 pp. (in Russian).

Grigoriev, M.N., 2017. Study of permafrost formations degradation of East Siberia coastal zone (subsequent to the results of expeditions of 2014–2016. Problemy Arktiki i Antarktiki [Arctic and Antarctic Research], No. 1 (111), 89–96.

Klimovskiy, I.V., 2008. Academician Pavel Ivanovich Melnikov. Zhang, R.V., Shepelev, V.V. (Eds.). Acad. Publ. House "Geo", Novosibirsk, 306 pp. (in Russian).

Kuzmin, G.P., Kuvaev, V.A., 2019. Water as an accumulator of solar energy. Applied Journal of Applied and Fundamental Research, No. 9, 80–84.

Kuzmin, G.P., Zhang, R.V., Yakovlev, A.V., et al., 2012a. RF Useful Model Patent 112219. A device for cooling permafrost soils. Patent Holder Permafrost Institute SB RAS. – No. 2011146997. Claimed 18.11.2011. Published 10.09.2012, Bull. No. 25 (in Russian).

Kuzmin, G.P., Zhang, R.V., Remizov, V.A., et al., 2012b. RF Useful Model Patent No. 112219. A device for indoor temperature stabilization. Patent Holder Permafrost Institute SB RAS. – No. 2011133062. Claimed 21.07.2011. Published 10.01.2012, Bull. No. 1 (in Russian).

Shakhova, N., Semiletov, I., Gustafsson, O., et al., 2017. Observational evidence for current rates and mechanisms of permafrost degradation in the East Siberian Arctic Shelf. Nature Communications, No. 8, 1–13, DOI: 10.1038/ncomms15872. – https://www.nature.com/articles/ncomms15872.pdf IF13.092

Shepelev, V.V., 2011. Suprapermafrost Waters in the Cryolithozone. Acad. Publ. House "Geo", Novosibirsk, 169 pp. (in Russian).

Shepelev, V.V., Zhang, T.R., 2011. The hydrogeology of urban areas on permafrost and the main problems in water logging control: a case study of Yakutsk. National Geology, No. 6, 58–63 (in Russian).

Shepelev, V.V., Zheleznyak, M.N., 2019. Main results of Melnikov Permafrost Institute SB RAS research and organizational activities. Annual report 2018. Melnikov Permafrost Institute SB RAS, Yakutsk, 222 pp. (in Russian).

Shepelev, V.V., Zheleznyak, M.N., 2020. Main results of Melnikov Permafrost Institute SB RAS research and organizational activities. Annual report 2019. Melnikov Permafrost Institute SB RAS, Yakutsk, 210 pp. (in Russian).

Shestakova, A.A., Spektor, V.B., Torgovkin, Ya.I., Spektor, V.V., 2016. Summarized data on the permafrost zone on the 1:1 500 000-scale engineering and geological map of the Sakha Republic (Yakutia). In: Proceedings of the Fifth Conference of Geocryologists (Moscow, June 14–17, 2016). Univ. Kniga, Moscow, vol. 3, pp. 290–297 (in Russian).

Velikin, S.A., 2012. Particularities of geophysical monitoring of hydrotechnical structures in the cryolithozone. Nauka i Obrazovanie [Science and Education], No. 4, 29–34.

Vlasov, V.P., Gulyi, S.A., Zhang, R.V., 2012. Guidelines for design and construction of pile foundations in thawing and thawed ground in the Magadan Oblast. Melnikov Permafrost Institute SB RAS, Yakutsk, 64 pp. (in Russian).

Zhang, R.V., Kuznetsov, G.I., Shepelev, V.V., et al., 2012. Small Dams on Permafrost in Yakutia: Guidelines for design and construction. Melnikov Permafrost Institute SB RAS, Yakutsk, 124 pp. (in Russian).

Zhang, R.V., Velikin, S.A., Kuznetsov, G.I., Kruk, N.V., 2019. Embankment Dams in the Permafrost Zone of Russia. Acad. Publ. House "Geo", Novosibirsk, 427 pp. (in Russian).

Zheleznyak, M.N., Semenov, V.P., 2020. Subsurface Temperature Field and Permafrost in the Vilyui Syneclise. SB RAS Publ., Novosibirsk, 121 pp. (in Russian).

Zheleznyak, M.N., Shepelev, V.V., Zhang, R.V., 2020. Environmental and infrastructure integrity in permafrost regions. Proceedings of the Russian Conference with International Participation on the Occasion of the 60th Anniversary of the Melnikov Permafrost Institute (Yakutsk, September 28–30, 2020). Melnikov Permafrost Institute SB RAS, Yakutsk, 462 pp. (in Russian).

Received November 6, 2020
Revised version received November 15, 2020
Accepted November 26, 2020

EARTH'S CRYOSPHERE
SCIENTIFIC JOURNAL

Kriosfera Zemli, 2021, vol. XXV, No. 1, pp. 61–62

ADVERTISING

CONTACT AND VISIT US IN THE KOLYMA REGION FOR JOINT RESEARCH!

The North-East is a resource base of strategic importance and, according to the development plans of the Russian Federation, in the near future it should become one of the most dynamically developing regions located in the permafrost zone. In this regard, it becomes relevant to study the response of all components of the natural environment to climatic and anthropogenic impacts.

The team of North-Eastern Permafrost Station (NEPS) of Melnikov Permafrost Institute, SB RAS located in Magadan, seeks for cooperation in various fields of research on natural processes in the North-East and their impact on society.

In 2020, an initiative group of young hydrologists has moved to work in Magadan and is ready to assist in organizing and conducting scientific research in the North-East of Russia.

Our main research sites (the Anmangynda aufeis and the Kolyma water balance station, KWBS) are located along the Tenkinskaya highway in the Magadan region, we also conduct research in Kyubyume (the federal highway of Kolyma R-504 in Eastern Yakutia). We are carrying out the studies, the purpose of which is to assess changes in the conditions of water exchange of groundwater and surface waters in natural and disturbed conditions, establish the sources of river runoff, forecast changes in the hydrological conditions of rivers in the North-East of Russia. At the research plots, we investigate the dynamics of formation and ablation of aufeis; the monitoring gauges have been equipped to determine hydrogeological, hydrometeorological and

The Anmangynda aufeis in summer.

The view of the Kolyma water balance station.

The team and the transport.

Hydrological observations.

The formation of the Anmangynda aufeis. December 2020.

Winter work.

geocryological characteristics, including sampling for isotopic and hydrogeochemical analysis; geophysical and drilling operations are planned to establish permafrost-hydrogeological conditions.

NEPS has a vehicle (seven-seater jeep) to move around research objects in the Magadan Region and Eastern Yakutia. There is a three-room apartment with heating and hot water, as well as an excellent view of the nearby mountains located in the town of Ust-Omchug. The house with a stove is available for living in the Stokovoye (KWBS).

We have collected a large array of hydrometeorological and other observational data over a long period, based on which it is possible to conduct studies of the impact of climate change on the natural processes of the region. We have here the equipment and implements necessary for carrying out field work. The established contacts with the local administration and the business community will make it possible to quickly and efficiently organize scientific work at the highest level.

Within the framework of cooperation, we will be glad to:

- meet you at the Sokol (Magadan) airport;
- provide living arrangements in the city of Magadan and at our facilities adjacent to research sites in the Magadan region;
- provide transport for people and goods to the research sites;
- install equipment and monitor environmental characteristics, collect samples;
- receive students and young scientists for research and upon arrival to the Magadan region provide them with everything they need;
- collect archival data from organizations of the Magadan region;
- assist in carrying out a range of field work in permafrost, hydrology and other fields of Earth Sciences;
- represent your interests in the region and resolve all issues on the local level.

Welcome to our hospitable land!

CONTACT DETAILS

North-Eastern Permafrost Station, Melnikov Permafrost Institute,
Siberian Branch of the Russian Academy of Sciences, Portovaya str. 16, Magadan, 685017, Russia

Sergey Gulyi (Head of the station), svnims@mail.ru, +7(914)853-40-19

Olga Makarieva (leading researcher, responsible for cooperation), omakarieva@gmail.com, +7(911)213-26-57
https://vk.com/other_hydrology